A dark quencher genetically encodable voltage indicator (dqGEVI) for high fidelity recordings in murine and human *in vitro* systems

Dissertation

Therese Christine Alich

A dark quencher genetically encodable voltage indicator (dqGEVI) for high fidelity recordings in murine and human *in vitro* systems

Dissertation

zur

Erlangung des Doktorgrades (Dr. rer. nat.)

der

Mathematisch-Naturwissenschaftlichen Fakultät

der

Rheinischen Friedrich-Wilhelms-Universität Bonn

Vorgelegt von

Therese Christine Alich

aus

Bonn

Bonn 2023

Angefertigt mit Genehmigung der Mathematisch-Naturwissenschaftlichen Fakultät

der Rheinischen Friedrich-Wilhelms-Universität Bonn

Gutachter und Betreuer: Prof. Dr. Istvan Mody
Gutachter: Prof. Dr. Günter Mayer

Tag der Promotion: 12. September 2023
Erscheinungsjahr: 2023

Contents

1 Introduction 1

1.1 Aim and scope of this thesis 1

1.2 Electrode-based measurements 2

1.3 Optical methods 3

1.3.1 Calcium imaging 3

1.3.1.1 Synthetic Ca^{2+} indicators 4

1.3.1.2 Genetically encoded Ca^{2+} indicators 4

1.3.2 Voltage imaging 5

1.3.2.1 Challenges of voltage imaging 5

1.3.2.2 Synthetic voltage indicators 6

1.3.2.3 Genetically encoded voltage indicators 7

2 A new and promising genetically encodable voltage indicator (dqGEVI) (Publication #1) 13

3 Application of dqGEVI in human iPSC-derived sensory and cortical neurons (Publication #2) .. 16

4 Summary 19

5 References 23

6 Appendices 31

A Publication #1: A dark quencher genetically encodable voltage indicator (dqGEVI) exhibits high fidelity and speed 31

B Publication #2: Bringing to light the physiological and pathological firing patterns of human induced pluripotent stem cell-derived neurons using optical recordings 49

7 Acknowledgements 69

1 Introduction

1.1 Aim and scope of this thesis

This thesis describes experiments carried out on murine and human induced pluripotent stem cells (iPSC)-generated neurons in order to test and verify a novel genetically encoded voltage indicator (GEVI).

GEVIs represent an ideal tool for visualizing neuronal electrical activity directly at the plasma membrane. They can be targeted to specific neuronal subtypes, and are suitable for both microscopic and mesoscopic recording of neuronal activity. That has made them the object of intense research efforts. However, many existing GEVIs have major drawbacks. These include poor time resolution, bad signal-to-noise ratios – making averaging of the signals necessary –, production of photocurrents upon illumination, poor photostability, and non-linear voltage responses. They may also interfere with the integrity of the cell by increasing the capacitance of the plasma membrane.

The experiments carried out in the framework of this thesis have been reported in two publications, which are presented here. The first paper aims at developing and characterizing a novel GEVI which addresses the above-mentioned shortcomings. This optical tool, or sensor, was validated and characterized in murine cell cultures. The second publication reports experiments proving the usefulness of this sensor in a model *in vitro* system of neurons derived from human induced pluripotent stem cells (iPSCs).

Publication #1 describes the development and verification of a GEVI with a novel dark quencher (dq). This dqGEVI was developed based on the hVOS principle (see Section 1.3.2.3) optimizing this approach by replacing the quencher dipicrylamine (DPA), which has major shortcomings, such as toxicity, increasing membrane capacitance, and explosiveness. The replacement for DPA is a benign new quenching molecule, Disperse Orange 3 (D3). Experiments in murine cell cultures and brain slices show that dqGEVI does not increase the capacitance of the plasma membrane, is slow to photobleach on constant illumination, has a high temporal resolution, and is therefore ideally suited for the visualization of fast trains of action potentials. It has a linear response to hyperpolarized and depolarized membrane potentials, and produces sufficiently large signals to avoid the need for signal averaging to resolve the single trace fluorescence.

1. Alich, T.C., Pabst, M., Pothmann, L., Szalontai, B., Faas, G.C., Mody, I., 2021. A dark quencher genetically encodable voltage indicator (dqGEVI) exhibits high fidelity and speed. Proc. Natl. Acad. Sci. U. S. A. 118(6), 1-12. DOI: 10.1073/pnas.2020235118.

Following these initial promising results, the novel dqGEVI was applied to neurons derived from human induced pluripotent stem cells (hiPSCs). Publication #2 shows that the dqGEVI is capable of closely monitoring the activity of hiPSC-derived sensory and cortical neurons. In hiPSC-derived sensory neurons from a patient suffering from a chronic pain disorder the high temporal resolution and non-invasiveness of the dqGEVI enables monitoring of the pathological action potential firing patterns in the patient group, which were not detected with previous methods.

2. Alich TC‡, Röderer P‡, Szalontai B, Golcuk K, Tariq S, Peitz M, Brüstle O and Mody I (2023) Bringing to light the physiological and pathological firing patterns of human induced pluripotent stem cell-derived neurons using optical recordings. Front. Cell. Neurosci. 16:1039957, 1-15. DOI: 10.3389/fncel.2022.1039957. (‡ equal contribution)

Sections 1.2 and 1.3 of this thesis trace the main methods traditionally used to visualize neuronal activity, and discuss how the optical methods employed in this work provide an improved way of monitoring the activity. Chapter 2 summarizes the published work on the dqGEVI developed in the course of this research. It briefly describes the methods used and the obtained results. The paper itself is reproduced in Appendix A. Chapter 3 describes the successful application of this sensor to another *in vitro* system, in this case to human induced pluripotent stem cell (iPSC)-derived neurons. That paper is reproduced in Appendix B.

1.2 Electrode-based measurements

Visualizing the activity of large ensembles of neurons in parallel is one of the most challenging goals in neuroscience. The first attempts to monitor the activity of single neurons came from Cole and Curtis already in 1938, who first introduced a glass microelectrode to measure the impedance of single marine eggs (Cole KS, 1938), and from Hodgkin and Huxley, who were awarded the Nobel prize for their discovery of the ionic mechanism that takes place in the plasma membrane of the squid axon during excitation and inhibition (Hodgkin, 1939). Methodologically Hodgkin and Huxley introduced the use of glass electrodes, which penetrate the membrane and measure electrical currents, the so-called intracellular sharp electrode recording method. This technique was further developed by Neher and Sakmann in 1976 (Neher and Sakmann, 1976), who introduced the patch clamp technique, which presently constitutes the most widely used electrophysiological method to determine the electrophysiological properties of individual nerve cells.

Of late, the patch clamp technique has improved in throughput even to record from up to 384 cells in parallel (Obergrussberger et al., 2022). However, the patch clamp technique still suffers from major disadvantages. It is associated with high labor costs, and its invasiveness is marked in the whole cell configuration that ruptures the plasma membrane to exchange the cells' interior with an artificial intracellular solution.

Microelectrode arrays (MEAs) are a non-invasive electrode-based alternative. The method was first applied by in 1972 by Thomas and colleagues (Thomas et al., 1972) to study the development and plasticity of cultured cells and is used until today for visualization of overall spontaneous activity of a large number of cells in parallel. New microelectrode probes such as ultrathin CMOS arrays can offer more than 5000 recording sites (Steinmetz et al., 2016).

Compared to patch clamp approaches, MEAs are non-invasive and cells can be monitored over long time periods. Furthermore, the method is associated with little work for the experimenter compared to labor-intensive patch clamp experiments. The downside of the MEA is the lack of cellular resolution to resolve action potential kinetics. Moreover, the technique does not allow studying either the contribution of certain subtypes of cells within a mixed network or the contribution of certain ion channels to a specific activity pattern.

1.3 Optical methods

Optical methods seem to be an ideal solution for measuring neuronal activity as they overcome most of the shortcomings mentioned above and offer a wide range of possibilities for monitoring cellular activity.

Optical methods enable monitoring cellular excitability simply by examining the photons emitted by activity-sensing probes. The activity of multiple cells within an ensemble can be visualized in parallel. In addition, optical methods enable visualized interactions between multiple subcellular compartments of the same neurons, such as dendrites, axons and somata. Cells tagged with optical probes can be monitored with high and low magnification. Single cell resolution can be achieved using a standard microscopes equipped with an extremely light-sensitive camera with high sampling rates (Alich et al., 2021). High-throughput monitoring of huge ensembles of cells, in contrast, is made possible in a multi-well format using semi-automated or fully automated plate readers (Bedut et al., 2021).

Optical methods, compared to traditional electrophysiological methods, are relatively non-invasive avoiding rupture of the membrane by the recording pipette and the exchange of intracellular constituents as in whole-cell patch clamp recordings. The real degree of non–invasiveness of optical methods, however, depends on the optical tool that is used as will be discussed below (see Sections 1.3.2.1 and 1.3.2.3).

1.3.1 Calcium imaging

By far the most widely used optical method to monitor activity in cells of the nervous system is to measure activity-associated changes in intracellular Ca^{2+} using Ca^{2+} indicators. The following Sections will give an overview of synthetic and genetically encoded Ca^{2+} indicators and outline the advantages and drawbacks of this indirect method.

1.3.1.1 Synthetic Ca^{2+} indicators

The first Ca^{2+} indicators were bioluminescent calcium-binding photoproteins. The first calcium-binding photoprotein, Aequorin, was discovered as a new luminescent system in 1962 when Shimomura and colleagues discovered that Aequorin gives a light emitting reaction on addition of Ca^{2+} (Shimomura et al., 1962).

Later, in 1982, fluorescent, highly selective Ca^{2+} indicators have been developed, which are able to visualize and quantify free Ca^{2+} concentrations inside neurons. Tsien and colleagues (Tsien et al., 1982) developed the selective Ca^{2+} indicator, Quin2, a tetracarboxylic acid, whose fluorescence increases about five-fold upon Ca^{2+} binding. This initial probe was followed by Fluo-3 AM and Fluo-4 AM, which are widely used until today (Dissanayake et al., 2022; Wang et al., 2021). Fluo3-AM dyes are fluorescein-based acetoxymethyl (AM) esters that mask the carboxyl groups where Ca^{2+} is bound are highly hydrophobic and readily pass through the cell membrane. After entering the cell, esterases hydrolyze the esters, which enables the dyes to detect calcium.

These Ca^{2+} indicators are bright, photostable, show high Ca^{2+} affinity, and have very large calcium-dependent fluorescence. They can be delivered to the cells via bulk loading or cell permeabilization by a whole-cell patch clamp (Piatkevich et al., 2019).

1.3.1.2 Genetically encoded Ca^{2+} indicators

Genetically encoded Ca^{2+} indicators (GECIs), which have first been developed in 1997 (Miyawaki et al., 1997; Persechini et al., 1997), bypass most of the drawbacks of the cell-loading indicators. The genetically driven expression of the GECI avoids bulk loading of the dye and related background staining. The genetic tag of the indicators enables targeting specific neuronal subpopulations and neuronal subcompartments can be imaged without prior laborious loading. Additionally, imaging at specific developmental stages can be achieved through an appropriate developmental stage-dependent promoter. Various GECIs have been developed during the last decades, which have improved in terms of response time, photostability, and signal size. To avoid spectral overlap with optogenetic actuators and to GECIs have been developed in different colors or to multicolor imaging (Reviewed in Oh et al., 2019, Table 2).

As mentioned above, Ca^{2+} indicators, whether synthetic or genetically encoded, are the most widely used tools to visualize neuronal activity (Looger and Griesbeck, 2012). The widespread use of Ca^{2+} indicators can be assigned to the large fluorescent changes that can be easily detected with two-photon microscopy.

Changes in intracellular Ca^{2+} take place throughout the whole cytoplasm, which serves as a huge volume for sensor molecules to be present, thus creating a good signal-to-noise ratio (SNR).

Despite their widespread use as a proxy for activity indicators, Ca^{2+} indicators are associated with major disadvantages. First, they are only an indirect measure of neuronal activity measuring the Ca^{2+} influx that follows action potentials, which makes them inherently unable to resolve hyperpolarizations or subthreshold events below the action potential initiation threshold.

Moreover, the high Ca^{2+} affinities of presently available GECIs render the recorded Ca^{2+} signals inherently slower than action potentials, which makes them unsuitable for resolving trains of high-frequency action potentials or finer details encoded by high-frequency action potential firing. Finally, Ca^{2+} indicators are Ca^{2+} buffers (McMahon and Jackson, 2018), and thereby have a high chance for interfering with intracellular calcium-dependent signaling pathways. For these reasons, the ideal optical tool is a voltage indicator, that measures electrical changes at the plasma membrane (see Sections 1.3.2.2 and 1.3.2.3).

1.3.2 Voltage imaging

In contrast to the more widely used indirect method of Ca^{2+} imaging, optical imaging of electrical activity directly at the plasma membrane using genetically encoded voltage indicators (GEVIs) is the ultimate method to assess neuronal activity. However, voltage imaging is challenging for many reasons, as discussed in the following section.

1.3.2.1 Challenges of voltage imaging

The necessity of targeting the voltage indicator to the plasma membrane, where the electrical activity to be monitored takes place, brings up the first difficulty in this approach. The vast majority of cellular membranes are located intracellularly and targeting solely to the plasma membrane presents a special challenge. Any nonspecific labelling of intracellular membranes causes background noise, which decreases the signal.

The thinness of the plasma membrane represents the second major challenge, as it is a very thin compartment of only a few nm thickness. Compared to Ca^{2+} imaging where the sensor can occupy the entire cytoplasm, the space for placement of the voltage sensor molecules is thus minimal, restricted only to the plasma membrane. The volume ratio of the plasma membrane to that of the cytoplasm is approximately 1:1000.

This demands high illumination intensities to excite the few voltage-sensor molecules sufficiently to emit a large number of photons. This leads to rapid photobleaching and phototoxic effects such as photodamage from the generation of reactive oxygen radicals. The minimal space for sensor molecule placement also demands highly efficient chromophores. Nonetheless, signals often have to be spatially or temporally averaged to extract the signal from noise. Averaging, however, is problematic since the signals are very fast (in the millisecond range) and not necessarily repetitive, as they take place at the tiny space of the dendritic and axonal arbors.

In order to reflect the whole spectrum of neuronal activity, a voltage indicator should respond to depolarizing and hyperpolarizing voltages in a linear fashion, which represents a major challenge. Furthermore, the integrity of the plasma membrane needs to be preserved in spite of the loading of the sensor into the membrane. As the plasma membrane constitutes the barrier of the cell protecting it from outside factors, its integrity is of foremost importance. To visualize electrical activity directly, the sensor molecules have to be targeted to the plasma membrane, but the addition of large molecules to the membrane can increase its capacitance and interfere with the electrical or biochemical properties of the cell by adding additional charges or interfering with intracellular signaling cascades.

The speed of the biological electrical events of interest represents another major challenge. The speed of an action potential with just 1-2ms time-span and about 250µs rise time is challenging to capture with any dye. Voltage indicators have a very limited period to deliver photons to the light detector, which makes the signal noisier compared to Ca^{2+} imaging. Ca^{2+} events persist for 10 – 100s, enough time to deliver sufficient photons to the imaging detector to produce a bright signal. The speed of the events also demands high sampling rates of >1kHz, which, paired with the desired large field of view, is technically very challenging given the huge amount of data.

1.3.2.2 Synthetic voltage indicators

The first experiments using *intrinsic* optical properties of neurons to monitor electrical changes in the membrane were conducted in 1949 by Hill and Keynes (Hill and Keynes, 1949), who discovered the light scattering changes that accompanied trains of stimuli to nerves (Reviewed in Cohen, 1989). Later, Cohen and colleagues extended these observations and used a signal average to observe very small changes and observe light scattering and birefringence changes that accompany an action potential (Cohen et al., 1968). Notably, these relatively small signals could only be detected by averaging over several trials.

Improved signals of electrical changes in the membrane could be achieved by adding *extrinsic* fluorescent indicators, so-called voltage-sensitive dyes (VSDs). VSDs are charged, lipid-soluble molecules that bind to the plasma membrane and act as molecular transducers that transform changes in membrane potential into optical signals.

The use of VSDs was first reported by Shtrankfeld and Frank in 1964, who conducted initial experiments reporting changes in *extrinsic* fluorescence upon stimulation of giant axons (Shtrankfeld and Frank, 1964). However, the experimental setup only allowed a very poor time resolution. The first optical recordings with improved time resolution were made by Tasaki and colleagues on giant axons, squid fin nerves and crab nerves, who measured the fluorescence change after electrical stimulation after the nervous tissue was stained with a voltage sensitive dye (VSD), 1-anilino-8-naphthalene sulfonate (ANS) and 12 other VSDs (Tasaki, I., Carnay, L., Watanabe, 1969; Tasaki et al., 1968).

Subsequently, Cohen, Salzberg and colleagues tested 300 commercially available synthetic dyes, mainly fluorescent dyes used in histology, for improved fluorescent signals that would allow optical monitoring of membrane potential in neurons and succeeded with more than 180 of them including trinuclear-heterocyclic, cyanine, merocyanine and styryl dyes (Cohen et al., 1974) (reviewed in Cohen et al., 1978). Unfortunately, roughly a third of the tested dyes turned out to have pharmacological effects, such as the reduction of sodium or potassium currents. Additionally, intense illumination of the cells caused photodynamic damage and rapid photobleaching.

Improved dyes, organic voltage sensing chromophores, have been used to visualize the activity of different neuron types in invertebrates (Salzberg et al., 1977; Wu et al., 1994) and in cultured neurons (Grinvald et al., 1981; Nemet et al., 2004) and to visualize electrical activity in dendrites by injecting the dye into individual cells (Acker et al., 2016). The high temporal resolution of VSDs, which has been shown to be an astonishing 1.2µs measured as responses to voltage clamp pulses in squid axons (Loew et al., 1985), makes VSDs ideally suited to investigate action potentials occurring at high frequencies and even for the study of action potential waveforms.

However, much like synthetic Ca^{2+} indicators (see Section 1.3.1.1) VSDs have several drawbacks, as they do not differentiate between cells with different genetic identities. Bulk loading of the dyes results in strong background staining, which diminishes the signal and prevents differentiation between individual cells. Imaging of dendrites with VSDs is thus only possible after the cell has been laboriously individually laoded with the dye (Popovic et al., 2015). The improved way to selectively target single cells' membranes with voltage indicators is to equip the sensor with a genetic tag (see Section 1.3.2.3).

1.3.2.3 Genetically encoded voltage indicators

If the voltage sensor is genetically encoded, targeting of specific cells can be accomplished with the help of cell-specific promoters. Moreover, no background is generated as opposed to bulk loading of the dye and no laborious and potentially harmful loading of single cells is required. Genetic targeting is useful for discrimination in intact tissue, where cells are different subpopulations of cells are closely spaced and often perform different functions.

Three different major GEVI approaches have been developed starting with GEVIs that are based on voltage-sensitive domains (see Section 1.3.2.3 "Voltage-sensitive domain-based GEVIs" below) over GEVIs that use a microbial rhodopsin (see Section 1.3.2.3 "Rhodopsin-based GEVIs") and finally hybrid voltage sensors, which consist of a genetically expressed and a synthetic component, so-called hybrid indicators (see Section 1.3.2.3 "Hybrid GEVIs"). All approaches are based on the fact that membrane voltage acts on transmembrane proteins and changes in the electric field bring about conformational changes of proteins or movements of synthetic molecules in the membrane.

In the following representative sensors from each group are presented and their advantages and shortcomings are outlined.

Voltage-sensitive domain-based GEVIs

In 1997 the first genetically encoded voltage indicator (GEVI), FlaSh, was developed. This GEVI is composed of a voltage sensitive domain of a drosophila *Shaker* K^+ channel (Flash = fluorescent *Shaker*)(Siegel and Isacoff, 1997), which constitutes the detector, fused to a single fluorescent protein, green fluorescent protein (GFP), which constitutes the reporter. This sensor changes GFP fluorescence emission in response to voltage-dependent changes in the K^+ channel.

A few years later VSFP1 was developed using the same detector. This sensor had superior fluorescent properties as it used a fluorescent pair, cyan and yellow mutants of GFP, which interact via a Förster resonance electron transfer (FRET) (Sakai et al., 2001). The change in transmembrane voltage thereby alters the amount of FRET, which generates the optical signal.

Unfortunately, these first sensors were of minor success in mammalian preparations probably due to poor targeting to the plasma membrane. The discovery of a VSD from a phosphatase of a sea squirt, *Ciona intestinalis* (Murata et al., 2005), then led to more successful approaches displaying clear targeting to the plasma membrane in mammalian cells (Dimitrov et al., 2007). After that an improved sensor, Arclight, was developed by fusion of the voltage sensitive domain of the phosphatase of *Ciona intestinalis* with a novel fluorescent protein, super ecliptic pHluorin (Jin et al., 2012). Arclight showed improved signal size and was able to detect single action potentials in cultured neurons. The kinetics, however, were slow, limiting its use for action potential detection, especially at high frequencies. To improve upon this, an Accelerated Sensor of Action Potential (ASAP) was developed (St-Pierre et al., 2014a). ASAP harbored a circularly permutated GFP, which was inserted into an extracellular loop of a *G. Gallus* voltage-sensing phosphatase, a region known to undergo rapid conformational change after depolarization (Jensen et al., 2012). These conformational changes perturb the GFP fluorescence generating the optical signal. Depolarizations thus producing a decrease in fluorescence which is why they are referred to as negative indicators. This sensor, indeed, showed improved kinetics. A 2 ms decay time constant compared to a 17 ms decay time of Arclight allowed the detection of action potentials to up to 200Hz. Then different mutations were introduced into ASAP in order to improve the sensor yielding further generations of the sensor that were successfully used for different purposes as for two-photon excitation and for *in vivo* recordings (Chamberland et al., 2017; Villette et al., 2019), although the kinetics of the two-photon compatible variant is slower than earlier ASAP variants (Chamberland et al., 2017). Most recently the response kinetics of two-photon compatible ASAP variants have been compared to a hybrid GEVI, which shown much faster responses in response to action potential waveforms injected in HEK293T cells (Alich et al., 2021).

Lately, Cornejo and colleagues developed "postASAP", which was used to measure membrane potential in dendritic spines in vivo and under two-photon excitation (Cornejo et al., 2022). This sensor used ASAP as backbone modified with mutations for enhanced sensitivity and PSD95.FingR (Fibronectin intrabodies generated with mRNA display)(Gross et al., 2013) nanobody domain to enrich expression in spines. This elegant way of expression of a GEVI in spines surely opens the path to unravel the spatiotemporal patterns of depolarizations in dendritic trees. However, a limiting factor when using ASAP backbones is the photostability of the indicator, observing substantial photobleaching when recording for just a few seconds (Wu et al., 2020).

A way to improve photostability is the development of, positive voltage-sensitive domain-based indicators, which respond to depolarizations with an increase in fluorescence and show low fluorescence during resting state (Abdelfattah et al., 2016; Tsutsui et al., 2008). These indicators have been developed to prevent rapid photobleaching. The downside is that the low fluorescence during resting state impedes the detailed visualization of small hyperpolarizations.

An improved version of ASAP has therefore recently been optimized in terms of photostability. The new GEVI jellyfish-derived electricity reporting designer indicator for 2-photon (JEDI-2P) (Liu et al., 2022) has been selected in a high throughput platform under two-photon illumination from a library of GEVI variants constructed by side directed polymerase chain reaction (PCR) mutagenesis of ASAP. In combination with resonant scanning and ultrafast local volume excitation (ULoVE) random-access microscopy (Villette et al., 2019), JEDI-2P enables monitoring of individual cortical neurons in awake behaving mice for more than 30 minutes under two-photon illumination.

Despite this progress a major shortcoming of voltage-sensitive domain-based GEVIs is that they have a relatively narrow response range to voltage as the voltage-gated ion channels undergo conformational changes over a narrow voltage range and thus a relatively low sensitivity. Another intrinsic problem of voltage sensitive domain based GEVIs is the targeting of the sensor to the plasma membrane, as the voltage gated ion channels preferentially tend to be trapped into intracellular compartments (Capera et al., 2019).

Besides these drawbacks the overexpression of trans-membrane domains per se represents a fundamental disadvantage of these types of voltage indicators as a major challenge in voltage imaging is to minimally interfere with the integrity of the plasma membrane (see Section 1.3.2.1).

Rhodopsin-based GEVIs

The discovery of a microbial green absorbing proteorhodopsin (GPR), a light-driven proton pump found in the ocean (Beja et al., 2000), led to the first opsin-based GEVI, called Proteorhodopsin Optical Proton sensor (PROPS) (Kralj et al., 2011). It was speculated that the mechanism can be run in reverse to use the GPR as voltage sensor with optical readout. Indeed, through mutagenesis the natural light-driven

transport of protons in the microbial rhodopsin, which induces changes in fluorescence, was abolished and the system was adapted so that voltage-dependent repositioning of the protons induced the colour change in the retinal chromophore under illumination (Maclaurin et al., 2012).

Unfortunately, this first-generation opsin-based GEVI was limited to use in *E. coli* as the protein did not localize to the plasma membrane in eukaryotic cells, despite several attempts using different targeting and localization sequences. Therefore, other microbial rhodopsins suitable for use in mammalian cells were needed. Archaerhodopsin 3 (also known as *Arch*) is expressed by the extremely halophilic archaeon *Halorubrum sodomense*, an organism first identified in the Dead Sea and was cloned in 1999 by Ihara and colleagues (Ihara et al., 1999) and successfully used for voltage imaging in cultured rat neurons (Kralj et al., 2012).

Based on *Arch* several opsin-based voltage indicators such as the *Arch* D95N, D95S and *Arch* D95T mutations, Arch-EEN and –EEQ (Gong et al., 2013), QuasAr 1 and 2 (Hochbaum et al., 2014) and Archon 1 and 2 (Piatkevich et al., 2018) have been developed. Furthermore, opsin-based GEVIs have been coupled to bright FPs in order to overcome the intrinsic dimness of the rhodopsin protein and still keep the speed of the opsin. In this case the FP deals as donor in a Förster resonance electron transfer (FRET) reaction and the opsin deals as FRET acceptor. A promising GEVI using this principle is *Acetabularia chemigenetiacetabulum* rhodopsin (Ace2N) (Gong et al., 2015), which uses the rhodopsin from the giant unicellular marine alga *Acetabularia acatabulum* (Tsunoda et al., 2006) and mNeonGreen as bright fluorescent protein (FP) and the voltage-activated red neuronal activity monitor (VERNAM) (Kannan et al., 2018), using the same rhodopsin but a red fluorescent protein, mRuby3 both of which have been applied to monitor intake brains of freely behaving mice.

One of the major caveats of rhodopsin-based GEVIs is the intrinsic dimness of the rhopsins. This can be overcome by coupling bright FPs in a FRET-based approach, however, depending on the FP used rapid photobleaching upon illumination might occur. Additionally, localization of the sensors to the plasma membrane is often problematic.

Another basic problem is the residual photocurrent originating from the fact that rhodopsins are proton pumps that are driven by light. Although all attempts have been made to eliminate these photocurrents (Gong et al., 2013) they are still present and have a high risk of perturbing the endogenous membrane potential the ultimately needs to be monitored.

As with voltage-sensitive domain-based indicators (see Section 1.3.2.3 “voltage-sensitive domain-based GEVIs”), a fundamental disadvantage lies in the overexpression of trans-membrane domains in the plasma membrane, as a major challenge in voltage imaging is to minimally interfere with the integrity of the plasma membrane (see Section 1.3.2.1).

Hybrid GEVIs

Hybrid GEVIs combine a genetically expressed component with a synthetic or organic component. A most recently developed indicator, Voltron, combines a genetically expressed rhodopsin, Ace2, with a self-labeling protein tag, which allows covalent binding of a synthetic fluorophore, a Janelia Fluor ® (JF) dye that has to be administered separately (Abdelfattah et al., 2019). After covalent binding the JF dye and the rhodopsin domain are in close proximity so that the emission of the acceptor, the rhodopsin, can be recognized by the donor, the JF dye, in a FRET reaction. The absorption spectrum of the rhodopsin changes depending on the transmembrane voltage thereby modulating the degree of fluorescence quenching of the JF dye in the FRET reaction.

Voltron has been successfully used for two photon recordings in awake animals (Abdelfattah et al., 2019) and, to improve upon photostability, has even been modified to a positive indicator, which increases in brightness upon depolarizations called Positron (Abdelfattah et al., 2020).

Early studies have introduced the mechanism for achieving fast ratiometric voltage-sensitive fluorescence changes in single cells using FRET. These studies used fixed fluorescent donors, a fluorescently labelled lectin, which were not genetically encoded, and translocating oxonol acceptors (González and Tsien, 1995).

The acceptors are located at the outer layer of the phospholipid bilayer of the plasma membrane at hyperpolarized potentials, in close vicinity with the donor, where they quench the donor's fluorescence via a FRET reaction. The acceptors then rapidly move in the membrane upon changes in membrane potential. If the cell depolarizes the acceptors are "pulled" to the inner side of the plasma membrane and further apart from the donor thereby disturbing FRET between the two fluorophores and generating a fluorescent read out of electrical activity at the membrane.

To maximize the sensitivity to voltage the translocating acceptors should be able to translocate nearly all the way through the membrane and it should be negatively charged, delocalized, and hydrophobic in order to achieve fast translocation and a near real time read out of the electrical changes across the membrane (González and Tsien, 1995). Different FRET pairs, such as pentamethineoxonol as acceptor and phospholipids as alternative donors to lectin, have been tested for sensitivity and speed and a < 0.4 ms time constant was reached using a pentamethineoxonol and a phosphatidylethanolamine (González and Tsien, 1997). Dipicrylamine (DPA, synonym: hexanitrodiphenylamine, HNDA) is another good candidate acceptor molecule in this approach as it has been shown to produce displacement currents in excitable tissue with sub-millisecond kinetics (Benz et al., 1976; Benz and Conti, 1981). In combination with the lipophilic fluorescent neuronal tracer dye DiO (3,3-Dioctadecyl oxacarbocyanine perchlorate) DPA yielded large optical voltage signals with sub-millisecond resolution enabling the detection of subthreshold activity and high frequency spiking in somatic, axonal and dendritic membrane compartments (Bradley et al., 2009).

Another hybrid GEVI, called hVOS (hybrid voltage sensor) (Chanda et al., 2005), is built on the same principle but the donor is genetically encoded. This approach differs substantially from all before mentioned GEVIs in that it does not make use of transmembrane domains, neither rhodopsins nor voltage sensitive domains from ion channels or phosphatases. hVOS, as several sensors described before (González and Tsien, 1997), makes use of a fluorescence quenching reaction to visualize changes in membrane voltage. The genetically expressed fluorescent protein, enhanced Green Fluorescent Protein (eGFP), which constitutes one part of the hybrid sensor, namely the donor in the quenching reaction, is attached to the inner leaflet of the lipid bilayer via a fatty anchor, a farnesylation tag (Jiang and Hunter, 1998). The other component of the hybrid sensor constitutes a synthetic voltage sensing molecule, dipicrylamine (DPA), which is the fluorescent quencher in the reaction, but itself non-fluorescent, which is why it is also referred to as "dark quencher". Through voltage-dependent movement of DPA in the membrane the distance and thereby the degree of quenching varies and membrane potential changes can be mapped by recording the quenched eGFP fluorescence. Just as those previous studies using the same FRET-based approach, though with a genetically expressed donor, hVOS shows fast response times (time constant of 500 µs) and is therefore ideally suited to examine action potential waveforms in cultured cells and brain slices (Ma et al., 2019).

Due to its high temporal resolution hVOS was a desired tool to systematically image genetically defined cell types and study action potential waveforms characteristic for each cell type. To this end a mouse line has been generated with an hVOS probe inserted into floxed Reverse Oriented Splice Acceptor, Clone 26 (ROSA26) locus enabling Cre-recombinase-dependent expression of hVOS in the desired cell type (Bayguinov et al., 2017). Furthermore, in brain slices, hVOS has been used to detect subthreshold synaptic potentials from many neurons simultaneously in a single trial (Ghitani et al., 2015).

Although hVOS seemed like a very promising GEVI there are major problems associated with the use of DPA as quenching molecule: First DPA has dramatic effects on cell capacitance and increases capacitance significantly at concentrations near the required concentrations for voltage imaging (Chanda et al., 2005). Furthermore, DPA is an explosive as it is composed of two trinitrotoluene (TNT) molecules, which complicates handling the substance. DPA has also been shown to interfere with diverse neurotransmitter systems such as γ-aminobutyric acid $(GABA)_A$ receptors (Chisari et al., 2011) GABAρ1 receptors (Limon et al., 2016) and N-methyl-D-aspartate receptor (NMDA) receptors (Linsenbardt et al., 2013). Another drawback of DPA is that it accumulates at hyperpolarized membrane potentials below -50mV (Ghitani et al., 2015), which makes the visualization of small hyperpolarizations more difficult.

Aside from the problems encountered when using DPA as a quencher, the hVOS approach is a very promising GEVI and overcomes most of the challenges described above (see Section 1.3.2.1). To

circumvent the drawbacks of using DPA, the work outlined in this thesis describes a replacement molecule for DPA in the hVOS approach.

2 A new and promising genetically encodable voltage indicator (dqGEVI) (Publication #1)

The first part of this thesis consists of the Publication

A dark quencher genetically encodable voltage indicator (dqGEVI) exhibits high fidelity and speed. Proc Natl Acad Sci U S A, 2021.

Involved in this work were M Pabst (who sadly passed away on September 26, 2016), L Pothmann, B Szalontai, and TC Alich from the University of Bonn, Institute of Experimental Epileptology and Cognition Research, working group Neuronal Networks in Health and Disease Laboratory, under the direction of I Mody, in the scope of his collaborative research lab in Bonn, and GC Faas and I Mody from Los Angeles, CA, The David Geffen School of Medicine at UCLA, Department of Neurology.

As discussed in Section 1.2 the electrical activity of neurons has traditionally been monitored with electrode-based approaches (Cole KS, 1938; Hodgkin, 1939; Neher and Sakmann, 1976), but due to the invasiveness of manual patch clamp recordings and poor spatial resolution of multi-electrode arrays, a better alternative is desirable. As mentioned above, optical methods offer such an alternative as they are less invasive and can be used in low and high magnification. However, as outlined in Section 1.3.1, the most widely used optical indicators are Ca^{2+} indicators, which provide only indirect measures of neuronal activity. They are unable to visualize hyperpolarizations and subthreshold events, and are invasive due to Ca^{2+} buffering properties, and too slow to resolve fast trains of action potentials.

As outlined in Section 1.3.2 direct visualization of electrical changes at the plasma membrane using voltage indicators is a more promising approach. In combination with a genetic tag (Section 1.3.2.3) voltage indicators can be used to monitor the entire spectrum of the activity of distinct neuronal subtypes. Various genetically encoded voltage indicators (GEVIs) exist and have been successfully used to image neuronal activity in several species *in vivo* as discussed in Section 1.3.2.3. However, all these approaches have major shortcomings related to their often poor temporal resolution and the fact that multiple copies of transmembrane domains have to be inserted into the plasma membrane, which may destroy the integrity of the membrane and increase the capacitance of the cell.

As mentioned in Section1.3.2.3 an alternative approach, which is not based on the insertion of transmembrane domains into the plasma membrane, is a hybrid genetically encoded voltage indicator (hVOS) (Chanda et al., 2005). The first component of the hVOS sensor is a genetically expressed fluorophore, green fluorescent protein (GFP), that is tagged to the inner leaflet of the plasma membrane with a lipid anchor and acts as donor in a Förster resonance electron transfer (FRET) reaction. The

second component, a synthetic voltage-sensing molecule, dipicrylamine (DPA) acts as the quencher. In voltage imaging experiments, DPA in the extracellular fluid attaches to the plasma membrane due to its high lipophilicity. The optical signal is then generated by the voltage-dependent movement of DPA in the plasma membrane. Movement from one leaflet of the plasma membrane to the other changes the distance between the quencher and the fluorophore, thereby varying the degree of quenching. This in turn modifies the optical signal.

However, DPA is a highly toxic and explosive substance which increases the capacitance of the cell and antagonizes GABA and NMDA receptors (Chisari et al., 2011; Limon et al., 2016). For this reason, a search was carried out for alternative quenching molecules to replace DPA. In the framework of this thesis, dozens of compounds were tested for their quenching functionality, using simultaneous optical and electrical recordings in murine cell cultures. Of these, Disperse Orange 3 (D3) was identified as a functional quencher.

Publication #1 "A dark quencher genetically encodable voltage indicator (dqGEVI) exhibits high fidelity and speed" (Appendix A publication #1), describes how the promising dqGEVI approach is optimized by replacing the quencher DPA with D3. To enhance the method even further, a glycosylphosphatidylinositol (GPI) linkage was utilized by B Szalontai to attach the enhanced green fluorescent protein (eGFP) to the outer leaflet of the plasma membrane in order to minimize any potential disruption to intracellular signaling pathways.

TC Alich, the author of this thesis, tested the substance extensively for effects on active and passive membrane properties (supplementary figure S2 in Publication #1). D3, when applied at high concentrations of 20µM, which is 10 times the concentration needed for optical measurements, did not show any effect on passive or active membrane properties including cell capacitance. TC Alich also demonstrated the significant effect of DPA on the capacitance of cultured murine neurons in direct comparison with D3 (supplementary figure S3). DPA significantly increases capacitance, even at such low concentrations as 3µM. TC Alich also tested the effect of D3 on synaptic responses in murine acute cortical brain slices. For that purpose, spontaneous excitatory postsynaptic currents (sEPSCs) and spontaneous inhibitory postsynaptic currents (sIPSCs) were recorded after application of 10µM D3. The lack of an effect of D3 on synaptic responses further confirmed its superiority as a benign quencher in a hybrid GEVI approach.

In the scope of this thesis, a multitude of simultaneous optical and patch clamp recordings were carried out to further characterize the novel sensor. Significantly, TC Alich demonstrated the speed of the sensor in direct comparison with a non-hybrid GEVI, ASAP2s. To that end TC Alich recorded action potential waveforms in HEK293T cells transfected with ASAP2s and GPI-eGFP in voltage clamp. The fluorescence signal obtained from D3-GPI-eGFP dqGEVI exhibited a significantly greater ability to accurately replicate the electrophysiological action potential waveform when compared to the

fluorescence signal generated by ASAP2s (Fig. 3E in Publication #1). As mentioned above, subthreshold changes and hyperpolarizations are not well monitored by other optical indicators. Therefore, another objective of this thesis was to test the ability of dqGEVI to resolve subthreshold changes in membrane potential. To accomplish that, TC Alich carried out simultaneous electrical and optical measurements on cultured neurons expressing dqGEVI and applied a stimulus protocol that systematically and reproducibly alters membrane potential according to a chirp function. The dqGEVI demonstrated exceptional speed and precision in detecting even the smallest subthreshold events and hyperpolarizations (Fig. 4 in Publication #1).

As photobleaching is a great concern in voltage imaging (see Section 1.3.2.1) and since previous voltage indicators have poor photostability, the photostability of dqGEVI was tested as part of this thesis. To that end, TC Alich conducted optical measurements on HEK293T cells transfected with GPI-GFP and the non-hybrid voltage indicators Positron and Voltron under constant illumination (Fig. 5 in Publication #1). The baseline fluorescence as well as the signal-to-noise ratio was only minimally decreased in the dqGEVI as compared with the rapidly bleaching Voltron and Positron optical traces.

Another objective of this thesis was to test if dqGEVI is applicable to monitor neuronal activity at the subcellular level. As electrode-based methods with all the disadvantages mentioned in Section 1.2 are still the gold standard for monitoring subcellular compartments, non-invasive tools for this are highly desirable. To that aim, TC Alich conducted optical measurements in spontaneously active murine primary neurons and successfully imaged the activity at proximal and more distal parts of the dendritic tree. The dqGEVI has thus proved to be suitable even for monitoring activity at subcellular compartments such as the dendrites.

In addition to conducting the experiments described above, TC Alich analyzed the data, generated the corresponding figures, and prepared the manuscript under the guidance of I Mody.

The published version of this work is reproduced in Appendix A.

3 Application of dqGEVI in human iPSC-derived sensory and cortical neurons (Publication #2)

The second part of this thesis was published in *Bringing to light the physiological and pathological firing patterns of human induced pluripotent stem cell-derived neurons using optical recordings, Front. Cell. Neurosci., 2022.* This work was carried out by TC Alich, B Szalontai, from the University of Bonn, Institute of Experimental Epileptology and Cognition Research, Neuronal Networks in Health and Disease Laboratory, under the direction of I Mody, in the scope of his collaborative research lab in Bonn, as well as K Golcuk from the University of Bonn, Institute of Experimental Epileptology and Cognition Research, Circuit Mechanisms of Behavior Laboratory, P Roederer, S Tariq, M Peitz, and O Brüstle from the University of Bonn. Institute of Reconstructive Neurobiology.

The work reported in Publication #1 (Appendix A) showed the outstanding characteristics of the new dqGEVI. It was then considered that these properties, shown in a murine *in vitro* cell system, could potentially be helpful to elucidate the activity in other *in vitro* systems.
Human induced pluripotent stem cell (hiPSC)-derived neurons are an appealing option, given that they are the most physiologically relevant and advanced *in vitro* tool available for modeling human neuropsychiatric and neurological disorders (Okano and Yamanaka, 2014). Human iPSC-derived neurons can be generated from patients with specific genetic mutations or disease phenotypes. This allows for the study of disease mechanisms, which can provide insights into the pathology of the disorders and help to identify potential therapeutic targets.

The primary method for characterizing the activity of these neurons is through electrode-based electrophysiological methods (see Section 1.2). The heterogeneity of these cells, however, presents a considerable challenge for effectively characterizing their functionalities using manual patch-clamp electrophysiology, not to mention the invasiveness of the technique. Conversely, while multielectrode arrays (MEAs) provide large throughput capabilities, there is a limitation in terms of spatial precision and the ability to discriminate between neuronal subtypes. Therefore, a non-invasive tool to visualize the undisturbed activity of these neurons in large-scale recordings would be highly desirable for better and faster characterization of iPSC-derived neuronal cultures.

In the framework of this thesis, the dqGEVI was utilized in a model of inherited erythromelalgia (EM). EM is a genetic chronic pain disease characterized by recurrent episodes of pain, swelling, and redness of the distal extremities (Tham and Giles, 2018). The pain episodes are triggered by mild increases in ambient or body temperature (Mcdonnell et al., 2016). EM is associated with a gain of function mutation in the SCN9A gene encoding a voltage-gated sodium channel, Nav 1.7, which plays an important role in action potential firing in human sensory neurons (Yang et al., 2004). Action potential firing patterns

of neurons are important for the communication between and within neurons. Firing patterns range from sporadically firing cells to bursting activity. Of these patterns, bursting activity stands out as a critical factor in neuronal computation, as it enhances transmitter release and reduces the likelihood of synaptic transmission failures (Lisman, 1997). Hyperexcitable burst firing is a major indicator of pathology in many neurological and neuropsychiatric diseases (Cain et al., 2018; Fremont et al., 2014; Lobb CJ, 2014; Sanabria et al., 2001) and plays an important role in pain transmission.

In order to examine the neuronal phenotype associated with individual mutations in the SCN9A gene, a previous study used manual patch clamp recordings to characterize iPSC-derived sensory neurons from EM patients (Cao et al., 2016). As part of this thesis the dqGEVI was used to carry out measurements on this disease model.

The iPSC-derived sensory neurons from an EM patient and a non-EM control were provided by P Röderer and O Brüstle from the University of Bonn, Institute of Reconstructive Neurobiology.
After confirmation of the integrity of the cells upon dqGEVI expression using patch-clamp recordings, TC Alich optically detected the spiking activity of iPSC-derived sensory neurons from the EM patient and the non-EM patient. A comparison of the firing frequencies between sensory neurons derived from EM patient iPSCs and controls confirmed the increased excitability of the EM patient neurons compared to the control (Fig. 2 in Publication #2) which had already been observed in the above-mentioned publication (Cao et al., 2016).

TC Alich analyzed the firing patterns of the cells using various measures of burst characterization. Interestingly, analysis of the firing patterns revealed a significantly higher fraction of sensory neurons exhibiting bursting activity among the EM patient cells compared to controls (Table 1 in Publication #2). A deeper analysis of the firing patterns using a continuous metric of burstiness (Goh and Barabási, 2008; Schleiss and Smith, 2016) confirmed that the firing patterns of the sensory neurons derived from iPSCs from the EM patient fire in a more bursty fashion compared to the control (Fig. 3 in Publication #2). As mentioned above, EM patients suffer from recurrent pain attacks that are triggered by mild increases of temperature. To test the physiology of the model, a heat experiment was conducted by TC Alich in the framework of this thesis. Ambient temperature was slightly increased. The sensory neurons derived from the EM patient showed a significant increase in firing frequencies, reflecting their hypersensitivity to heat. The control cell, in contrast, did not discharge in a faster fashion upon increased ambient temperature (Fig. 4 in Publication #2).

To explore whether dqGEVI is applicable to a broader field of *in vitro* models, dqGEVI was tested in hiPSC-derived cortical neurons. TC Alich, in the scope of this thesis, conducted optical measurements of human iPSC-derived forebrain neurons transduced with dqGEVI. These induced forebrain GABAergic and glutamatergic cocultures were provided by S Tariq, M Peitz, and O Brüstle, from the University of Bonn, Institute of Reconstructive Neurobiology. The optical traces revealed that the cells

exhibited synchronous bursting activity (Fig. 5 in Publication #2). Synchronicity is important for communication between neurons in neuronal networks. Disturbances in synchronous firing behavior of neurons are known to play a role in a number of neurological and neuropsychiatric diseases such as schizophrenia, epilepsy, autism spectrum disorder, Alzheimer's and Parkinson's disease (Uhlhaas and Singer, 2006). Thus, the finding that the dqGEVI sensor can detect synchronous firing patterns in forebrain neurons suggests that it may indeed be widely applicable for studying different neuronal systems as well as disease models *in vitro*.

In addition carrying out the optical measurements, TC Alich analysed the electrophysiological data, generated the corresponding figures and prepared the manuscript under the guidance of I Mody.

The published version of this work is reproduced in Appendix B.

4 Summary

Understanding how neurons communicate with each other and how they generate patterns of activity is a fundamental goal of neurosciences research. Traditionally, electrode-based techniques, including patch clamp recording, have been used to monitor the activity of individual neurons and neuronal networks. They provide high temporal resolution enabling the precise timing of neuronal activity to be tracked.

Despite their advantages, electrode-based methods have major limitations. They can only record the activity of a limited number of neurons at the same time, making it difficult to study large-scale neuronal networks. Moreover, the patch clamp recordings that involve the rupture of the membrane and the exchange of the intracellular fluid are considered invasive.

Optical methods provide a viable alternative mainly because of their high spatial precision allowing simultaneous recording from large numbers of cells in a less invasive way. The optical method that is most commonly used involves Ca^{2+} imaging, but it has major drawbacks, as outlined above.

Direct visualizing of voltage changes at the plasma membrane using optical voltage indicators may be an ideal approach, but it presents special challenges: the space for fluorophore placement is minimal as it is restricted to the thinness of the plasma membrane. Since the plasma membrane is a delicate compartment, preserving its integrity is crucial.

Genetically encoded voltage indicators (GEVIs) have emerged as a promising approach for visualizing neuronal activity *in vivo* across various species. Many voltage indicators have been developed based on the insertion of voltage-sensitive domains (Cornejo et al., 2022; St-Pierre et al., 2014b; Villette et al., 2019) and rhodopsins (Hochbaum et al., 2014; Kannan et al., 2018; Piatkevich et al., 2018) into the plasma membrane, thereby directly translating voltage changes into optical signals. While attempts with GEVIs have been successful, their non-invasiveness remains uncertain.

By contrast, in the hybrid voltage indicator (hVOS) approach (Chanda et al., 2005), the fluorophore is attached to the plasma membrane using a fatty anchor, thus minimally interfering with the integrity of the membrane. hVOS is based on a Förster resonance electron transfer (FRET) reaction between the fluorophore and a small synthetic quencher molecule. This highly lipophilic additive moves from one leaflet of the plasma membrane to the other in a voltage-dependent fashion, thereby quenching and unquenching the fluorescence.

While hVOS generates fast voltage responses, the quencher dipicrylamine (DPA) used in the original work (Chanda et al., 2005) is toxic and explosive and has a significant impact on the capacitance of the plasma membrane. Furthermore, it accumulates on the outer surface of the plasma membrane at voltages below approximately -50 mV and is therefore not suited to resolve small hyperpolarizations.

Due to these factors the objective of this thesis was to identify an alternative quencher for this approach. After extensive experimentation with numerous substances, the diazobenzene quencher Disperse Orange 3 (D3) was ultimately selected. D3 was found to be a highly effective quencher in a FRET pair with eGFP. In addition, it is characterized as a dark quencher (dq) because it does not exhibit

autofluorescence. Therefore the novel sensor is referred to as dqGEVI. Using dqGEVI, the activity of primary mouse neurons was visualized with unprecedented accuracy (Alich et al., 2021).

The dqGEVI sensor exhibits exceptional speed (as described in Publication #1, Appendix A). With this high temporal resolution dqGEVI is ideally suited to resolve fast trains of action potentials with exceptional sensitivity. In a direct comparison to a commonly used non-hybrid voltage indicator, Accelerated Sensor of Action Potential (ASAP) 2s, a considerably faster voltage response was detected during action potentials. In addition, the validation of the novel voltage indicator shows that the sensor responds to changes in voltage in both directions - hyperpolarizing and depolarizing - with a linear response, which is important for demonstrating the whole spectrum of neuronal activity equally well.
Photostability is a major concern in voltage imaging. The fact that the space for sensor molecule placement is minimal creates a high illumination demand. Extensive testing of photostability was conducted in this study and the data were directly compared to two of the most commonly used voltage indicators, Voltron and the positive GEVI Positron (Abdelfattah et al., 2020, 2019). Even after 15 minutes of continuous illumination, bleaching of dqGEVI was negligible in contrast to the other non-hybrid sensors. This feature offers the opportunity for long-term recordings of neuronal activity.
Furthermore, this work demonstrated that the sensor is suitable for imaging voltage changes at subcellular compartments as dqGEVI has successfully visualized the activity at proximal and more distal parts of the dendrite.

Properties demonstrated in the murine *in vitro* cell system as described in Publication #1, (Appendix A) could aid in clarifying the activity of other *in vitro* systems. One promising option for modeling human neuropsychiatric and neurological diseases is human induced pluripotent stem cell (iPSC)-derived neurons. These neurons can be generated from patients with specific genetic mutations or disease phenotypes, allowing for the study of disease mechanisms and potential therapeutic targets (Okano and Yamanaka, 2014). The primary method for characterizing the activity of iPSC-derived neurons is through electrode-based electrophysiological methods. However, the low throughput that is obtained with patch clamp recordings does not compensate for the high number of cells that are required for their characterization due to the heterogeneity of these cells. Multielectrode arrays (MEA) provide large throughput capabilities, but they have limitations in terms of spatial precision and neuronal subtype discrimination. The non-invasive tool provided by the optical method described in this thesis was able to fill this gap.

Action potential firing patterns, characterized by either single spikes or complex bursting behavior, are typically the most accurate means of describing the cells' activity. The temporal characteristics of spike trains are particularly important in communication between pre- and postsynaptic neurons. Bursting activity has been found to enhance information transfer within neuronal networks by increasing the probability of inducing postsynaptic neurons to fire action potentials (Lisman, 1997). As a result,

understanding the mechanisms that govern these firing patterns is fundamental to comprehending the functioning of neural networks and their communication. Consequently, the study of burst patterns has emerged as an essential technique in both clinical and fundamental research.
In the work comprising this thesis, dqGEVI was applied in a model of the chronic pain disease inherited erythromelalgia (EM). Sensory neurons derived from a patient suffering from EM and a control were provided by the laboratory of O Brüstle. Previous findings using the invasive patch clamp technique (Cao et al., 2016) had indicated that EM sensory neurons exhibited considerably higher levels of neuronal excitability and firing frequencies in comparison to controls.
This finding could be well reproduced using dqGEVI.

Furthermore, the physiology of the model was confirmed in experiments in which the ambient temperature was slightly raised. As a result, iPSC-derived sensory neurons obtained from an EM patient demonstrated a marked elevation in firing frequencies, while cells obtained from the non-EM cells did not display any heat-induced increase in firing frequencies. These results replicate the heat-induced pain attacks commonly observed in EM patients.

Significantly, the precision of the dqGEVI sensor revealed a hitherto undiscovered difference in firing patterns, as the EM patient group displayed a remarkable difference in several measures of burst classification. A considerably greater proportion of cells displayed bursting activity in comparison to those that fired sporadically. This observation was confirmed using a continuous measure of burstiness, which was calculated according to well-established metrics of burstiness (Chen et al., 2018; Goh and Barabási, 2008; Schleiss and Smith, 2016). The sensory neurons derived from an EM patient showed significantly higher burstiness compared to sensory neurons derived from a healthy donor. This finding may be of important pathophysiological relevance. The potentiation of synaptic transmission and postsynaptic action potential firing plays an important role in the context of pain transmission as burst firing in sensory neurons can increase the probability of transmitting pain information to the postsynaptic pain projection neuron. Thus since in this exemplary EM model the dqGEVI proved to be an invaluable tool for visualizing the firing patterns of neurons undisturbed by disruptive methods it may help to elucidate potential pathomechanisms for EM patient cells.

The wide applicability of dqGEVI was also demonstrated in optical voltage recordings in mixed cultures of human iPSC-derived glutamatergic and GABAergic forebrain neurons, which were also provided by the laboratory of O Brüstle. The results of the optical measurements demonstrated that the cells discharged in a bursty fashion with a high degree of synchrony. As discussed in Chapter 3, the results regarding synchronous firing suggest that dqGEVI may be applicable for studying a variety of neurological and neuropsychiatric disease models *in vitro.*

Alongside the applications of dqGEVI examined in the framework of this thesis, some potential new fields for the implementation of this novel sensor may be suggested.

In addition to neurological and neuropsychiatric disorders associated with changes in action potential firing patterns, it may be worthwhile to use dqGEVI for the study of disorders associated with hyperpolarizations such as neuropsychiatric disorders associated with mutations in potassium channels (Imbrici et al., 2013). As shown in Chapter 2 the dqGEVI is able to precisely monitor small deviations from resting membrane potential in the hyperpolarizing and depolarizing direction. This makes it a sensitive detector of such neuronal signals.

While *in vitro* models using human iPSC-derived neurons are very useful since they offer a controlled environment for studying specific cellular mechanisms, *in vivo* experiments on mice provide a more comprehensive and accurate representation of biological processes within a living organism. The advantages of dqGEVI should thus also be considered for *in vivo* recordings in mice. However, this is considerably easier in non-hybrid GEVI approaches (Abdelfattah et al., 2019; Chamberland et al., 2017; Cornejo et al., 2022; Villette et al., 2019), as the application of the quencher to the living brain during the recordings represents a major challenge. Nonetheless, since precise visualization of subthreshold and fast spiking activities is of invaluable importance for studying the function of the brain, efforts to develop an *in vivo* setting for the dqGEVI approach should be made.

To conclude, this thesis presents the development, validation and characterization of dqGEVI. This sensor has unique properties such as its exceptionally high temporal resolution, its excellent photostability and non-invasiveness, which distinguishes it from other GEVIs.
The application to several *in vitro* models proves its broad applicability in this area. In addition to that, the extension to *in vivo* systems would offer unique insights into the entire spectrum of neuronal networks.

5 References

Abdelfattah, A.S., Kawashima, T., Singh, A., Novak, O., Liu, H., Shuai, Y., Huang, Y.C., Campagnola, L., Seeman, S.C., Yu, J., Zheng, J., Grimm, J.B., Patel, R., Friedrich, J., Mensh, B.D., Paninski, L., Macklin, J.J., Murphy, G.J., Podgorski, K., Lin, B.J., Chen, T.W., Turner, G.C., Liu, Z., Koyama, M., Svoboda, K., Ahrens, M.B., Lavis, L.D., Schreiter, E.R., 2019. Bright and photostable chemigenetic indicators for extended in vivo voltage imaging. Science. 365, 699–704. https://doi.org/10.1126/science.aav6416

Abdelfattah, A.S., Samouil, X., Farhi, L., Zhao, Y., Brinks, D., Zou, X.P., Ruangkittisakul, A., Platisa, J., Pieribone, V.A., Ballanyi, K., Cohen, A.E., Campbell, R.E., 2016. Cellular/Molecular A Bright and Fast Red Fluorescent Protein Voltage Indicator That Reports Neuronal Activity in Organotypic Brain Slices. https://doi.org/10.1523/JNEUROSCI.3484-15.2016

Abdelfattah, A.S., Valenti, R., Zheng, J., Wong, A., Chuong, A.S., Hasseman, J.P., Jayaraman, V., Kolb, I., Korff, W., Lavis, L.D., Liang, Y., Looger, L.L., Merryweather, D., Reep, D., Spruston, N., Svoboda, K., Tsang, A., Tsegaye, G., Turner, G., Podgorski, K., Koyama, M., Kim, D.S., Schreiter, E.R., 2020. A general approach to engineer positive-going eFRET voltage indicators. Nat. Commun. 11. https://doi.org/10.1038/s41467-020-17322-1

Acker, C.D., Hoyos, E., Loew, L.M., 2016. EPSPs measured in proximal dendritic spines of cortical pyramidal neurons. eNeuro 3, 1524–1541. https://doi.org/10.1523/ENEURO.0050-15.2016

Alich, T.C., Pabst, M., Pothmann, L., Szalontai, B., Faas, G.C., Mody, I., 2021. A dark quencher genetically encodable voltage indicator (dqGEVI) exhibits high fidelity and speed. Proc. Natl. Acad. Sci. U. S. A. 118, 1–12. https://doi.org/10.1073/pnas.2020235118

Bayguinov, P.O., Ma, Y., Gao, X.Y., Zhao, X.X., Jackson, X.M.B., 2017. Imaging Voltage in Genetically Defined Neuronal Subpopulations with a Cre Recombinase-Targeted Hybrid Voltage Sensor. J. Neurosci. 37, 9305–9319. https://doi.org/10.1523/JNEUROSCI.1363-17.2017

Bedut, S., Seminatore-nole, C., Lamamy, V., Caignard, S., Boutin, J.A., Nosjean, O., Stephan, J., Coge, F., 2021. High-throughput drug profiling with voltage- and calcium-sensitive fluorescent probes in human iPSC-derived cardiomyocytes 44–53. https://doi.org/10.1152/ajpheart.00793.2015

Beja, O., Aravind, L., Koonin, E. V., Suzuki, M.T., Hadd, A., Nguyen, L.P., Jovanovich, S.B., Gates, C.M., Feldman, R.A., Spudich, J.L., Spudich, E.N., DeLong, E.F., 2000. Bacterial Rhodopsin : Evidence for a New Type of Phototrophy in the Sea. Science. 289, 1902–1907.

Benz, R., Conti, F., 1981. Structure of the squid axon membrane as derived from charge-pulse relaxation studies in the presence of absorbed lipophilic ions. J Membr Biol. 59, 91–104.

Benz, R., Läuger, P., Janko, K., 1976. Transport kinetics of hydrophobic ions in lipid bilayer membranes Charge-pulse relaxation studies. BBA - Biomembr. 455, 701–720. https://doi.org/10.1016/0005-2736(76)90042-0

Bradley, J., Luo, R., Otis, T.S., Digregorio, D.A., 2009. Submillisecond Optical Reporting of Membrane Potential In Situ Using a Neuronal Tracer Dye. https://doi.org/10.1523/JNEUROSCI.1240-09.2009

Cain, S.M., Tyson, J.R., Choi, H.B., Ko, R., Lin, P.J.C., LeDue, J.M., Powell, K.L., Bernier, L.P., Rungta, R.L., Yang, Y., Cullis, P.R., O'Brien, T.J., MacVicar, B.A., Snutch, T.P., 2018. CaV3.2 drives sustained burst-firing, which is critical for absence seizure propagation in reticular thalamic neurons. Epilepsia 59, 778–791. https://doi.org/10.1111/epi.14018

Cao, L., McDonnell, A., Nitzsche, A., Alexandrou, A., Saintot, P.P., Loucif, A.J.C., Brown, A.R., Young, G., Mis, M., Randall, A., Waxman, S.G., Stanley, P., Kirby, S., Tarabar, S., Gutteridge, A., Butt, R., McKernan, R.M., Whiting, P., Ali, Z., Bilsland, J., Stevens, E.B., 2016. Pharmacological reversal of a pain phenotype in iPSC-derived sensory neurons and patients with inherited erythromelalgia. Sci Transl Med. 8, 225–245. https://doi.org/10.1126/scitranslmed.aad7653

Capera, J., Serrano-Novillo, C., Navarro-Pérez, M., Cassinelli, S., Felipe, A., 2019. The potassium channel odyssey: Mechanisms of traffic and membrane arrangement. Int. J. Mol. Sci. 20. https://doi.org/10.3390/ijms20030734

Chamberland, S., Yang, H.H., Pan, M.M., Evans, S.W., Guan, S., Chavarha, M., Yang, Y., Salesse, C., Wu, H., Wu, J.C., Clandinin, T.R., Toth, K., Lin, M.Z., States, U., States, U., 2017. Fast two-photon imaging of subcellular voltage dynamics in neuronal tissue with genetically encoded indicators 1–35. https://doi.org/10.7554/eLife.25690

Chanda, B., Blunck, R., Faria, L.C., Schweizer, F.E., Mody, I., Bezanilla, F., 2005. A hybrid approach to measuring electrical activity in genetically specified neurons. Nat. Neurosci. 8, 1619–1626. https://doi.org/10.1038/nn1558

Chen, L., Saito, T., Saido, T.C., Mody, I., 2018. Novel quantitative analyses of spontaneous synaptic events in cortical pyramidal cells reveal subtle parvalbumin-expressing interneuron dysfunction in a knock-in mouse model of alzheimer's disease. eNeuro 5, 1–15. https://doi.org/10.1523/ENEURO.0059-18.2018

Chisari, M., Wu, K., Zorumski, C.F., Mennerick, S., 2011. Hydrophobic anions potently and uncompetitively antagonize GABA A receptor function in the absence of a conventional binding site. Br. J. Pharmacol. 164, 667–680. https://doi.org/10.1111/j.1476-5381.2011.01396.x

Cohen, L., 1989. special topic: optical approaches to neuron function. Annu. Rev.Physiol. 51, 487–490.

Cohen, L.B., Keynes, R.D., Hille, B., 1968. Light scattering and birefringence changes during nerve activity. Nature 218, 438–441. https://doi.org/10.1038/218438a0

Cohen, L.B., Salzberg, B.M., Davila, H. V, Ross, W.N., Landowne, D., Waggoner, A.S., Wang, C.H., 1974. Changes in Axon Fluorescence during Activity" Molecular Probes of Membrane Potential, J. Membrane Biol.

Cohen, L.B., Salzberg, B.M., Grinvald, A., 1978. Optical methods for monitoring neuron activity. Annu.

Rev. Neurosci. 1, 171–182. https://doi.org/10.1146/annurev.ne.01.030178.001131

Cole KS, K.H., 1938. Electric impedance of single marine eggs. J. Gen. Physiol. 591–599.

Cornejo, V.H., Ofer, N., Yuste, R., 2022. Voltage compartmentalization in dendritic spines in vivo. Science. 375, 82–86. https://doi.org/10.1126/science.abg0501

Dimitrov, D., He, Y., Mutoh, H., Baker, B.J., Cohen, L., Akermann, W., Knöpfel, T., 2007. Engineering and characterization of an enhanced fluorescent protein voltage sensor. PLoS One 2, 2–6. https://doi.org/10.1371/journal.pone.0000440

Dissanayake, K.N., Redman, R.R., Mackenzie, H., Eddleston, M., Ribchester, R.R., 2022. " Calcium bombs " as harbingers of synaptic pathology and their mitigation by magnesium at murine neuromuscular junctions. Front. Mol. Neurosci. 15, 1–18. https://doi.org/10.3389/fnmol.2022.937974

Fremont, R., Paola Calderon, D., Maleki, S., Khodakhah, K., 2014. Abnormal high-frequency burst firing of cerebellar neurons in rapid-onset dystonia-parkinsonism. J. Neurosci. 34, 11723–11732. https://doi.org/10.1523/JNEUROSCI.1409-14.2014

Ghitani, N., Bayguinov, P.O., Ma, Y., Jackson, M.B., 2015. Single-trial imaging of spikes and synaptic potentials in single neurons in brain slices with genetically encoded hybrid voltage sensor. J Neurophysiol 113, 1249–1259. https://doi.org/10.1152/jn.00691.2014.-Genetically

Goh, K., Barabási, A., 2008. Burstiness and memory in complex systems. Epl 81, 1–5. https://doi.org/10.1209/0295-5075/81/48002

Gong, Y., Huang, C., Li, J.Z., Grewe, B.F., Zhang, Y., Eismann, S., Schnitzer, M.J., 2015. High-speed recording of neural spikes in awake mice and flies with a fluorescent voltage sensor. Science. 350, 1361–1366. https://doi.org/10.1126/science.aab0810

Gong, Y., Li, J.Z., Schnitzer, M.J., 2013. Enhanced Archaerhodopsin Fluorescent Protein Voltage Indicators 8, 1–10. https://doi.org/10.1371/journal.pone.0066959

González, J.E., Tsien, R.Y., 1997. Improved indicators of cell membrane potential that use fluorescence resonance energy transfer. Chem. Biol. 4, 269–277. https://doi.org/10.1016/S1074-5521(97)90070-3

González, J.E., Tsien, R.Y., 1995. Voltage sensing by fluorescence resonance energy transfer in single cells. Biophys. J. 69, 1272–1280. https://doi.org/10.1016/S0006-3495(95)80029-9

Grinvald, A., Ross, W.N., Farber, I., 1981. Simultaneous optical measurements of electrical activity from multiple sites on processes of cultured .neurons (tissue culture/neurons/membrane potential/fluorescence/growth cone). Neurobiology 78, 3245–3249.

Gross, G.G., Junge, J.A., Mora, R.J., Kwon, H.-B., Olson, C.A., Takahashi, T.T., Liman, E.R., Ellis-Davies, G.C.R., McGee, A.W., Sabatini, B.L., Roberts, R.W., Arnold, D.B., 2013. Recombinant probes for visualizing endogenous synaptic proteins in living neurons. Neuron 78, 971–985. https://doi.org/10.1016/j.neuron.2013.04.017.Recombinant

Hill, D., Keynes, R., 1949. Opacity changes in stimulated nerve. J. Physiol. 278–281.

Hochbaum, D.R., Zhao, Y., Farhi, S.L., Klapoetke, N., Werley, C.A., Kapoor, V., Zou, P., Kralj, J.M., MacLaurin, D., Smedemark-Margulies, N., Saulnier, J.L., Boulting, G.L., Straub, C., Cho, Y.K., Melkonian, M., Wong, G.K.S., Harrison, D.J., Murthy, V.N., Sabatini, B.L., Boyden, E.S., Campbell, R.E., Cohen, A.E., 2014. All-optical electrophysiology in mammalian neurons using engineered microbial rhodopsins. Nat. Methods 11, 825–833. https://doi.org/10.1038/NMETH.3000

Hodgkin, H., 1939. Nature (6) (7). Nature 144, 710–711.

Ihara, K., Umemura, T., Katagiri, I., Kitajima-Ihara, T., Sugiyama, Y., Kimura, Y., Mukohata, Y., 1999. Evolution of the archaeal rhodopsins: evolution rate changes by gene duplication and functional differentiation. J. Mol. Biol. 285, 163–174. https://doi.org/10.1006/JMBI.1998.2286

Imbrici, P., Camerino, D.C., Tricarico, D., 2013. Major channels involved in neuropsychiatric disorders and therapeutic perspectives. Front. Genet. 4, 1–19. https://doi.org/10.3389/fgene.2013.00076

Jensen, M.Ø., Jogini, V., Borhani, D.W., Leffler, A.E., Dror, R.O., Shaw, D.E., 2012. Mechanism of Voltage Gating in Potassium Channels 229–234.

Jiang, W., Hunter, T., 1998. Analysis of cell-cycle profiles in transfected cells using a membrane-targeted GFP. Biotechniques 24, 349–50, 352, 354.

Jin, L., Han, Z., Platisa, J., Wooltorton, J.R.A., Cohen, L.B., Pieribone, V.A., 2012. Single action potentials and subthreshold electrical events imaged in neurons with a novel fluorescent protein voltage probe. Neuron 75, 779–785. https://doi.org/10.1016/j.neuron.2012.06.040.Single

Kannan, M., Vasan, G., Huang, C., Haziza, S., Li, J.Z., Inan, H., Schnitzer, M.J., Pieribone, V.A., 2018. Fast, in vivo voltage imaging using a red fluorescent indicator. Nat. Methods 15, 1108–1116. https://doi.org/10.1038/s41592-018-0188-7

Kralj, J.M., Douglass, A.D., Hochbaum, D.R., Maclaurin, D., Cohen, A.E., 2012. Optical recording of action potentials in mammalian neurons using a microbial rhodopsin. Nat Methods 9, 90–95. https://doi.org/10.1038/nmeth.1782.Optical

Kralj, J.M., Hochbaum, D.R., Douglass, A.D., Cohen, A.E., 2011. Electrical Spiking in Escherichia coli Probed with a Fluorescent Voltage-Indicating Protein. Science. 333, 345–349.

Limon, A., Estrada-Mondragón, A., Reyes Ruiz, J.M., Miledi, R., 2016. Dipicrylamine Modulates GABAr1 Receptors through Interactions with Residues in the TM4 and Cys-Loop Domains. Mol. Pharmacol. 89, 446–456. https://doi.org/10.1124/mol.116.103432

Linsenbardt, A.J., Chisari, M., Yu, A., Shu, H.J., Zorumski, C.F., Mennerick, S., 2013. Noncompetitive, voltage-dependent NMDA receptor antagonism by hydrophobic anions. Mol. Pharmacol. 83, 354–366. https://doi.org/10.1124/mol.112.081794

Lisman, J.E., 1997. Bursts as a unit of neural information: Making unreliable synapses reliable. Trends Neurosci. 20, 38–43. https://doi.org/10.1016/S0166-2236(96)10070-9

Liu, Z., Lu, X., Villette, V., Gou, Y., Colbert, K.L., Lai, S., Guan, S., Land, M.A., Lee, J., Assefa, T., Zollinger, D.R., Korympidou, M.M., Vlasits, A.L., Pang, M.M., Su, S., Cai, C., Froudarakis, E.,

Zhou, N., Patel, S.S., Smith, C.L., Ayon, A., Bizouard, P., Bradley, J., Franke, K., Clandinin, T.R., Giovannucci, A., Tolias, A.S., Reimer, J., Dieudonné, S., St-Pierre, F., 2022. Sustained deep-tissue voltage recording using a fast indicator evolved for two-photon microscopy. Cell 185, 3408-3425.e29. https://doi.org/10.1016/j.cell.2022.07.013

Lobb CJ, 2014. Abnormal Bursting as a Pathophysiological Mechanism in Parkinson's Disease. Basal Ganglia 3, 187–195. https://doi.org/10.1016/j.baga.2013.11.002.Abnormal

Loew, L.M., Cohen, L.B., Salzberg, B.M., Obaid, A.L., Bezanilla, F., 1985. Charge-shift probes of membrane potential. Characterization of aminostyrylpyridinium dyes on the squid giant axon. Biophys. J. 47, 71–77. https://doi.org/10.1016/S0006-3495(85)83878-9

Looger, L.L., Griesbeck, O., 2012. Genetically encoded neural activity indicators. Curr. Opin. Neurobiol. 22, 18–23. https://doi.org/10.1016/j.conb.2011.10.024

Ma, Y., Bayguinov, P.O., Jackson, M.B., 2019. Optical studies of action potential dynamics with hVOS probes. Curr. Opin. Biomed. Eng. 12, 51–58. https://doi.org/10.1016/j.cobme.2019.09.007

Maclaurin, D., Venkatachalam, V., Lee, H., Cohen, A.E., 2012. Mechanism of voltage-sensitive fluorescence in a microbial rhodopsin. PNAS 110, 5939–5944. https://doi.org/10.1073/pnas.1215595110

Mcdonnell, A., Schulman, B., Ali, Z., Dib-hajj, S.D., Brock, F., Cobain, S., Mainka, T., Vollert, J., Tarabar, S., Waxman, S.G., 2016. Inherited erythromelalgia due to mutations in SCN9A : natural history , clinical phenotype and somatosensory profile 1052–1065. https://doi.org/10.1093/brain/aww007

McMahon, S., Jackson, M., 2018. An Inconvenient Truth: Calcium Sensors Are Calcium Buffers. Trends Neurosci. 41, 880–884. https://doi.org/10.1016/j.tins.2018.09.005.An

Miyawaki, A., Llopis, J., Heim, R., Michael McCaffery, J., Adams, J.A., Ikura, M., Tsien, R.Y., 1997. Fluorescent indicators for Ca2+ based on green fluorescent proteins and calmodulin. Nature 388, 882–887. https://doi.org/10.1038/42264

Murata, Y., Iwasaki, H., Sasaki, M., Inaba, K., Okamura, Y., 2005. Phosphoinositide phosphatase activity coupled to an intrinsic voltage sensor. Nature 435, 1239–1243. https://doi.org/10.1038/nature03650

Neher, E., Sakmann, B., 1976. Single-channel currents recorded from membrane. Nature 260, 799–802. https://doi.org/10.1038/260799a0

Nemet, B.A., Nikolenko, V., Yuste, R., 2004. Second harmonic imaging of membrane potential of neurons with retinal. https://doi.org/10.1117/1.1783353

Obergrussberger, A., Rinke-Weiß, I., Goetze, T.A., Rapedius, M., Brinkwirth, N., Becker, N., Rotordam, M.G., Hutchison, L., Madau, P., Pau, D., Dalrymple, D., Braun, N., Friis, S., Pless, S.A., Fertig, N., 2022. The suitability of high throughput automated patch clamp for physiological applications. J Physiol 600, 277–297. https://doi.org/10.1113/JP282107#support-information-section

Oh, J., Lee, C., Kaang, B.K., 2019. Imaging and analysis of genetically encoded calcium indicators linking neural circuits and behaviors. Korean J. Physiol. Pharmacol. 23, 237–249. https://doi.org/10.4196/kjpp.2019.23.4.237

Okano, H., Yamanaka, S., 2014. iPS cell technologies: significance and applications to CNS regeneration and disease. Mol Brain 7, 1–12. https://doi.org/10.1186/1756-6606-7-22

Persechini, A., Lynch, J.A., Romoser, V.A., 1997. Novel fluorescent indicator proteins for monitoring free intracellular Ca2+. Cell Calcium 22, 209–216. https://doi.org/10.1016/S0143-4160(97)90014-2

Piatkevich, K.D., Bensussen, S., Tseng, H. an, Shroff, S.N., Lopez-Huerta, V.G., Park, D., Jung, E.E., Shemesh, O.A., Straub, C., Gritton, H.J., Romano, M.F., Costa, E., Sabatini, B.L., Fu, Z., Boyden, E.S., Han, X., 2019. Population imaging of neural activity in awake behaving mice. Nature 574, 413–417. https://doi.org/10.1038/s41586-019-1641-1

Piatkevich, K.D., Jung, E.E., Straub, C., Linghu, C., Park, D., Suk, H.J., Hochbaum, D.R., Goodwin, D., Pnevmatikakis, E., Pak, N., Kawashima, T., Yang, C.T., Rhoades, J.L., Shemesh, O., Asano, S., Yoon, Y.G., Freifeld, L., Saulnier, J.L., Riegler, C., Engert, F., Hughes, T., Drobizhev, M., Szabo, B., Ahrens, M.B., Flavell, S.W., Sabatini, B.L., Boyden, E.S., 2018. A robotic multidimensional directed evolution approach applied to fluorescent voltage reporters article. Nat. Chem. Biol. 14, 352–360. https://doi.org/10.1038/s41589-018-0004-9

Popovic, M.A., Carnevale, N., Rozsa, B., Zecevic, D., 2015. Electrical behaviour of dendritic spines as revealed by voltage imaging. Nat. Commun. 6, 1–12. https://doi.org/10.1038/ncomms9436

Sakai, R., Repunte-Canonigo, V., Raj, C.D., Knöpfel, T., 2001. Design and characterization of a DNA-encoded, voltage-sensitive fluorescent protein. Eur. J. Neurosci. 13, 2314–2318.

Salzberg, B.M., Grinvald, A., Cohen, L.B., Davila, H. V., Ross, W.N., 1977. Optical recording of neuronal activity in an invertebrate central nervous system: simultaneous monitoring of several neurons. J. Neurophysiol. 40, 1281–1291. https://doi.org/10.1152/jn.1977.40.6.1281

Sanabria, E.R.G., Su, H., Yaari, Y., 2001. Initiation of network bursts by Ca2+-dependent intrinsic bursting in the rat pilocarpine model of temporal lobe epilepsy. J. Physiol. 532, 205–216.

Schleiss, M., Smith, J.A., 2016. Two simple metrics for quantifying rainfall intermittency: The burstiness and memory of interamount times. J. Hydrometeorol. 17, 421–436. https://doi.org/10.1175/JHM-D-15-0078.1

Shimomura, O., Johnson, F.H., Saiga, Y., 1962. Extraction, purification and properties of aequorin, a bioluminescent. J. Cell. Comp. Physiol. 59, 223–239. https://doi.org/10.1002/jcp.1030590302

Shtrankfeld, I.G., Frank, G.M., 1964. on luminescence of giant nerve fibres during excitation. Biofizika 321–326.

Siegel, M.S., Isacoff, E.Y., 1997. A genetically encoded optical probe of membrane voltage. Neuron 19, 735–741. https://doi.org/10.1016/S0896-6273(00)80955-1

St-Pierre, F., Marshall, J.D., Yang, Y., Gong, Y., Mark, J., 2014a. High-fidelity optical reporting of

neuronal electrical activity with an ultrafast fluorescent voltage sensor 17, 884–889.

St-Pierre, F., Marshall, J.D., Yang, Y., Gong, Y., Schnitzer, M.J., Lin, M.Z., 2014b. High-fidelity optical reporting of neuronal electrical activity with an ultrafast fluorescent voltage sensor. Nat. Publ. Gr. https://doi.org/10.1038/nn.3709

Steinmetz, N.A., Aydin, C., Lebedeva, A., Okun, M., Pachitariu, M., Bauza4, M., Beau, M., Bhagat, J., Böhm, C., Broux, M., Chen, S., Colonell, J., Gardner, R.J., Bill Karsh7, F., 2016. Neuropixels 2.0: A miniaturized high-density probe for stable, long-term brain recordings †Corresponding. Physiol. Behav. 176, 139–148. https://doi.org/10.1126/science.abf4588.Neuropixels

Tasaki, I., Carnay, L., Watanabe, A., 1969. Fluorescence Changes during Conduction in Nerves Stained with Acridine Orange. Science. 163, 683–685.

Tasaki, I., Watanabe, A., Sandlin, R., Carnay, L., 1968. Changes in fluorescence, turbidity, and birefringence associated with nerve excitation. Proc. Natl. Acad. Sci. U. S. A. 61, 883–888. https://doi.org/10.1073/pnas.61.3.883

Tham, S.W., Giles, M., 2018. Current pain management strategies for patients with erythromelalgia : a critical review 1689–1698.

Thomas, C., Springer, P., Loeb, G., Berwald-Netter, Y., Okun, L., 1972. A miniature microelectrode array to monitor the bioelectric activity of cultured cells. Exp. Cell Res. 74, 61–66. https://doi.org/10.1016/0014-4827(72)90481-8

Tsien, R.Y., Pozzan, T., Rink, T.J., 1982. Calcium homeostasis in intact lymphocytes: Cytoplasmic free calcium monitored with a intracellularly trapped fluorescent indicator. J. Cell Biol. 94, 325–334. https://doi.org/10.1083/jcb.94.2.325

Tsunoda, S.P., Ewers, D., Gazzarrini, S., Moroni, A., Gradmann, D., Hegemann, P., 2006. H+-pumping rhodopsin from the marine alga Acetabularia. Biophys. J. 91, 1471–1479. https://doi.org/10.1529/biophysj.106.086421

Tsutsui, H., Karasawa, S., Okamura, Y., Miyawaki, A., 2008. Improving membrane voltage measurements using FRET with new fluorescent proteins 5, 683–685. https://doi.org/10.1038/NMETH.1235

Uhlhaas, P.J., Singer, W., 2006. Neural Synchrony in Brain Disorders: Relevance for Cognitive Dysfunctions and Pathophysiology. Neuron 52, 155–168. https://doi.org/10.1016/j.neuron.2006.09.020

Villette, V., Chavarha, M., Dimov, I.K., Bradley, J., Pradhan, L., Mathieu, B., Evans, S.W., Chamberland, S., Shi, D., Yang, R., Kim, B.B., Ayon, A., Jalil, A., St-Pierre, F., Schnitzer, M.J., Bi, G., Toth, K., Ding, J., Dieudonné, S., Lin, M.Z., 2019. Ultrafast Two-Photon Imaging of a High-Gain Voltage Indicator in Awake Behaving Mice. Cell 179, 1590-1608.e23. https://doi.org/10.1016/j.cell.2019.11.004

Wang, L., Lei, Q., Zhao, S., Xu, W.J., Dong, W., Ran, J.H., Shi, Q.H., Fu, J.F., 2021. Ginkgolide B Maintains Calcium Homeostasis in Hypoxic Hippocampal Neurons by Inhibiting Calcium Influx

and Intracellular Calcium Release. Front. Cell. Neurosci. 14, 1–10. https://doi.org/10.3389/fncel.2020.627846

Wu, J., Liang, Y., Chen, S., Hsu, C.L., Chavarha, M., Evans, S.W., Shi, D., Lin, M.Z., Tsia, K.K., Ji, N., 2020. Kilohertz two-photon fluorescence microscopy imaging of neural activity in vivo. Nat. Methods 17, 287–290. https://doi.org/10.1038/s41592-020-0762-7

Wu, J.Y., Cohen, L.B., Falk, C.X., 1994. Neuronal activity during different behaviors in aplysia: A distributed organization? Science. 263, 820–823. https://doi.org/10.1126/science.8303300

Yang, Y., Wang, Y., Li, S., Xu, Z., Li, H., Ma, L., Fan, J., Bu, D., Liu, B., Fan, Z., Wu, G., Jin, J., Ding, B., Zhu, X., Shen, Y., 2004. Mutations in SCN9A , encoding a sodium channel alpha subunit, in patients with primary erythermalgia. J Med Genet 41, 171–174. https://doi.org/10.1136/jmg.2003.012153

6 Appendices

A Publication #1: A dark quencher genetically encodable voltage indicator (dqGEVI) exhibits high fidelity and speed

A dark quencher genetically encodable voltage indicator (dqGEVI) exhibits high fidelity and speed

Therese C. Alich[a], Milan Pabst[a,1,2], Leonie Pothmann[a,2], Bálint Szalontai[a,2], Guido C. Faas[b], and Istvan Mody[a,b,3]

[a]Neuronal Networks in Health and Disease Laboratory, Institute of Experimental Epileptology and Cognition Research, Life and Brain Center, University of Bonn Medical Center, 53127 Bonn, Germany; and [b]Department of Neurology, The David Geffen School of Medicine at UCLA, Los Angeles, CA 90095

Edited by György Buzsáki, New York University Langone Medical Center, New York, NY, and approved January 6, 2021 (received for review October 2, 2020)

Voltage sensing with genetically expressed optical probes is highly desirable for large-scale recordings of neuronal activity and detection of localized voltage signals in single neurons. Most genetically encodable voltage indicators (GEVI) have drawbacks including slow response, low fluorescence, or excessive bleaching. Here we present a dark quencher GEVI approach (dqGEVI) using a Förster resonance energy transfer pair between a fluorophore glycosylphosphatidylinositol–enhanced green fluorescent protein (GPI-eGFP) on the outer surface of the neuronal membrane and an azo-benzene dye quencher (D3) that rapidly moves in the membrane driven by voltage. In contrast to previous probes, the sensor has a single photon bleaching time constant of ∼40 min, has a high temporal resolution and fidelity for detecting action potential firing at 100 Hz, resolves membrane de- and hyperpolarizations of a few millivolts, and has negligible effects on passive membrane properties or synaptic events. The dqGEVI approach should be a valuable tool for optical recordings of subcellular or population membrane potential changes in nerve cells.

genetically encoded voltage indicator | GEVI | fluorescent membrane potential measurement | cultured neurons

The most widely used genetically encodable indicators of neuronal activity are Ca^{2+}-binding proteins that change fluorescence upon binding Ca^{2+} after it enters through voltage-gated Ca^{2+} channels. However, these genetically encodable Ca^{2+} indicators are not ideally suited for accurate detection of single action potentials (APs) and are unable to record membrane hyperpolarizations or depolarizations below AP threshold (1, 2). In contrast, direct optical voltage sensing using genetically expressed probes is highly promising for large-scale recordings of neuronal activity. Many of the various genetically encodable voltage indicators (GEVIs) currently in use were subject to several recent reviews and comparative studies (3–10) observing the rapid development of these valuable probes together with highly sensitive fluorescent probes for membrane voltage monitoring that are not genetically encoded (11).

One of the most promising starting approaches has been to fuse the voltage sensor of the *Acetabularia chemigenetiacetabulum* rhodopsin (Ace2N) and the fluorescent protein mNeonGreen to enable voltage-sensitive Förster resonance energy transfer (FRET) (12). This sensor has been shown to work in expression systems, neurons in culture, slices, in the intact brains of awake mice, and in dendrites of olfactory neurons in intact flies. Since then, several other approaches have been developed (13–15) that work well for determining cell-specific behavioral correlates in mice. The development of the Optopatch3 mouse line (13) was a revolutionary milestone in advancing research using GEVIs. The most recent advances in the field combine a voltage-sensitive microbial rhodopsin with a self-labeling protein domain that covalently binds the synthetic Janelia Fluor fluorophore that has to be administered separately. The degree of FRET is modulated by the voltage-sensitive absorption spectrum of the rhodopsin. This type of GEVI has been termed chemigenetic as it has a chemical and a genetic component. Voltron (16) and its latest derivative, Positron (17), have been used in various expression systems including intact mouse brains. Another chemigenetic fluorescent voltage sensing approach, also called hybrid GEVI, is based on FRET, or rather quenching (18) between two components, but the voltage sensor is not genetically encoded. A fluorescent particle is anchored to one side of the membrane and a small lipophilic anion (dark quencher) is used as the voltage sensor that is rapidly moved inside the membrane by the electric field. The approach was pioneered over 20 y ago (19) and has been refined by using the FRET reaction between a stationary fluorescent lipid and a mobile dye, which gave an astonishing >50% fluorescence change per 100 mV with a time constant of <0.4 ms (20). The principle was turned into a genuine GEVI approach by using a genetically encodable membrane-targeted fluorescent protein as the membrane-anchored fluorophore (usually myristoylated and palmtoylated at Gly and Cys residues), and dipicrylamine (DPA) as its FRET quencher pair (21). DPA was known from early charge-pulse relaxation experiments to electrophorese through lipid membranes with a submillisecond translocation rate (22) that was as fast as gating currents in the squid axon (23). When used in combination with the lipophilic fluorescent dye DiO, that had to be fastidiously loaded into individual neurons, DPA gave very fast and large optical voltage signals (24–26). As the DPA absorption and enhanced green fluorescent protein (eGFP) emission spectra do not greatly overlap (*SI Appendix*, Fig. S1*A*), improvements in the method have been attained by using the blue-shifted enhanced cyan fluorescent protein (18), by developing a

Significance

Voltage sensing with genetically expressed optical probes is highly desirable for large-scale recordings of neuronal activity and detection of localized voltage signals in single neurons. Here we describe a method for a two-component (hybrid) genetically encodable fluorescent voltage sensing in neurons. The approach uses a glycosylphosphatidylinositol-tagged fluorescent protein (enhanced green fluorescent protein) that ensures the fluorescence to be specifically confined to the outside of the plasma membrane and D3, a voltage-dependent quencher. Previous hybrid genetically encoded voltage sensing approaches relied on a single quenching molecule, dipycrilamine (DPA), which is toxic, increases membrane capacitance, interferes with neurotransmitters, and is explosive. Our method uses a nontoxic and nonexplosive compound that performs better than DPA in all aspects of fluorescent voltage sensing.

Author contributions: G.C.F. and I.M. designed research; T.C.A., M.P., L.P., B.S., and I.M. performed research; T.C.A., M.P., L.P., G.C.F., and I.M. analyzed data; and T.C.A., B.S., and I.M. wrote the paper.

The authors declare no competing interest.

This article is a PNAS Direct Submission.

[1]Deceased September 26, 2016.

[2]M.P., L.P., and B.S. contributed equally to this work.

[3]To whom correspondence may be addressed. Email: mody@ucla.edu.

This article contains supporting information online at https://www.pnas.org/lookup/suppl/doi:10.1073/pnas.2020235118/-/DCSupplemental.

Published February 2, 2021.

membrane localized fluorophore (hVOS 1.5, a cerulean fluorescent protein tagged at its C terminus with a truncated farnesylation motif) (27), and by proposing various optimizations of the approach (28).

In general, this two-component approach provides good signal-to-noise ratio (SNR) for the detection of APs and for recording subthreshold synaptic events in various preparations (21, 29–31), but in all of these studies the voltage-dependent dark quencher remained the same: DPA. While this molecule satisfies many of the original requirements (19) for voltage sensing, it also has several drawbacks. These include its accumulation on the outer surface of the membrane below approximately −50 mV, thus making it difficult to report small membrane hyperpolarizatios (29), the considerable capacitive membrane load near the required concentrations for voltage sensing (21, 28, 32) that causes time-dependent deterioration of APs (26), and its interactions with various neurotransmitter systems (33–35). In addition, as it is made up of two trinitrotoluene molecules joined together, DPA (also known as hexanitrodiphenylamine, or HND) is highly explosive; indeed, it was actively used as an explosive in World War II.

In order to replace DPA in the two-component GEVI approach we have set out to carry out a systematic search for different dark quenching molecules. After testing several dozens of compounds, we identified an organic nitroazobenzene dye (Disperse Orange 3 or 4-amino-4′-nitroazobenzene, CAS number 730-40-5, herein referred to as D3) with an absorption spectrum better suited than DPA to quench eGFP fluorescence (*SI Appendix*, Fig. S1*A*). Importantly, as a dark quencher D3 does not have any autofluorescence, and therefore, despite being a voltage indicator, it does not report a fluorescence signal by itself. Here we report on the superior properties of the dark quencher D3 in combination with eGFP for a dark quencher GEVI (dqGEVI) approach with the fluorophore anchored to the outside of the membrane by the glycosylphosphatidylinositol (GPI) motif (36) (GPI-eGFP; *SI Appendix*, Fig. S1*B*) in neuronal cultures and demonstrate its innocuous effects on passive membrane properties and synaptic events. Some GEVIs are quite adequate for 2P imaging (37–39), and our approach should also perform well in this mode, as 2P fluorescent voltage measurements have been very successful with another quencher (DPA) paired with a nongenetically encoded membrane fluorophore (25, 26). We have compared the speed of our voltage sensor to one of the GEVIs used for 2P imaging, ASAP2s (37), and find a considerable faster fluorescence response during APs.

Results

Fast, High-Fidelity Reporting of AP Firing and Membrane Hyperpolarizations. We have recorded from mouse and rat cortical and hippocampal neurons in culture that were transduced with the GPI-eGFP construct carrying recombinant adeno-associated viruses. The neurons expressed the fluorophore in their membranes including their somata, dendrites, and axons even as long as 6 wk after viral transduction (*SI Appendix*, Fig. S1*C*). In our recordings we typically used neurons after 2 to 3 wk of viral transduction. Simultaneous whole-cell patch-clamp recordings and optical recordings were done at 32 ± 1 °C starting at ∼5 min following addition of 2 to 10 μM D3. Several of our recordings persisted for >60 min, which allowed us to determine the lasting presence of D3 in the membrane following its washout that lasted at least 48 h (discussed below). Most recorded neurons were subjected to a standardized current injection protocol consisting of eight 300-ms-duration current injections (staircased as three hyperpolarizing and five depolarizing pulses, usually ranging between −200 and +300 pA, in steps set to provide −30 to −40 mV initial hyperpolarizations from the resting membrane potential (RMP) of −60 to −68 mV and AP firing upon depolarizations). Such an experiment is shown in Fig. 1 with the optical recording sampled at 1.08 kHz and the electrical recording sampled at 50 kHz. Note that in addition to the accurate detection of APs (Fig. 1 *A* and *D–H*), small hyperpolarizations were also truthfully detected by the dqGEVI (Fig. 1 *B–D* and *F*). In this particular cell, the SNR (z-score equivalent) (29) of the first AP in the train was 31.4. The mean (± SEM) fluorescence change (ΔF/F) of the 27 APs in this recording was 5.01 ± 0.05%. Cohen's d statistic for the same 27 APs was 288.3 when the SD of a 200-ms baseline was considered for the analysis. However, since the pooled SD (*Materials and Methods*) is reduced by the large number of points present in a long baseline, we also calculated the d values using 27 baseline points to match that of the APs. In this case, the d values ranged between 103.0 and 112.3 for 12 randomly selected baselines, an outstanding statistical effect size (40). Remarkably, in a total of 24 neurons the average SNR (z-score equivalent), calculated from unsmoothed single fluorescence traces of the first APs evoked by the injected current, was 17.95 ± 1.12 (mean ± SEM; $n = 24$).

The standardized current protocol experiments also allowed us to correlate the membrane potential (V_m) changes measured by electrophysiology with the fluorescence changes (ΔF/F) as measured by the mean gray levels in the regions of interest (ROIs) (usually the somatic membrane). For these measurements the electrophysiology traces were downsampled to match the sampling of the fluorescence (∼1.08 or 2.225 kHz) (Fig. 2 *A* and *B*). In this manner, the two traces could be plotted against each other to obtain the graph of ΔF/F as a function of the membrane potential through a point-by-point correspondence. The slope of the line fitted to the ∼3,000 to 6,000 point pairs in each cell yielded the ΔF/F for a V_m change of 100 mV (Fig. 3*C*). In $n = 10$ cells, under matching experimental conditions, except for the sampling rate of the fluorescence, the average ΔF/F for a 100-mV change was 6.604 ± 0.421% (± SEM). In all cases, the responses were consistently linear in the V_m range of −100 mV to +40 mV.

Fluorescence Signals Using D3 dqGEVI Detect Rapid Changes in V_m Associated with APs. The relatively low maximal sampling rate of the fluorescent signals with our electron-multiplying charge-coupled device (EM-CCD) camera (∼2.2 kHz) precluded accurate measurements of the rising phase of APs or fitting exponential functions to the rising phases of square-shaped voltage pulses. Therefore, we decided to compare fluorescent and electrical measurements of fast changes in V_m by measuring the decay time constants (τ) of APs where more sample points were available in the fluorescence traces. We divided the APs into two groups: the rapidly decaying APs, usually those that were elicited first in a train of spikes, and slowly decaying APs, that is, those that were the last in the train when due to various biophysical factors the recovery of the membrane potential following an AP is hindered. In these experiments the APs recorded by fluorescence (sampled at ∼2.2 kHz) or through electrophysiology (sampled at 50 kHz) were normalized to their peaks and single exponentials were fitted to the decay phases (Fig. 3 *A* and *B*). Comparison of the fast AP decays shown nearly one-to-one correspondence between the two measurements. In six cells a total of 27 fast APs (τ range: 1 to 3 ms; Fig. 3*C*) and 20 slow APs (τ range: 3 to 22 ms; Fig. 3*D*) were compared. The linear fit to the fast AP data has a slope = 1.0334 ± 0.0366 and $R^2 = 0.746$ (Fig. 3*C*), while the linear fit to the slower decaying APs has a slope = 1.0495 ± 0.026 and $R^2 = 0.939$ (Fig. 3*D*). The high correlation between the τs indicates the accurate and fast rendition of membrane potential changes by the D3-GPI-eGFP dqGEVI. We also compared the performance of our dqGEVI approach with that of another GEVI, ASAP2s. The D3-GPI-eGFP dqGEVI fluorescence followed with much higher fidelity the electrophysiological AP waveform than the fluorescent signal generated by ASAP2s (Fig. 3*E*). The summary data show the AP half-width measurements that were obtained by the two approaches, indicating a significantly faster measurement with the D3 dqGEVI approach (Fig. 3*F*).

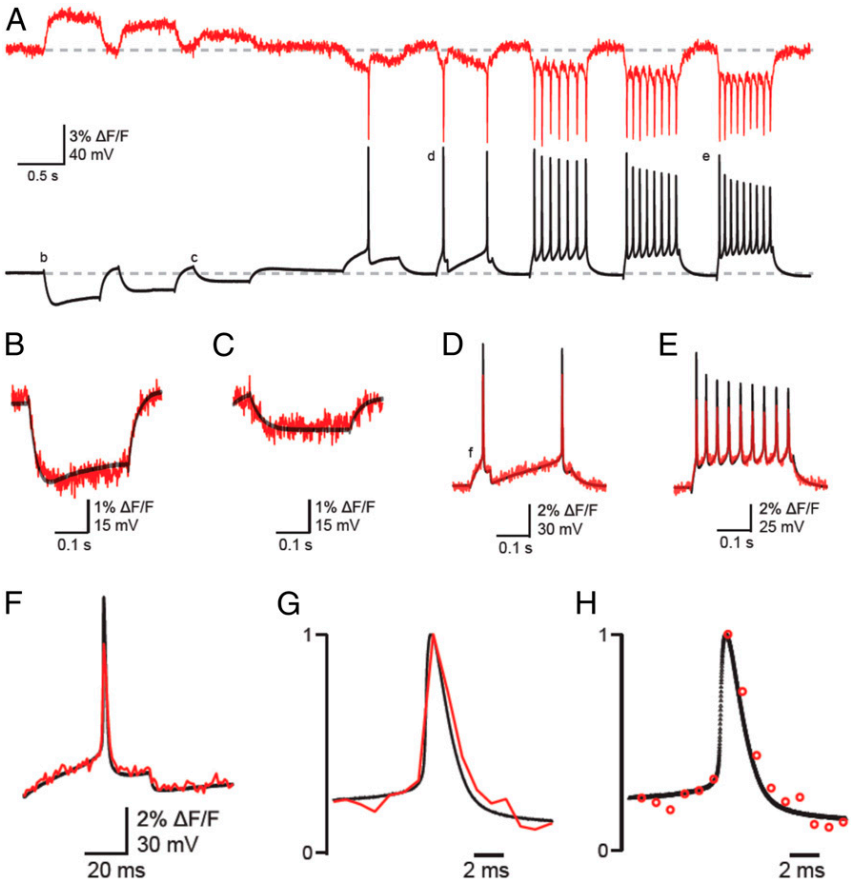

Fig. 1. Simultaneous optical and electrical recordings of membrane potential changes in a cultured neuron using the dqGEVI approach with 10 μM D3. (*A*) Single continuous traces of optical recordings (red) without image processing or filtering, as sampled at 1.08 kHz with an EM-CCD camera. The patch-clamp recordings in the I-clamp configuration (black) were sampled at 50 kHz. Various current pulses of 300-ms duration were injected into the neuron to produce hyper- and depolarizations of the membrane and AP firing. The average ΔF/F (± SEM) for the 27 APs depicted in this trace was 5.01 ± 0.05%. Horizontal dashed line indicates the RMP of −65 mV. (*B–E*) Parts of the traces labeled with the respective letters on panel *A* are shown in enlarged snapshots as superimposed traces of optical (red) and electrical (black) recordings. Note the highly accurate temporal overlap between the fluorescence and membrane potential changes. (*F*) Overlay of fluorescence (red) and membrane voltage (black) during an AP at higher temporal resolution. Note the superimposition of the two traces during both the pre-AP voltage rising to threshold and during the post-AP hyperpolarization. (*G*) Fluorescence and membrane potential are shown normalized to the peak of the AP. (*H*) The sampling data points are shown for the two recording modalities to illustrate the rapid change in fluorescence despite the relatively low sampling frequency.

Recordings of Subthreshold Changes in V_m. We wanted to know how accurately the dqGEVI approach reflects subthreshold changes in V_m. Therefore, we created a stimulus protocol that systematically and reproducibly altered the V_m in voltage-clamped cultured neurons expressing GPI-eGFP. The protocol changed the V_m according to a chirp function (*Materials and Methods*) that increased from 10 Hz to 100 Hz over 4 s and had a peak-to-peak amplitude of 40 mV (± 20 mV from the RMP). We then carried out extensive analyses of the correlations between the V_m (downsampled to the sampling rate of the fluorescence) and the ΔF/F over the 4 s of the chirp pulse of increasing frequency. Fig. 4*A* shows such an experiment together with the Morlet wavelet transforms of the two signals (ΔF/F and V_m). Using the Hilbert transform (*Materials and Methods*) we also calculated the phases of the two responses (Fig. 4 *B* and *C*) during the duration of the 4-s chirp wave. For each experiment we plotted the point-by-point correlation between the phase of the ΔF/F and the phase of the V_m signals. These plots were binned in three-dimensional histograms (Fig. 4*D*), and Pearson's R value was calculated, together with its significance based on the t distribution of R/SQRT [(1 − R^2)/(N − 2)], where N is the number of point pairs. Furthermore, we calculated the cross-correlation between the phase of ΔF/F and that of V_m (Fig. 4*E*). The values of the cross-correlations were normalized using the root-mean-square (RMS) values of each signal (*Materials and Methods*). Finally, for each experiment we subtracted the phase of the V_m signal from the ΔF/F phase in a point-by-point manner. The values of the subtracted points were binned at 0.1 rad, and a histogram was generated for each experiment. We then fitted a Gaussian to the histogram (Fig. 4*F*) that provided the mean difference between the two phases (in rad). A negative value of the difference indicates that the phase of the ΔF/F lags behind that of the V_m signal. The value of the phase difference expressed in rad was converted to milliseconds using the average frequency over the entire duration of the chirp function (55 Hz, i.e., 2π rad = 18.182 ms). From eight chirp sweeps recorded in six different neurons at their RMP of −68 to −72 mV, the mean (± SEM) values were as follows: R (ΔF/F phase, V_m phase correlation) 0.476 ± 0.056; *t* value 40.34 ± 6.90; degrees of freedom (range) 4,330 to 8,872; *P* (range) 0.00 to 1.92E-67; normalized R (ΔF/F, V_m cross-correlation) 0.596 ± 0.063; degrees of freedom (range) 4,330 to 8,872; *P* (range) 0.00 to 5.27E-122; average (ΔF/F phase – V_m phase) in rad: −0.0097 ± 0.0084, in microseconds: −276 ± 240. Taken together, our measurements indicate that the dqGEVI approach highly accurately reflects slow (10 Hz) and fast (100 Hz) subthreshold changes in V_m.

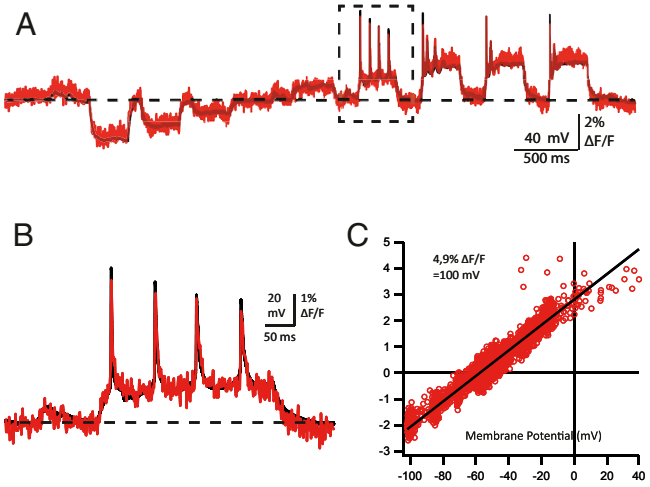

Fig. 2. Calculation of the correspondence between ΔF/F and membrane potential. (*A*) A current injection protocol similar to that used in Fig. 1 in another cultured neuron expressing GPI-eGFP recorded in the presence of 10 μM D3. Superimposed traces of nonimage processed fluorescence sampled at 1.08 kHz (red) and the I-clamped membrane voltage (black) downsampled to the same sampling interval from the original 50 kHz. The horizontal dashed line indicates the RMP of −60 mV. (*B*) A portion of the traces is shown from the part enclosed in the dashed lined box of *A*. Note the excellent overlay between the optical and electrical recordings as indicated by the accurate reporting of the decreasing AP amplitudes during the train, and the subthreshold depolarizing events (~5 mV) prior to the current injection (probably spontaneous excitatory postsynaptic potentials; arrowhead) of <10 mV amplitudes. (*C*) The relationship between ΔF/F and membrane potential was calculated by plotting the two traces point-by-point against each other. The slope of the linear regression (black line) yields the relationship for this cell as indicated in the inset.

Very Slow Single-Photon Photobleaching. One of the inherent problems of using GEVIs is the rapid photobleaching upon continuous single-photon illumination. The longest of the bleaching time constants for several GEVIs is ~400 s for QuasAr2 (6), while during two-photon illumination these values are extended by three- to fourfold (6). We measured the single photobleaching time constant of our dqGEVI under 15-min continuous illumination conditions in cultured neurons (Fig. 5*A*). The decay time constant from five averaged experiments was 2,629.6 s (~44 min), which compares very favorably to the newly developed two-component GEVIs Voltron (16) and Positron (17), and the SNR measured periodically during the continuous illumination had a similarly slow decay (Fig. 5 *B* and *C*).

Receiver Operating Characteristic Analyses of Induced AP Firing at 50 Hz and 100 Hz. During 300-ms-long depolarizing current pulse injections, cultured cortical or hippocampal neurons under our recording conditions did not fire at frequencies of >30 Hz (e.g., Fig. 1*E*). As previously reported (12) for other GEVI approaches, at these relatively low frequencies there was a one-to-one correspondence between the APs detected in the optical voltage traces and the APs recorded by the patch-clamp method. However, we wanted to know whether the dqGEVI method is also capable of detecting APs elicited at higher frequencies. We injected short (4 ms) high-amplitude (800 to 1,500 pA) current pulses to elicit APs at 50 Hz (Fig. 6 *A* and *B*) and at 100 Hz (Fig. 6 *C* and *D*) in a highly controlled manner. For these experiments, the ΔF/F traces were smoothed according to the Savitzky–Golay method by a 17-point (for 2.225-kHz sampling) and 7-point (for 1.08-kHz sampling) fourth-order polynomial. The threshold for AP detection in the smoothed ΔF/F traces was set at 75% of the peak amplitude of the first fluorescent AP. Point-to-point correlations between smoothed ΔF/F traces and the V_m traces downsampled to match the fluorescence sampling rates were >0.9 (Fig. 6 *B* and *D*). In six neurons each, we performed a binary receiver operating characteristic (ROC) analysis of several sweeps with a total 579 APs and 102 failures elicited at 50 Hz and 396 APs and 296 failures elicited at 100 Hz (Fig. 6*E*). Such an analysis, primarily used for determining the reliability of a diagnostic test, reveals the accuracy of the applied detection method. However, in contrast to a diagnostic test, where the precise prevalence of the disease in the population is rarely known, in our experiments the V_m recordings provided the true rates of APs and failures elicited by the current pulses, thereby making this a very powerful analytical tool. It should also be noted that the failures are not simply absences of APs but represent quite large subthreshold depolarizations elicited by the short current pulses, thus making the distinction between APs and failures more difficult. The ROC analysis indicates very high levels of sensitivity (50 Hz: 98.8%; 100 Hz: 97.7%) and specificity (50 Hz: 98.0%; 100 Hz: 92.9%) for discriminating between APs and failures at these two frequencies. A valuable statistic is the diagnostic odds ratio (DOR) of the test (41) that represents the ratio of the odds of ΔF/F positivity when APs are present in the V_m trace relative to the odds of ΔF/F positivity when there are AP failures in the V_m. The DOR values were >4,000 (50 Hz) and >500 (100 Hz), while the calculated values for the area under the curve (AUC) were 0.999 (50 Hz) and 0.993 (100 Hz). Such large values of DOR and AUC are indicative of a test of extremely high diagnostic value (41). In addition to the ROC analysis that does not account for consecutive APs, we also calculated the rates of detection of two or more successive APs at 50 Hz and 100 Hz. Of the total of 579 APs elicited at 50 Hz stimulation, 561 were part of bursts of ≥2 APs. Of these, 554 (98.75%) were also detected optically. Of the 396 APs elicited by 100 Hz stimulation 197 occurred in bursts of ≥2 APs. Of these, 193 (97.97%) were also detected optically. As previous studies did not make an effort to induce high-frequency APs but mainly relied on the intrinsic firing rates of the recorded neurons (<40 Hz), the sizeable detection rates by our dqGEVI approach are encouraging for its usefulness to detect APs from rapidly firing cell types such as interneurons. Accordingly, the dqGEVI method is sufficiently sensitive to detect small V_m deflections, yet its dynamic range is adequately large to enable a very simple threshold detection to differentiate between APs and failures.

Simultaneous Recordings from Two Neurons and from Subcellular Compartments. GEVIs offer the possibility to record simultaneously from a large number of neurons, thus allowing the monitoring of both subthreshold activities in some cells and AP firing in others. We recorded membrane fluorescence changes with 2 μM D3 after inducing synchronous activity by exposing neuronal cultures for at least 45 min to the K^+ channel blocker 4-aminopyridine (4-AP; 50 μM), a compound known for inducing epileptiform bursting activity (42). Usually, we recorded from two neurons within the same field of view (Fig. 7*A*). One of the two cells also underwent whole-cell recording in I-clamp configuration. Recordings from such an experiment are shown in Fig. 7 *B–D*. Both electrophysiological and optical recordings of the membrane voltage indicated the presence of subthreshold and suprathreshold activities (Fig. 7 *B–D*). Similar recordings were obtained in five other cell pairs in different cultures, indicating that simultaneous optical recordings of membrane voltage using the D3 dqGEVI method will be a valuable tool to detect neuronal synchrony and the temporal activation in a synaptically interconnected network. We have also measured the fluorescence in different ROIs recorded in different subcellular compartments. In Fig. 7*E* we show two dendritic locations that were on average 12.6 μm and 40.6 μm away from the soma. These two dendritic locations received the back-propagating somatic

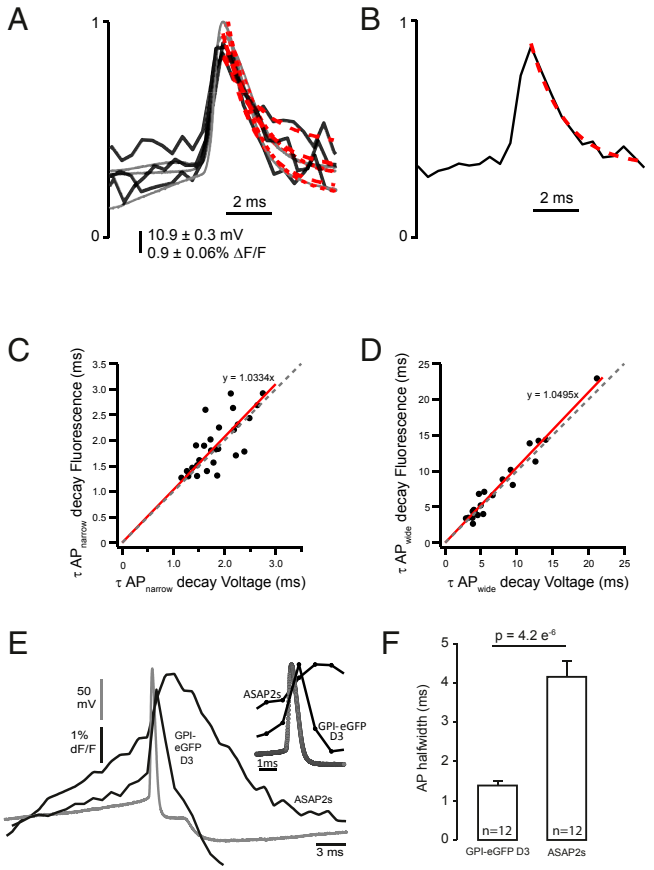

Fig. 3. Speed of the dqGEVI approach as measured during the decay of APs. (*A*) Rapidly decaying APs (usually those early on during a current pulse injection) were normalized to their peaks (gray: electrophysiology; black: fluorescence) and single exponentials were fitted to their decay phases (dotted red lines). (*B*) The same was done for slower APs (usually recorded during the late phases of the depolarizing current injections). (*C*) Comparison of the fast AP decays show a remarkable one-to-one correspondence between the optical and the electrical measurements (dotted line with a slope = 1 for comparison; red line is the linear fit to the data; slope = 1.0334 ± 0.0366; R^2 = 0.746). (*D*) Similar to *C* but for the APs with slower decays (slope = 1.0495 ± 0.026; R^2 = 0.939). Values expressed as mean ± SD. (*E*) AP waveforms recorded in HEK293T cells transfected with ASAP2s and GPI-eGFP D3 in voltage clamp mode. Optical traces (black) show the average of 12 traces from 12 cells. The AP waveform voltage trace is indicated in gray. (*Inset*) The lower sampling rate (1 kHz) of the fluorescent traces makes it look as if the upswing on the AP voltage trace is delayed, which is not the case. (*F*) Comparison of AP width of the optical traces measured at 50% amplitude. Significance was assessed by Wilcoxon rank-sum test.

depolarizations elicited by 4-AP with delays proportional to the dendritic distance from the soma (Fig. 7*F*).

Recordings after Washout of D3. The GEVI that uses a single molecule for voltage sensing or the FRET between two fluorescent proteins differ from the dqGEVI approach in that the latter uses a small molecule that first has to be added to the extracellular compartment to eventually partition itself into the membrane. An open question remains whether the small quenching molecule needs to be continuously present in the extracellular space, or whether it is sufficient to load the membrane only once. This question has not been addressed in previous voltage-sensing experiments with DPA, and therefore it is not known if DPA can reside long enough in the cell membrane to allow the optical recordings to persist following its washout from the environment. We have addressed this question with the D3-GPI-eGFP dqGEVI approach. Cells were exposed to 10 μM D3 for 10 min. Subsequently, the cells were perfused with a solution containing no D3 (and no dimethyl sulfoxide [DMSO]) at a flow rate (3 mL/min) that exchanged the recording chamber volume several times a minute. Both optical and electrophysiological recordings were undertaken immediately after washout was started and were continued for as long as 70 min. Fig. 8*A* illustrates such an experiment where the standard current clamp approach was applied to a cell every 10 min for 60 min after the start of the D3 washout. Presumably due to the high lipophilicity of D3, the optical recordings had a slow run down in the prolonged absence of D3 from the extracellular space. The SNR (z-score equivalent) for the first AP in the train remained constant: 13.83 at 0 min and 12.18 after 60 min (Fig. 8). In a total of six neurons the average (± SEM) SNR (z-score equivalent) of the first AP in the train was 15.4 ± 3.74 after 30 min and 12.21 ± 3.36 after 60 min of D3 washout. Considering the overall average (± SEM) value of AP SNR in the presence of 10 μM D3 of 17.95 ± 1.12 (n = 24), the slight loss of SNR upon D3 washout appears to be linear at a rate of 0.095 min^{-1}. Therefore, once loaded in the membrane, D3 does not need to be continuously present in the extracellular space to yield a decent SNR for AP detection even 60 min after its washout. A single membrane loading for 10 min provides ample amount of time for subsequent recordings from the GPI-eGFP expressing neurons. As illustrated in Fig. 8*B*, a cultured neuron loaded with D3 (2 μM) for 10 min 24 h before the recording still accurately resolves the electrophysiologically elicited APs through the fluorescent traces. In HEK293 cells we carried out experiments at 24 and 48 h after a 10-min exposure to D3 (2 μM). The AP voltage waveforms are shown in Fig. 8*C*, while the summary data in Fig. 8*D* indicate that the SNR decreases after 24 h by about 40%, but this level remains stable over the next 24-h period even after about two division cycles of the HEK293 cells. The long retention of D3 in the membrane after a single short exposure may be highly relevant and desirable for the future potential in vivo use of the D3-GPI-eGFP dqGEVI approach where continuous administration of the small quenching molecule may be impractical.

Comparison of DPA and D3 on Passive Membrane Properties and AP Firing. One of the major concerns with the dqGEVI approach is that the small-molecule quencher accumulates in the membrane sufficiently to cause considerable changes in capacitance and impede AP firing. The exact concentration threshold for DPA to cause such changes has not been adequately investigated but reports exist that at 5 μM DPA has deleterious effects on evoked responses in hippocampal slices (21). However, no such effects have been reported after incubation of slices with 4 μM DPA when it was used in conjunction with a new membrane-targeting approach for fluorescent proteins (29). First, we established that there was no difference between the AP width at half-amplitude between the cells expressing GPI-eGFP (mean ± SEM: 1.63 ± 0.26 ms, n = 16) and those that did not express the fluorescent protein (1.32 ± 0.07 ms, n = 36; P = 0.4878, Mann–Whitney U test). Next, we compared the effects of DPA and D3 on passive membrane properties and AP firing of cultured neurons without the expression of eGFP. We started by measuring the effects of 20 μM D3 (in 0.2% DMSO), a concentration twofold higher than we normally used for optical measurements, on whole-cell capacitance, input resistance, AP width at half-amplitude, and AP threshold. None of these parameters was affected by 20 μM D3 (*SI Appendix*, Fig. S2). In another series of experiments we systematically compared the effects of 0.2% DMSO; 2.5, 3, or 5 μM DPA (dissolved in 0.025, 0.03, and 0.05% DMSO, respectively); and 10 or 20 μM D3 (dissolved in 0.1 and 0.2% DMSO, respectively) on the same membrane parameters. The starting values for each of the properties were not different between the cells. In contrast to D3 and DMSO, DPA significantly increased

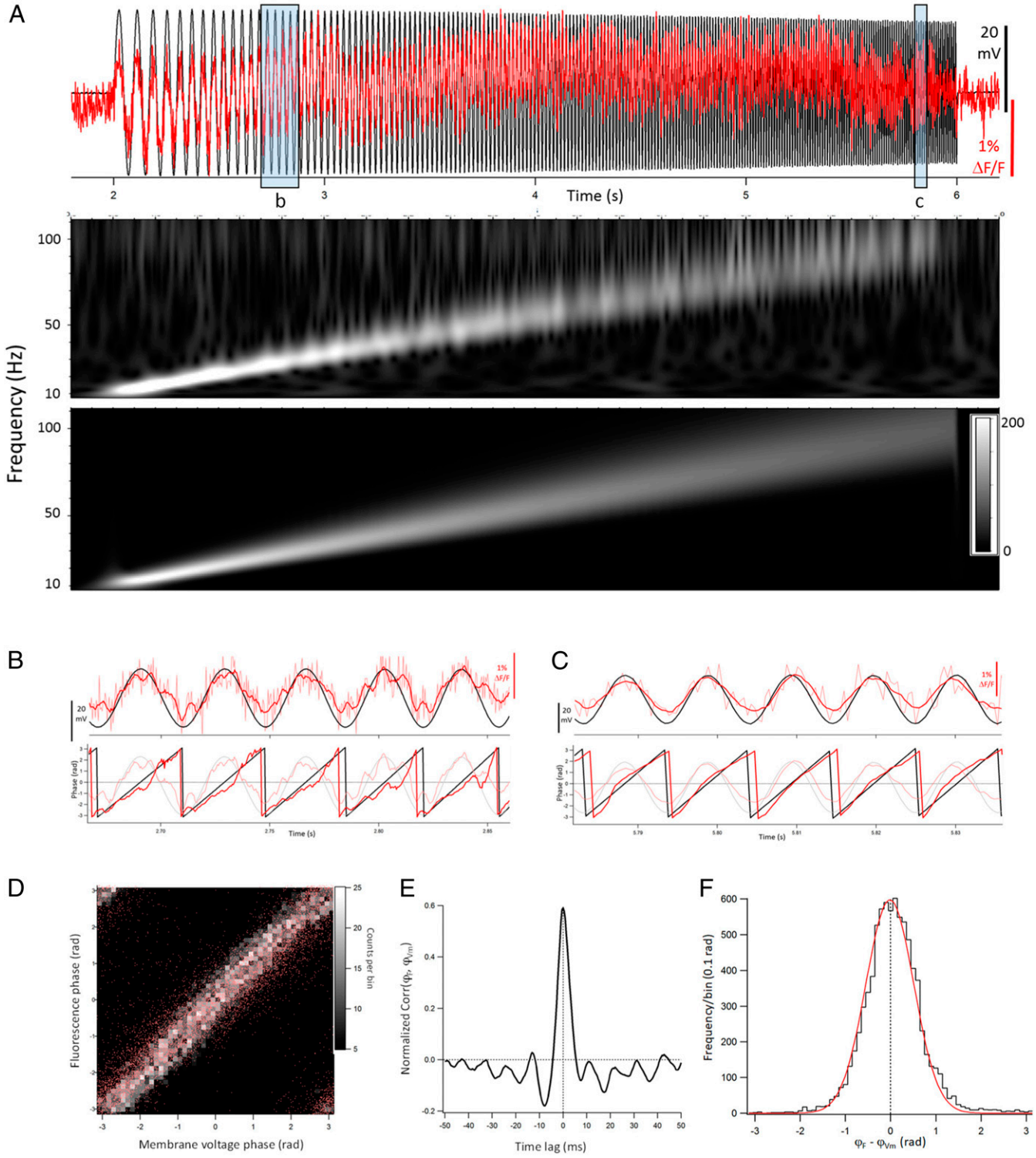

Fig. 4. Amplitude and phase correspondence between ΔF/F and V_m during subthreshold stimuli of increasing frequencies. (*A*) Superimposed plots of the ΔF/F (red) and V_m (black*)* during a 4-s chirp pulse (10 to 100 Hz). Morlet wavelet transforms of the ΔF/F trace (*Top*) and of the V_m trace (*Bottom*) showing the linearly increasing frequency responses. Note how the ΔF/F response faithfully follows the linear change in frequency. (*B* and *C*) Zoomed images of the ΔF/F and V_m traces from the shaded boxes labeled in *A*. (*Top*) The smoothed ΔF/F (dark red) and raw ΔF/F (light red) traces, superimposed with the V_m trace (black). (*Bottom*) The phases of the ΔF/F (red) and V_m (black) with the smoothed ΔF/F and V_m traces in the background shown in fainter colors. (*D*) Plot of ΔF/F phase vs. V_m phase. Individual points are represented in red, and the greyscale represents the binned histogram values with a bin width of 0.04π rad. Pearson's $R = 0.61$; $P = 0$. (*E*) Normalized cross-correlation between ΔF/F phase and V_m phase. The RMS normalization of the cross-correlogram was done as described in *Materials and Methods*. (*F*) Histogram of point-by-point differences between ΔF/F phase and V_m phase. The mean of the Gaussian fit (red) is at −0.011 rad, that is, −311 μs. The mean ± SEM lag betwen ΔF/F phase and V_m phase determined in this manner in eight experiments was −276 ± 240 μs.

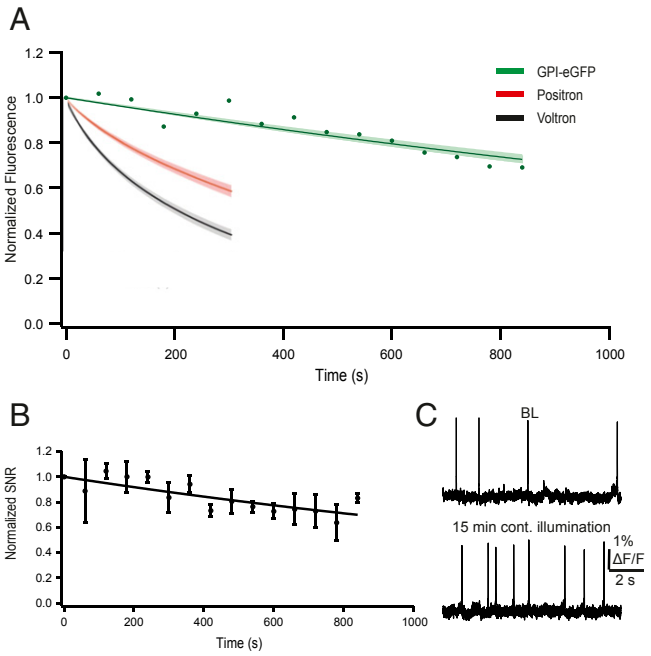

Fig. 5. High photostability of GPI-eGFP D3. (*A*) Normalized fluorescence intensity of GPI-eGFP D3 over 15-min continuous illumination with an LED (illumination intensity 4.3 mW × mm^{-2}, the standard intensity used in all of our experiments). Points are average fluorescence values sampled every 60 s in three cells. The fitted exponential decay (green line) has a time constant of 2,268 s (~38 min) with a ±SD (shaded green) of 177 s (~3 min). Graph is superimposed with the photostability curves for Voltron (black) and Positron (red) (17) (illuminated with an LED, light intensity 18 mW × mm^{-2}). (*B*) Normalized SNRs of GPI-eGFP D3 over 15-min continuous illumination ($n = 5$ neurons). Error bars indicate ± SEM. (*C*) Example raw traces from a single cultured neuron showing spontaneous APs at baseline (*Upper*) and after 15 min of continuous illumination (*Lower*).

membrane capacitance and AP width at half-maximal amplitude (*SI Appendix*, Fig. S3 *A* and *B*). The values prior to perfusion were compared to those measured at 5 or 10 min after the perfusion of the compounds. The concentration of DPA used was commensurate with that customarily employed in hybrid voltage sensing (21, 24, 29). In addition to increasing the membrane capacitance, 3 μM DPA had a toxic effect on the cells, as gradually fewer and fewer neurons survived for the entire duration of the 10-min perfusion (*SI Appendix*, Fig. S3*C*). In a small number of cells ($n = 3$) that expressed GPI-eGPF and lasted sufficiently long in 3 μM DPA we wanted to compare the optical recordings to those we obtained with D3. Unfortunately, in none of the recorded neurons did we obtain any fluorescent signals that correspond to evoked APs. It is possible that D3 and DPA have different energy requirements for voltage-dependent movements or changes in orientation in the membrane and therefore do not have similar charging effects. In the case of D3 such energy requirements may be sufficiently low not to perturb the passive membrane properties.

Lack of D3 Effects on Synaptic Responses in Slices. Another considerable concern with the use of the two-component voltage measurement approach with DPA is its effect on ligand-gated ion channels. DPA and other hydrophobic anions have been reported to antagonize $GABA_A$ (33, 34) and NMDA receptors (35). Therefore, we wanted to test the effects of 10 μM D3 on excitatory and inhibitory synaptic responses recorded in cortical slices. We recorded spontaneous excitatory postsynaptic currents (sEPSCs) (at $V_h = -60$ mV) and spontaneous inhibitory postsynaptic currents (sIPSCs) (at $V_h = 0$ mV) in L2/3 pyramidal cells of mouse cortical slices at 32 ± 1 °C. In eight neurons values are given as follows (mean ± SEM before D3 perfusion; at the end of a 10-min 10 μM D3 perfusion; the respective P values obtained by a Wilcoxon matched-pairs signed rank test): the frequencies of sEPSCs (6.55 ± 2.34 Hz; 5.90 ± 1.46 Hz; $P = 0.8438$) and sIPSCs (8.83 ± 1.91 Hz; 9.33 ± 1.61; $P = 0.5469$), 20 to 80% rise times of sEPSCs (1.29 ± 0.38 ms; 1.44 ± 0.43 ms; $P = 0.4609$) and sIPSCs (1.53 ± 0.38 ms; 1.32 ± 0.28 ms; $P = 0.8438$), weighted decay time constants for sEPSCs (6.93 ± 1.07 ms; 8.22 ± 1.12 ms; $P = 0.1484$) and sIPSCs (11.25 ± 0.65 ms; 10.64 ± 0.51 ms; $P = 0.6406$), and peak amplitudes of sEPSCs (13.47 ± 3.16 pA; 11.46 ± 2.09 pA; $P = 0.3125$) and sIPSCs (19.14 ± 1.07 pA; 20.96 ± 1.65 pA; $P = 0.3828$) were all unchanged by D3.

Discussion

We have discovered a FRET pair for a dqGEVI approach. Over the past decades, the dqGEVI method has been using the same small-molecule voltage sensor, DPA. The quenching compound D3 in combination with the membrane tagged GPI-eGFP performs better than previous FRET quenching pairs used for dqGEVI. In addition, at concentrations required for optical voltage sensing, D3 has a considerable advantage by not altering passive membrane properties or AP characteristics and by not affecting synaptic responses in cortical neurons. Moreover, it shows a linear response to voltages over a wide range (−100 to +40 mV) of membrane potentials, unlike the DPA-hVOS 1.5 or 2.0 probes that are less than optimal for recording membrane hyperpolarizations (29) and exhibit remarkably slow single-photon excitation photobleaching properties. Using no optical refinement or pixel enhancement methods, the D3-GPI-eGFP dqGEVI shows a satisfactory voltage sensitivity (6.6% ΔF/F per 100 mV) which is on average less than those of single-component GEVIs (6, 10). At our highest sampling rate of the fluorescence (~2.2 kHz) D3-GPI-eGFP showed a remarkable speed and accuracy of detecting APs as well as subthreshold depolarizing and hyperpolarizing responses without the need for signal averaging and pixel enhancement techniques. In GEVI recordings we performed a ROC analysis of optical AP detection. The values obtained for the sensitivity, specificity, DOR, and AUC of AP detection at 50 Hz and 100 Hz are truly remarkable and provide the basis for the future use of the dqGEVI approach presented here for the detection of APs in fast spiking cells, such as interneurons. At the low light intensities used, there was little bleaching observed, and recordings with good SNR could be maintained for over 60 min. The observation that D3 does not need to be present in the extracellular environment is also promising as it will permit preloading the plasma membrane with the molecule prior to in vivo experiments. Since eGFP has a much longer photobleaching half-time compared to the cerulean-based (43) hVOS 1.5, our approach should also be suitable for longer exposures to excitation light. Based on our preliminary findings possible differences between the membrane movements and orientations between DPA and D3 should be further explored in order to advance the dqGEVI approach. A way to improve upon ΔF/F is to increase the Förster radius (R_0), which can be described as (44) follows:

$$R_0 = 9.79 \times 10^3 \sqrt[6]{\frac{q_{em} J \kappa^2}{n^4}},$$

where q_{em} is the quantum yield of the donor, J is the overlap integral between the emission spectrum of the donor and the absorption spectrum of the acceptor, n is the refractive index of the medium, and κ accounts for the relative orientation between the transitional dipoles of the donor and acceptor (e.g., $\kappa = 0$ when the donor and acceptor transition dipoles are

NEUROSCIENCE

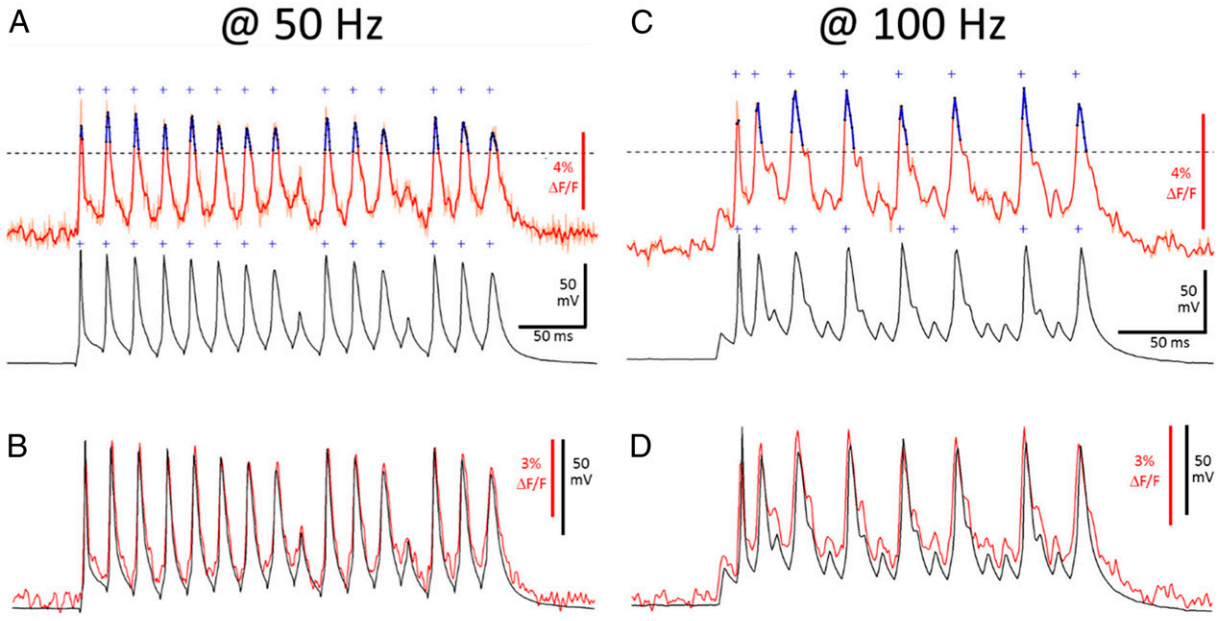

E

@ 50 Hz	APs (V_m)	n	Failures (V_m)	n	Total
APs (ΔF/F)	True Positive	$a = 572$	False Positive	$c = 2$	$a + c = 574$
Failures (ΔF/F)	False Negative	$b = 7$	True Negative	$d = 100$	$b + d = 107$
Total	$a + b = 579$		$c + d = 102$		681
N (cells)	6				
N (sweeps)	41				
@ 100 Hz	APs (V_m)	n	Failures (V_m)	n	Total
APs (ΔF/F)	True Positive	$a = 387$	False Positive	$c = 21$	$a + c = 408$
Failures (ΔF/F)	False Negative	$b = 9$	True Negative	$d = 275$	$b + d = 284$
Total	$a + b = 396$		$c + d = 296$		692
N (cells)	6				
N (sweeps)	33				

ROC Analysis	Formula	@ 50 Hz		@ 100 Hz	
		Value	95% CI	Value	95% CI
Sensitivity	$\frac{a}{a+b}$	98.79 %	97.52 - 99.51 %	97.73 %	95.73 - 98.96%
Specificity	$\frac{d}{c+d}$	98.04 %	93.10 - 99.76 %	92.91 %	89.36 - 95.55%
Positive Likelihood Ratio	$\frac{Sensitivity}{100 - Specificity}$	50.38	12.77 - 198.73	13.77	9.12 - 20.81
Negative Likelihood Ratio	$\frac{100 - Sensitivity}{Specificity}$	0.01	0.01 - 0.03	0.02	0.01 - 0.05
Prevalence	$\frac{a+b}{a+b+c+d}$	85.02 %	82.12 - 87.62 %	57.23 %	53.44 - 60.95 %
Positive Predictive Value	$\frac{a}{a+c}$	99.65 %	98.64 - 99.91 %	94.85 %	92.42 - 96.53 %
Negative Predictive Value	$\frac{d}{b+d}$	93.46 %	87.24 - 96.76 %	96.83 %	94.12 - 98.31 %
Diagnostic odds ratio (DOR)	$\frac{a/b}{c/d}$	4085.7	837 - 19951	563.1	254 - 1248
Area under the curve (AUC)	$\int_0^1 \frac{1}{1+\frac{1}{DOR\left(\frac{x}{1-x}\right)}} dx$	0.998984		0.992994	

Fig. 6. Accuracy of AP detection at 50 Hz and 100 Hz and its ROC analysis. (*A*) Detection of APs elicited with 4-ms current pulses at 50 Hz. (*Upper*) Raw (light red) and smoothed (red) ΔF/F signal of example recording. Threshold (dashed line) for detection of fluorescent APs (fAPs) was set at 75% peak amplitude of the first fAP, determined as the peak ΔF/F in a ±3-ms time window of the first electrophysiological (V_m) AP relative to a 180 ms baseline period. Crosses indicate threshold crossings, peaks of detected fAPs are indicated in blue. (*Lower*) Corresponding electrophysiological trace. Threshold for detection of V_m APs was set at 0 mV. (*B*) Superimposed raw fluorescent and electrophysiological traces from (*A*) ($R = 0.98$). (*C*) Same as *A* at 100 Hz. (*D*) Superimposed raw fluorescent and electrophysiological traces from *C* ($R = 0.95$). (*E*) ROC analysis of the indicated number of cells and traces with 579 APs and 102 failures elicited at 50 Hz and 396 APs and 296 failures elicited at 100 Hz.

perpendicular). Often the value of κ is assumed to be 2/3 to reflect a randomized alignment of the donor and acceptor dipoles during the former's fluorescence (28). However, since in theory $0 \leq \kappa^2 \leq 4$, it should be possible to determine whether other donor fluorescent proteins paired with different D3-like molecules might improve κ^2 to reach values >2/3. We are presently extending our search to identify fast voltage-sensing black-hole quencher molecules that would be capable of quenching at

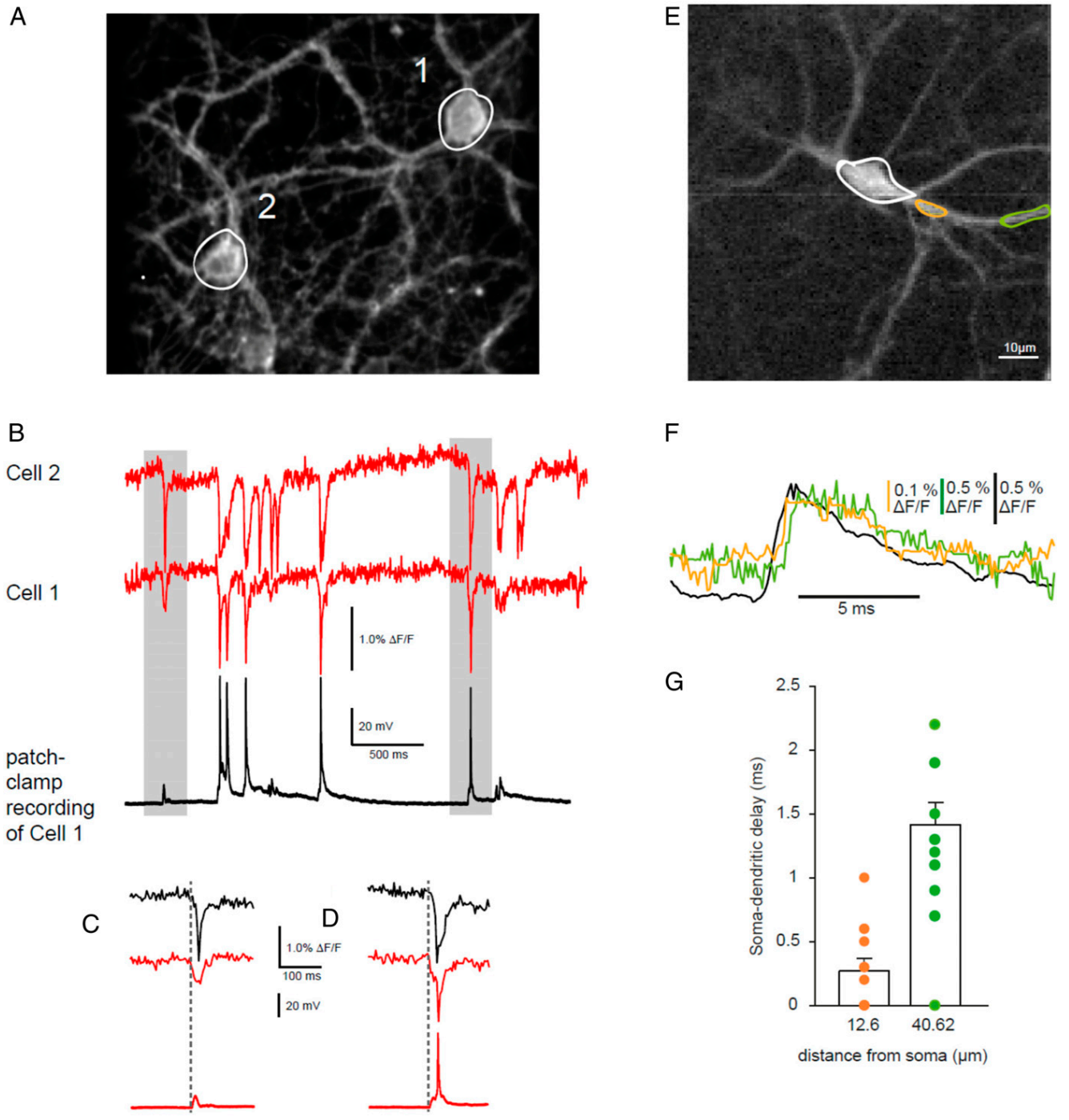

Fig. 7. Optical recordings of synchronous activity. (*A*) Two fluorescent cultured neurons on the same coverslip. Cell 1 was recorded in the I-clamp whole-cell mode. Cell 2 was only optically monitored. White circles indicate the ROI from which the imaging trace was taken. (*B*) When treated with 4-AP (50 μM) neurons developed epileptiform bursting. The simultaneous recordings show the fluorescent signals in the two cells (red and green traces) and the electrical recording in Cell 1 (black trace). (*C*) The area shaded in gray on the left of *B* magnified to show suprathreshold activity in Cell 2 and subthreshold activity in Cell 1. (*D*) The area shaded in gray on the right of *B* magnified to show suprathreshold activity in both cells. Note the alignment of the start of the synchronous discharges in both *C* and *D*. (*E*) A 128- × 128-pixel image of a GPI-eGFP–expressing cultured cortical primary mouse neuron imaged at 10 kHz. Spontaneous activity was elicited by incubation with 4-AP. (*F*) Superimposed single traces of the dendritic signals at a proximal location (orange) and at a more distal location (green). The somatic signal (black, ROI indicated at soma with white circle) precedes the dendritic signals. (*G*) Quantification of the soma–dendritic delay in a single neuron measured on average at a distance of 12.60 ± 0.09 μm (orange) and 40.62 ± 0.17 μm (green) from the soma (n = 13 depolarizations). Error bars indicate ± SEM.

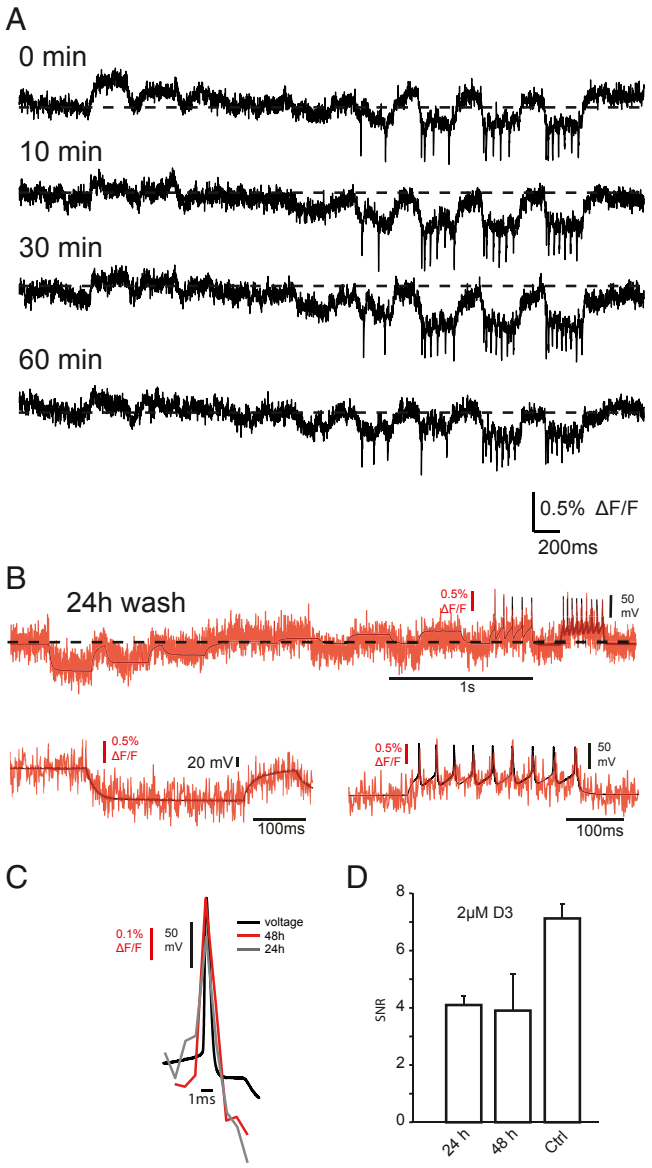

Fig. 8. Long-lasting optical measurements of membrane voltage following removal of the acceptor/quencher D3 from the extracellular space. (*A*) Individual traces of raw unfiltered and unprocessed fluorescent signals (sampled at 1.08 kHz) of membrane potential changes following the indicated times after the washout of 10 μM D3 from the recording chamber. The current injection protocol is the same as that shown in Figs. 2 and 3. Each protocol required a 6-s continuous illumination and was repeated four times every 10 min. Despite the multiple exposures to light, the SNR (z-score) of the first AP in the train was remarkably constant over time (at 0 min: 13.8 and at 60 min: 12.2). (*B*) Simultaneous optical (red) and electrical (black) recording from a mouse cultured neuron recorded 24 h after 10 min of incubation in 2 μM D3. The patch-clamp recordings in the I-clamp configuration (black) were sampled at 50 kHz. (*Upper*) Whole trace of current pulses of 300-ms duration injected into the neuron to produce hyper- and depolarizations of the membrane and AP firing. (*Lower*) Enlarged snapshots of hyperpolarizing (*Lower Left*) and depolarizing (*Lower Right*) current injections. (*C*) Superimposed average trace of five AP waveforms induced in a HEK293T cell expressing GPI-eGFP measured 24 and 48 h after 10 min of incubation with 2 μM D3. (*D*) Bar graph showing SNRs 24 and 48 h after incubation compared to Ctrl. Error bars indicate ± SEM.

the same time several fluorescent proteins separated in their emission spectra. This would enable a multispectral GEVI approach that would not be easily reproducible by other methods.

Compared to single-molecule GEVIs (6, 10) and other two-component GEVI approaches that do not use dark quenchers (16, 17, 45, 46) our approach may lack in the magnitude of ΔF/F response for a given voltage, but it makes up for this with a high SNR, lack of fast photobleaching, and a highly accurate and rapid electrical signal rendering without the need for averaging and pixel manipulations. The use of GEVIs in mice has been rendered considerably easier with the development of the Optopatch3 mouse line (13), but the use of GEVIs in other preparations such as neurons derived from human iPSCs (47) has not been widespread. Our dqGEVI approach works well in both dorsal root ganglion cells and cortical neurons derived from human iPSCs, presenting a stage where its many superior properties will be useful for unperturbed recordings of membrane potential changes.

Materials and Methods

Animals. Timed-pregnant Wistar rats and C57BL/6N mice were used to prepare cell cultures between days 16 and 18 of embryonic development. Adult (>11 wk old) C57BL/6N mice of both sexes were used to prepare brain slices. All animal storage, handling, and experiments were conducted in accordance with the guidelines of the Animal Care and Use Committee of the University of Bonn.

Cell Cultures. For cell culturing, molecular biological, and virus preparation procedures all reagents were purchased from Thermo Scientific unless indicated otherwise. Cortical neurons were obtained from Wistar rats or C57BL/6N mice mice between days 16 and 18 of embryonic development. Pregnant rats or mice were anesthetized with isoflurane and decapitated and the embryos were removed from the uterus. After decapitation of the embryos, the cortices were isolated in HBSS buffer and digested with trypsin (0.25%) and DNase I (1 mg/mL, purchased from Sigma). Cells were cultured in the mixture of basal medium Eagle enriched with fetal bovine serum (1%), B-27 supplement (2%), glucose (1%) and L-glutamine (0.23%). Cells were plated at a density of 20,000 to 35,000 cells per well onto poly-D-lysine–coated coverslips (d = 12 mm) in a 24-well plate. Twenty-four hours after preparation the plating medium was changed to 1 mL of fresh medium per well. As a second approach, we also used frozen cell stocks of rat cortical neurons (AMS Biotechnology). These were revived and put into culture according to the manufacturer's instructions with a plating density of 35,000 cells per well. All culturing procedures were similar to those described for the primary mouse neuronal cultures above. HEK293T cells were purchased from ATCC (CRL-3216) and cultured in DMEM bathing medium (+10% fetal calf serum and 1% penicillin–streptomycin). Cells were grown under standard conditions (37 °C, 5% CO_2) and transfected with Lipofectamine 3000 according to the manufacturer's protocol.

Molecular Biology. The pCAG:GPI-eGFP plasmid (48) encoding a fusion protein of proacrosin signal peptide, eGFP, and Thy-1 GPI anchoring signal (GPI-eGFP) was purchased from Addgene (Plasmid 32601; deposited by Anna-Katerina Hadjantonakis) as well as pAAV-hSyn-ASAP2s (Plasmid 101276; deposited by Francois St-Pierre). All other reagents were purchased from Thermo Scientific, if not indicated otherwise. To minimize nonneural expression, the open reading frame for GPI-eGFP was cloned to an AAV plasmid backbone (pAAV Syn1:MCS) under the human synapsin-1 promoter (49) with the XbaI and HindIII restriction sites (primers: forward XbaI GPI_KOZ and reverse HindIII GPI).

Virus Preparation and Transduction Procedures. Recombinant adeno-associated virus production and preparation were carried out as previously described (50, 51). Briefly, plasmids for viral vector production were grown in DH5 alpha bacteria while HEK293T cells (ATCC CRL-3216TM) were transfected using the $CaPO_4$ method. Virus particles were harvested 4 or 5 d after transfection and subsequently purified with HiTrap Heparin HP columns (GE Healthcare Life Sciences). After concentration and sterile filtration, viral proteins were separated using denaturizing polyacrylamide gel electrophoresis to detect major viral proteins VP1, VP2, and VP3 for quality control. For transduction of cultured neurons, virus particles were diluted in sterile phosphate-buffered saline and were added directly to the bathing medium.

Confocal Imaging. To demonstrate plasma membrane targeting of the GPI-eGFP fusion protein, images of transgene-expressing neurons were taken at 40× magnification on a TCS SP5 confocal platform and on an Olympus

IX81 confocal microscope (Olympus Corp.). Cells were fixed with 4% paraformaldehyde for ~3 min and then coated with Vectashield mounting medium (Vector Laboratories).

Combined Optical and Electrophysiological Recordings. Reagents for electrophysiological experiments were purchased from Sigma unless indicated otherwise. Most experiments were conducted using an Olympus BX61WI microscope (Olympus Corp.) equipped with epifluorescence and differential interference contrast. An EM-CCD camera (Evolve 512 Delta with LightSpeedTM) or a metal–oxide–semiconductor (CMOS) camera (Prime 95b, both cameras from Teledyne Photometrics) were used to visualize neurons and to verify fluorescence. Both cameras were controlled by μManager software (52). Expression of GPI-eGFP was verified using epifluorescence. Excitation illumination (470 nm) at 4.3 mW × mm^{-2} was provided with a custom-made light source (parts from Thorlabs Inc. with a Luxeon Rebel 470-nm light-emitting diode [LED] LXML-PB01-0040) that was driven by a custom-made transistor–transistor logic (TTL) switched stable current source. The excitation light as well as the collected fluorescence were filtered using a FITC filter set (Ex: HQ480/40×; Di: Q505LP; Em: HQ535/50m; Chroma Technology Corp.). For optical voltage imaging with the EM-CCD camera two different settings were used. Frame rates of ~1.08 kHz were achieved by measuring a 100- × 100-pixel ROI without binning. In order to gain more precise timing of the optically recorded peak of electrical events we also applied 4- × 4-pixel binning in a 100- × 80-pixel ROI resulting in 25- × 20-pixel ROI and frame rates of ~2.225 kHz.

For optical voltage imaging with the CMOS camera frame rates of 976 Hz were achieved by measuring a 96 × 96 pixel ROI. The timing of illumination and image acquisition were controlled by a digital stimulator (PG4000A; Cygnus Technology Inc.) that was triggered by the acquisition software WinWCP. No image processing was applied.

For dendritic recordings a Redshirt FastCMOS 128x camera mounted to a SliceScope Pro-1000 microscope (Scientifica) reconstructed using parts of the Olympus BX61WI by Scientifica was used. Excitation illumination (488 nm) at this setup was provided by an excelsior-488C-200_CDRH laser (Spectra-Physics) with a maximum power of 200 mW. During the dendritic measurements the laser power was set to 75 mW measured at the end of the light fiber. Frame rates of 10 kHz were achieved at full frame of 128 × 128 pixels (pixel size 15 μm) without binning. Recordings were started after a ~45-min preincubation period with artificial cerebrospinal fluid (ACSF) containing of 4-AP (50 μM) and the D3 (Millipore Sigma) (2 to 10 μM) in 0.02% DMSO at room temperature. Whole-cell patch clamp recordings were amplified using a Multiclamp 700B amplifier (Molecular Devices), low-pass-filtered at 10 kHz and digitized at 50 kHz with an NI USB-6341 (National Instruments) controlled by Strathclyde Electrophysiology software WinWCP (John Dempster, University of Strathclyde, Glasgow, United Kingdom). Data were stored on a hard disk for offline analysis. Pipettes were pulled from borosilicate glass (King Precision Glass, Inc.) using a DMZ Zeitz puller (Zeitz-Instruments). Patch pipettes had resistances of 3 to 5 MΩ and contained (in millimolar): 135 K-gluconate, 5 KCl, 10 Hepes, 0.1 ethylene glycol-bis(2-aminoethylether)-N,N,N′,N′-tetraacetic acid (EGTA), 1 MgCl2, 3 MgATP, and 0.2 Na2ATP at pH 7.2. GPI-eGFP–expressing cultured neurons 2 to 3 wk after viral transduction were transferred to a modified submerged chamber (52) and perfused with Hepes-buffered ACSF (3 mL/min at 32 ± 1 °C, in millimolar): 145 NaCl, 5 KCl, 1.5 $CaCl_2$, 2 $MgCl_2$, 26 2-(4-(2-hydroxyethyl)-1-piperazinyl)-ethanesulfonic acid (Hepes), and 10 glucose at pH 7.4. Recordings were started after a ~5 min preincubation period with ACSF containing D3 (10 μM) in 0.1% DMSO.

Imaging sequences were analyzed using ImageJ (53) and Igor Pro (Wavemetrics Inc.). Average gray values were extracted from the image sequences using the Z profiler-plugin for ImageJ. The precise timing of the images was obtained by digitally recording the "exposure out" TTL signal given off by the camera. This signal was then imported into Igor Pro and the rising and falling edges of the TTL pulses were detected. The midpoints between the detected edges constituted the precise time points for the image acquisition, which were then lined up with the digitized electrophysiology traces. The optically recorded AP peak and the decay time constant of the AP were analyzed in recordings with 2.225-kHz sampling. Exponential fits of the electrophysiological and optical signals were made using IgorPro. The SNR (z-score equivalent) for APs was measured as the ΔF/F of the AP divided by the SD of the 200-ms prior baseline (29) that contained no obvious spontaneous activity in the electrical recording. To analyze the ability of the dqGEVI approach to faithfully report high-frequency AP firing, trains of 16 or 21 high-amplitude (800 to 1,500 pA) 4-ms current pulses were applied at a frequency of 50 or 100 Hz in the I-clamp configuration. Prior to AP detection, fluorescent traces were detrended, smoothed using the Savitzky–Golay method by a 17-point (for 2.225-kHz sampling) and 7-point (for 1.08-kHz sampling) fourth-order polynomial, and aligned with the electrophysiological traces as described above. Detection threshold for optical APs was set as 75% peak amplitude of the first fluorescent AP in the train relative to the mean 180-ms prior baseline period. AP threshold in the electrophysiological (Vm) trace was set at 0 mV. In some of the cultured neurons APs and failures were not clearly distinguishable in the electrophysiological recording. Therefore, traces with events that exceeded −20 mV but did not reach 0 mV were omitted from analysis. To elicit spontaneous activity in a synaptically connected network of cultured neurons and to record from multiple neurons simultaneously, the K+-channel antagonist 4-AP was added to the ACSF. In some of the experiments simultaneous electrophysiological recordings from one of the imaged neuron was also performed.

Chirp Function and Phase Determination. The 10- to 100-Hz chirp function was generated by the following equation: $A \times \sin[2\pi(F_0 + ((F_{max} - F_0) \times t/2T) \times t)]$, where A is 50% of the peak-to-peak amplitude, F_0 is the starting frequency (10 Hz), F_{max} is the frequency at the end of the pulse (100 Hz), t is time, and T is the duration of the chirp pulse (4 s). This pulse, generated at a sampling rate of 1,000 s^{-1}, was fed into the digital-to-analog converter and subsequently low-pass-filtered at 300 Hz before feeding it into the amplifier to circumvent step-like changes in V_m. For determination of the phases of the equivalently sampled and mean subtracted ΔF/F and V_m signals, we first used the HilbertTransform function built into IgorPro. The phase was then determined by the value of the atan function of the point-by-point division between the HilbertTransform/signal.

Assessment of Quencher Effects on Passive and AP Properties. Nonfluorescent cultured neurons aged similarly to those used for combined optical and elecrophysiological recordings were used for these experiments. The procedures for whole-cell I-clamp recordings were identical to those described for the electrophysiological recordings above. Data were analyzed using Igor Pro. For passive membrane properties, a 300-ms hyperpolarizing voltage pulse was elicited by current injection every 5 s for a 5-min baseline period followed by the bath perfusion of the vehicle (0.2% DMSO) or the quencher, that is, 3 μM DPA (Biotium) (in 0.03% DMSO) or 10 or 20 μM D3 (in 0.1 and 0.2% DMSO, respectively) for 10 min. Membrane time constants were assessed by fitting an exponential to the hyperpolarization. APs were elicited by 200-ms-long depolarizing current injections. AP threshold was determined from the first peak of the third derivative of the voltage signal (54). AP full width at half amplitude was determined as the time difference between the two points between the rising and decaying phases of the APs both at 50% of AP amplitude.

Slice Recordings. Wild-type C57BL/6N mice (aged 11 to 14 wk) were anesthetized with isoflurane and decapitated. Brains were quickly removed and transferred into ice-cold cutting solution containing (in millimolar) 60 NaCl, 100 sucrose, 2.5 KCl, 1.25 NaH_2PO_4, 26 $NaHCO_3$, 1 $CaCl_2$, 5 $MgCl_2$, and 20 glucose (pH 7.3). Three hundred-micrometer coronal slices were prepared with a vibratome (Leica VT1200S) and gradually warmed to 37 °C. For electrophysiology, slices were transferred into a submerged chamber (55) and superfused with ACSF containing (in millimolar) 125 NaCl, 3.5 KCl, 1.25 NaH_2PO_4, 26 $NaHCO_3$, 2 $CaCl_2$, 2 $MgCl_2$, and 15 D-glucose (pH 7.3) and allowed to equilibrate for at least 20 min at room temperature. All solutions were bubbled with 95% O_2–5% CO_2. Whole-cell voltage clamp recordings were performed on visually identified cortical layer 2/3 pyramidal neurons. Patch pipettes (3 to 6 MΩ) were filled with (in millimolar) 135 Cs methansulfonate, 5 KCl, 10 Hepes, 0.16 EGTA, 2 $MgCl_2$, 3 NaCl, 4 Na_2-phosphocreatine, 2 MgATP, and 0.2 NaGTP (pH adjusted to 7.3 with CsOH, osmolarity 290 mosm/kg). Signals were low-pass-filtered at 3 kHz and sampled at 10 kHz. Series resistance was monitored before and after the recording. Experiments with series resistances >20 MΩ or a change >20% during the recording were excluded. sEPSCs were recorded at a holding potential (Vh) of −60 mV. sIPSCs were recorded at a Vh of 0 mV. sEPSCs and sIPSCs were recorded starting during a 2- to 3-min baseline period before bath application of 10 μM D3 in 0.1% DMSO and then continuously during D3 perfusion for >10 min. Events were analyzed during 1-min epochs collected during the baseline period and at least 10 min after bath application of D3. Data were analyzed using a custom-written LabView software (EVAN) which provided peak amplitudes, 20 to 80% rise times, weighted decay time constants, and averaged traces.

Quantification and Statistical Analyses. Cohen's d (difference between two means M1 and M2) was calculated as d = ABS(M1 − M2)/SD, where SD is the pooled SD given by SD = SQRT((SD1^2 + SD2^2)/(N1 + N2 − 2)). Here SD1 and SD2 are the sample SDs of the two distributions, respectively, and N1 and N2

NEUROSCIENCE

are the two corresponding Ns. The cross-correlation coefficients between the ΔF/F and Vm were normalized by dividing the value by RMS(ΔF/F) × SQRT[N(ΔF/F)] × RMS(Vm) × SQRT[N(Vm)]. Statistical significance levels were set at $P < 0.05$. For analysis of the fidelity of high-frequency AP firing, we performed a ROC analysis. The DOR was calculated (41) as (a/b)/(c/d), with a = true positives, b = false negatives, c = false positives, and d = true negatives, with the respective values indicated in Fig. 6. The AUC was calculated as

$$\int_0^1 \frac{1}{1+\frac{1}{DOR\left(x/1-x\right)}}dx$$

with $dx = 0.01$. All formulas for calculating the parameters of the ROC analysis are given in Fig. 6.

All results are expressed as mean ± SEM unless otherwise stated. Using variance estimates from the literature or from our own preliminary data, a power analysis was done to estimate the required sample size to obtain a power of 0.80, for a moderate effect size (0.25), and a significance level of 0.05. Statistical tests used for data comparisons and significance calculations are indicated for each comparison. Significance level was set at $P < 0.05$.

Data Availability. Excel files, Igor files, and Image files have been deposited in Sciebo (https://uni-bonn.sciebo.de/s/bd1mYM2AKbQXt7i). All study data are included in the article and/or *SI Appendix*.

ACKNOWLEDGMENTS. This research was initially supported by European Research Council Advanced Grant 339620 MULTIGEVOS. We thank Phuong Tran and Lydia Fischer for excellent technical assistance, S. Schoch and her laboratory for help with virus preparation, H. Beck for his generous help providing the Prime95B camera and him and his laboratoy members for discussions and comments, S. Remy and his laboratory members, F. Fuhrmann and H. Kaneko for their generous help and for the use of the setup for the dendritic recordings, W. F. Kunz for the use of the spectrophotometer, A. Zimmer's group for use of indispensable equipment, S. Opitz for preparation of cultured neurons, and M. Schwarz for confocal imaging. We acknowledge the assistance of the Microscopy Core Facility of the Medical Faculty within the Bonn Technology Campus Life Sciences, University of Bonn.

1. E. J. Hamel, B. F. Grewe, J. G. Parker, M. J. Schnitzer, Cellular level brain imaging in behaving mammals: An engineering approach. *Neuron* **86**, 140–159 (2015).
2. T. Knöpfel, Genetically encoded optical indicators for the analysis of neuronal circuits. *Nat. Rev. Neurosci.* **13**, 687–700 (2012).
3. M. Z. Lin, M. J. Schnitzer, Genetically encoded indicators of neuronal activity. *Nat. Neurosci.* **19**, 1142–1153 (2016).
4. D. Storace *et al*., Toward better genetically encoded sensors of membrane potential. *Trends Neurosci.* **39**, 277–289 (2016).
5. Y. Bando, C. Grimm, V. H. Cornejo, R. Yuste, Genetic voltage indicators. *BMC Biol.* **17**, 71 (2019).
6. Y. Bando, M. Sakamoto, S. Kim, I. Ayzenshtat, R. Yuste, Comparative evaluation of genetically encoded voltage indicators. *Cell Rep.* **26**, 802–813.e4 (2019).
7. M. Kannan, G. Vasan, V. A. Pieribone, Optimizing strategies for developing genetically encoded voltage indicators. *Front. Cell. Neurosci.* **13**, 53 (2019).
8. J. Platisa, V. A. Pieribone, Genetically encoded fluorescent voltage indicators: Are we there yet? *Curr. Opin. Neurobiol.* **50**, 146–153 (2018).
9. T. Knöpfel, C. Song, Optical voltage imaging in neurons: Moving from technology development to practical tool. *Nat. Rev. Neurosci.* **20**, 719–727 (2019).
10. M. M. Milosevic, J. Jang, E. J. McKimm, M. H. Zhu, S. D. Antic, *In vitro* testing of voltage indicators: Archon1, ArcLightD, ASAP1, ASAP2s, ASAP3b, Bongwoori-Pos6, BeRST1, FlicR1, and Chi-VSFP-Butterfly. *eNeuro* **7**, ENEURO.0060-20.2020 (2020).
11. P. Liu, E. W. Miller, Electrophysiology, unplugged: Imaging membrane potential with fluorescent indicators. *Acc. Chem. Res.* **53**, 11–19 (2020).
12. Y. Gong *et al*., High-speed recording of neural spikes in awake mice and flies with a fluorescent voltage sensor. *Science* **350**, 1361–1366 (2015).
13. Y. Adam *et al*., Voltage imaging and optogenetics reveal behaviour-dependent changes in hippocampal dynamics. *Nature* **569**, 413–417 (2019).
14. L. Z. Fan *et al*., All-optical electrophysiology reveals the role of lateral inhibition in sensory processing in cortical layer 1. *Cell* **180**, 521–535.e18 (2020).
15. K. D. Piatkevich *et al*., Population imaging of neural activity in awake behaving mice. *Nature* **574**, 413–417 (2019).
16. A. S. Abdelfattah *et al*., Bright and photostable chemigenetic indicators for extended in vivo voltage imaging. *Science* **365**, 699–704 (2019).
17. A. S. Abdelfattah *et al*.; GENIE Project Team, A general approach to engineer positive-going eFRET voltage indicators. *Nat. Commun.* **11**, 3444 (2020).
18. M. DiFranco, J. Capote, M. Quiñonez, J. L. Vergara, Voltage-dependent dynamic FRET signals from the transverse tubules in mammalian skeletal muscle fibers. *J. Gen. Physiol.* **130**, 581–600 (2007).
19. J. E. González, R. Y. Tsien, Voltage sensing by fluorescence resonance energy transfer in single cells. *Biophys. J.* **69**, 1272–1280 (1995).
20. J. E. González, R. Y. Tsien, Improved indicators of cell membrane potential that use fluorescence resonance energy transfer. *Chem. Biol.* **4**, 269–277 (1997).
21. B. Chanda *et al*., A hybrid approach to measuring electrical activity in genetically specified neurons. *Nat. Neurosci.* **8**, 1619–1626 (2005).
22. R. Benz, P. Läuger, K. Janko, Transport kinetics of hydrophobic ions in lipid bilayer membranes. Charge-pulse relaxation studies. *Biochim. Biophys. Acta* **455**, 701–720 (1976).
23. J. M. Fernández, R. E. Taylor, F. Bezanilla, Induced capacitance in the squid giant axon. Lipophilic ion displacement currents. *J. Gen. Physiol.* **82**, 331–346 (1983).
24. J. Bradley, R. Luo, T. S. Otis, D. A. DiGregorio, Submillisecond optical reporting of membrane potential in situ using a neuronal tracer dye. *J. Neurosci.* **29**, 9197–9209 (2009).
25. A. E. Fink, K. J. Bender, L. O. Trussell, T. S. Otis, D. A. DiGregorio, Two-photon compatibility and single-voxel, single-trial detection of subthreshold neuronal activity by a two-component optical voltage sensor. *PLoS One* **7**, e41434 (2012).
26. N. Shafeghat, M. Heidarinejad, N. Murata, H. Nakamura, T. Inoue, Optical detection of neuron connectivity by random access two-photon microscopy. *J. Neurosci. Methods* **263**, 48–56 (2016).
27. D. Wang, Z. Zhang, B. Chanda, M. B. Jackson, Improved probes for hybrid voltage sensor imaging. *Biophys. J.* **99**, 2355–2365 (2010).
28. L. Sjulson, G. Miesenböck, Rational optimization and imaging in vivo of a genetically encoded optical voltage reporter. *J. Neurosci.* **28**, 5582–5593 (2008).
29. N. Ghitani, P. O. Bayguinov, Y. Ma, M. B. Jackson, Single-trial imaging of spikes and synaptic potentials in single neurons in brain slices with genetically encoded hybrid voltage sensor. *J. Neurophysiol.* **113**, 1249–1259 (2015).
30. D. Wang, S. McMahon, Z. Zhang, M. B. Jackson, Hybrid voltage sensor imaging of electrical activity from neurons in hippocampal slices from transgenic mice. *J. Neurophysiol.* **108**, 3147–3160 (2012).
31. S. Weigel, T. Flisikowska, A. Schnieke, H. Luksch, Hybrid voltage sensor imaging of eGFP-F expressing neurons in chicken midbrain slices. *J. Neurosci. Methods* **233**, 28–33 (2014).
32. A. F. Oberhauser, J. M. Fernandez, Hydrophobic ions amplify the capacitive currents used to measure exocytotic fusion. *Biophys. J.* **69**, 451–459 (1995).
33. M. Chisari, K. Wu, C. F. Zorumski, S. Mennerick, Hydrophobic anions potently and uncompetitively antagonize GABA(A) receptor function in the absence of a conventional binding site. *Br. J. Pharmacol.* **164**, 667–680 (2011).
34. A. Limon, A. Estrada-Mondragón, J. M. Ruiz, R. Miledi, Dipicrylamine modulates $GABA_{\rho}1$ receptors through interactions with residues in the TM4 and Cys-loop domains. *Mol. Pharmacol.* **89**, 446–456 (2016).
35. A. J. Linsenbardt *et al*., Noncompetitive, voltage-dependent NMDA receptor antagonism by hydrophobic anions. *Mol. Pharmacol.* **83**, 354–366 (2013).
36. H. Ikezawa, Glycosylphosphatidylinositol (GPI)-anchored proteins. *Biol. Pharm. Bull.* **25**, 409–417 (2002).
37. S. Chamberland *et al*., Fast two-photon imaging of subcellular voltage dynamics in neuronal tissue with genetically encoded indicators. *eLife* **6**, e25690 (2017).
38. B. Li *et al*., Two-photon voltage imaging of spontaneous activity from multiple neurons reveals network activity in brain tissue. *iScience* **23**, 101363 (2020).
39. J. Wu *et al*., Kilohertz two-photon fluorescence microscopy imaging of neural activity in vivo. *Nat. Methods* **17**, 287–290 (2020).
40. S. Sawilowsky, New effect size rules of thumb. *J. Mod. Appl. Stat. Methods* **8**, 467–474 (2009).
41. A. S. Glas, J. G. Lijmer, M. H. Prins, G. J. Bonsel, P. M. Bossuyt, The diagnostic odds ratio: A single indicator of test performance. *J. Clin. Epidemiol.* **56**, 1129–1135 (2003).
42. M. Avoli, A. Williamson, Functional and pharmacological properties of human neocortical neurons maintained in vitro. *Prog. Neurobiol.* **48**, 519–554 (1996).
43. N. C. Shaner, P. A. Steinbach, R. Y. Tsien, A guide to choosing fluorescent proteins. *Nat. Methods* **2**, 905–909 (2005).
44. S. A. Latt, H. T. Cheung, E. R. Blout, Energy transfer. A system with relatively fixed donor-acceptor separation. *J. Am. Chem. Soc.* **87**, 995–1003 (1965).
45. V. Grenier, B. R. Daws, P. Liu, E. W. Miller, Spying on neuronal membrane potential with genetically targetable voltage indicators. *J. Am. Chem. Soc.* **141**, 1349–1358 (2019).
46. M. Sundukova *et al*., A chemogenetic approach for the optical monitoring of voltage in neurons. *Angew. Chem. Int. Ed. Engl.* **58**, 2341–2344 (2019).
47. E. Kiskinis *et al*., All-optical electrophysiology for high-throughput functional characterization of a human iPSC-derived motor neuron model of ALS. *Stem Cell Reports* **10**, 1991–2004 (2018).
48. J. M. Rhee *et al*., In vivo imaging and differential localization of lipid-modified GFP-variant fusions in embryonic stem cells and mice. *Genesis* **44**, 202–218 (2006).
49. K. M. van Loo *et al*., Zinc regulates a key transcriptional pathway for epileptogenesis via metal-regulatory transcription factor 1. *Nat. Commun.* **6**, 8688 (2015).
50. B. Hauck, L. Chen, W. Xiao, Generation and characterization of chimeric recombinant AAV vectors. *Mol. Ther.* **7**, 419–425 (2003).
51. C. McClure, K. L. Cole, P. Wulff, M. Klugmann, A. J. Murray, Production and titering of recombinant adeno-associated viral vectors. *J. Vis. Exp.*, e3348 (2011).
52. A. D. Edelstein *et al*., Advanced methods of microscope control using μManager software. *J. Biol. Methods* **1**, e10 (2014).
53. C. A. Schneider, W. S. Rasband, K. W. Eliceiri, NIH image to ImageJ: 25 years of image analysis. *Nat. Methods* **9**, 671–675 (2012).
54. D. A. Henze, G. Buzsáki, Action potential threshold of hippocampal pyramidal cells in vivo is increased by recent spiking activity. *Neuroscience* **105**, 121–130 (2001).
55. M. R. Hill, S. A. Greenfield, The membrane chamber: A new type of in vitro recording chamber. *J. Neurosci. Methods* **195**, 15–23 (2011).

BIOLOGICAL SCIENCES, Neuroscience

SUPPLEMENTARY INFORMATION

(Figures S1-S3)

A dark quencher genetically encodable voltage indicator (dqGEVI) exhibits high fidelity and speed

Therese C. Alich[1], Milan Pabst✞[1]*, Leonie Pothmann[1]*, , Bálint Szalontai[1*], Guido C. Faas[2], and Istvan Mody[1,2]

[1]Neuronal Networks in Health and Disease Laboratory
Institute of Experimental Epileptology and Cognition Research
University of Bonn Medical Center | Life and Brain Center
Venusberg-Campus 1
53127 Bonn/GERMANY

[2]Department of Neurology, NRB1
The David Geffen School of Medicine at UCLA
635 Charles Young Drive South
Los Angeles, CA 90095-733522
Tel: 310-206-4481

✞ *In memoriam*.

* These authors contributed equally to this study.

Correspondence to: Prof. Istvan Mody (see address above),
mody@ucla.edu

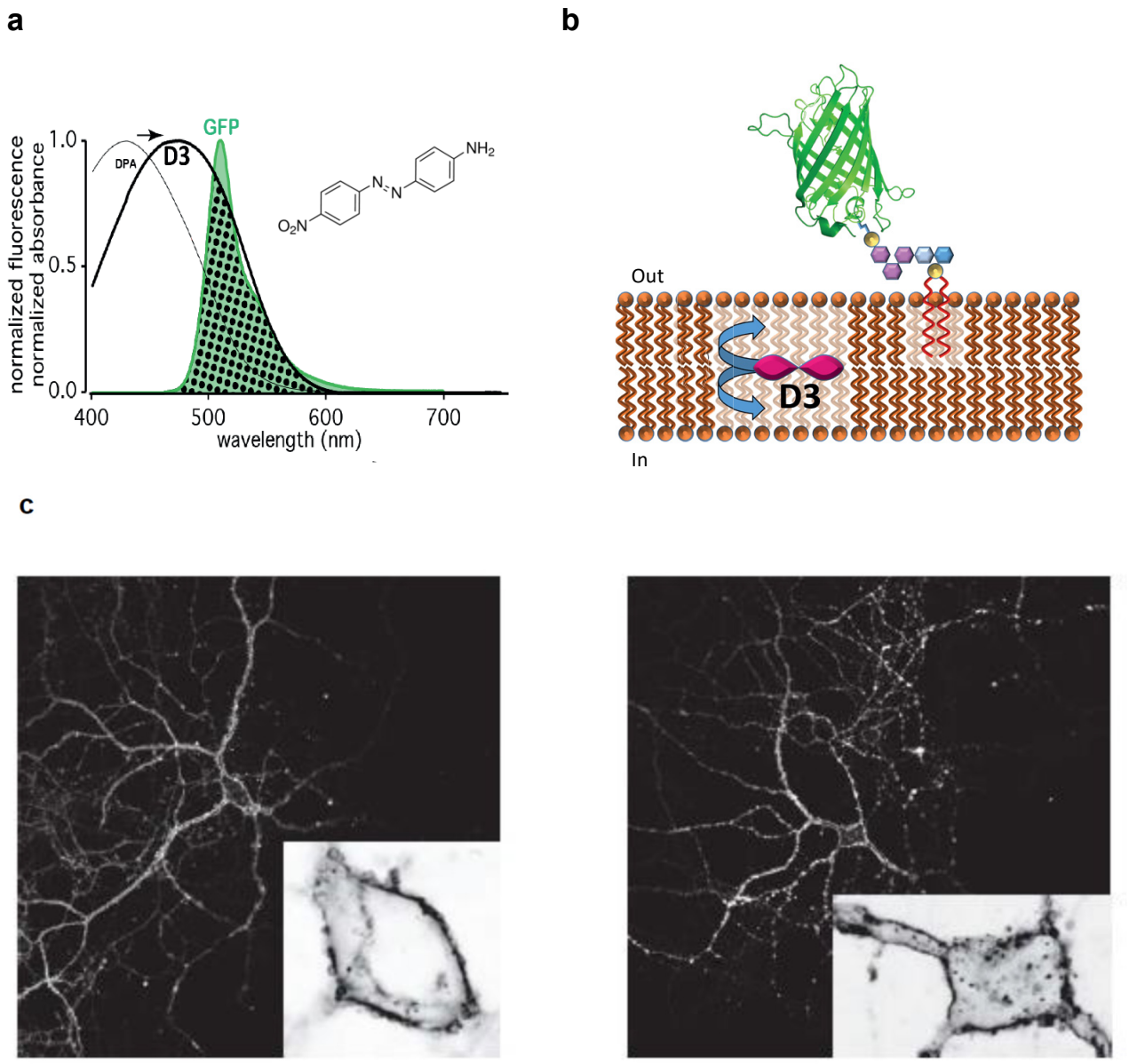

Figure S1. **The new hGEVI method and GPI-eGFP labelled neurons**. (**a**) Absorbance spectra of DPA and Disperse Orange 3 (D3) superimposed on the emission spectrum of eGFP. The regions of overlap between absorbance and eGFP emission are shaded. Note the better spectral overlap for D3 which should increase the FRET. *Inset*: Structure of D3 (4-amino-4'-nitroazobenzene). (**b**) The light emitted following the excitation of a genetically encodable fluorophore, preferably expressed only in the plasma membrane (here depicted as GPI-eGFP), is quenched by a small lipophilic molecule that rapidly changes FRET efficiency by changing the Förster radius and/or by moving in the membrane in a voltage-dependent manner (summarized here as movement of D3). (**c**) Confocal images of two rat cortical neurons in the same culture expressing GPI-eGFP 6 weeks after AAV transduction. Typically, neurons were used for experiments 2-3 weeks after transduction. Insets show the somata 4-fold magnified in reverse color to emphasize the fluorescence in the membrane.

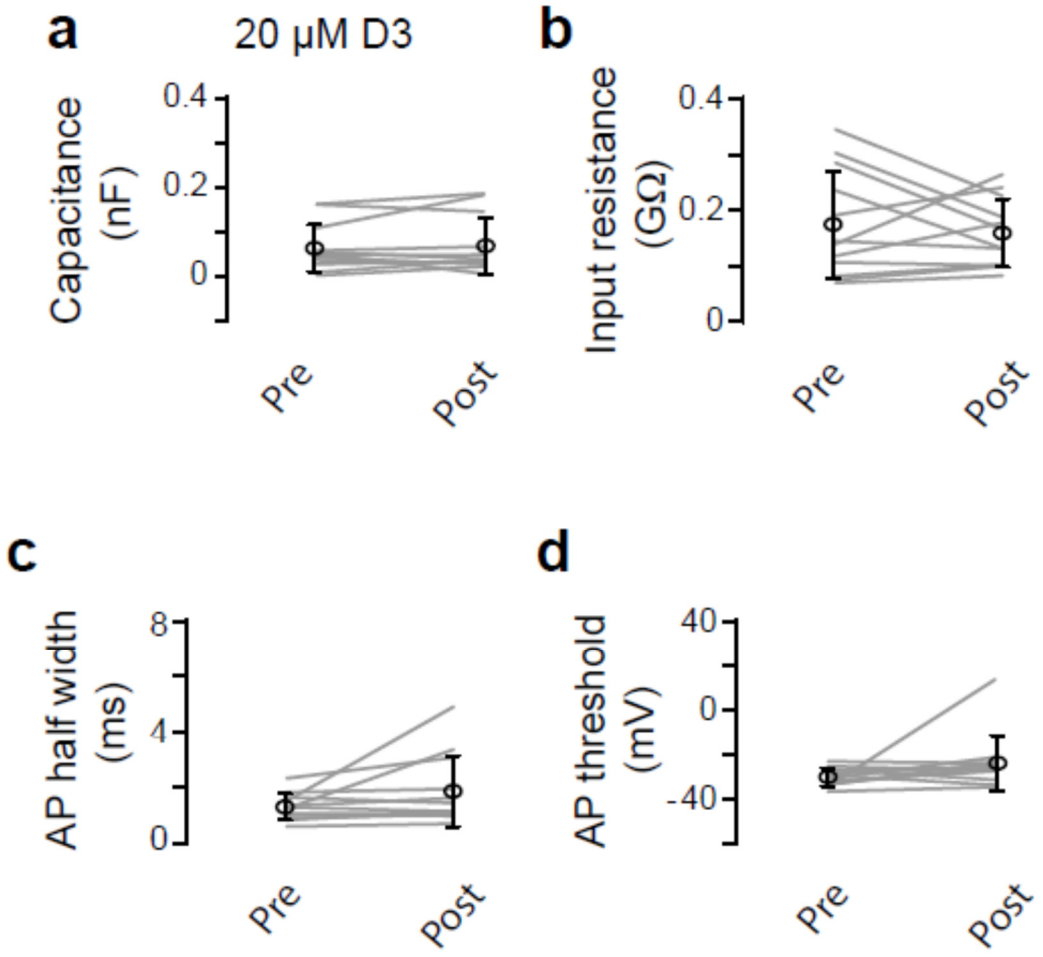

Figure S2. Lack of effects of D3 on passive membrane and AP properties. Whole-cell recordings were carried out in cultured neurons (n=12) without the expression of GPI-eGFP. Each measurement was taken before (*Pre*) and 10 min after (*Post*) the perfusion of 20 μM D3 (in 0.2% DMSO), a concentration 2-fold higher than that used in the hGEVI experiments. (**a**) Membrane capacitance, (**b**) input resistance, (**c**) AP width measured at 50% amplitude, also referred to as FWHM, and (**d**) AP threshold measured as the voltage at the first peak of the third derivative of the membrane potential. All statistical comparisons are done using Wilcoxon matched-pairs signed rank tests.

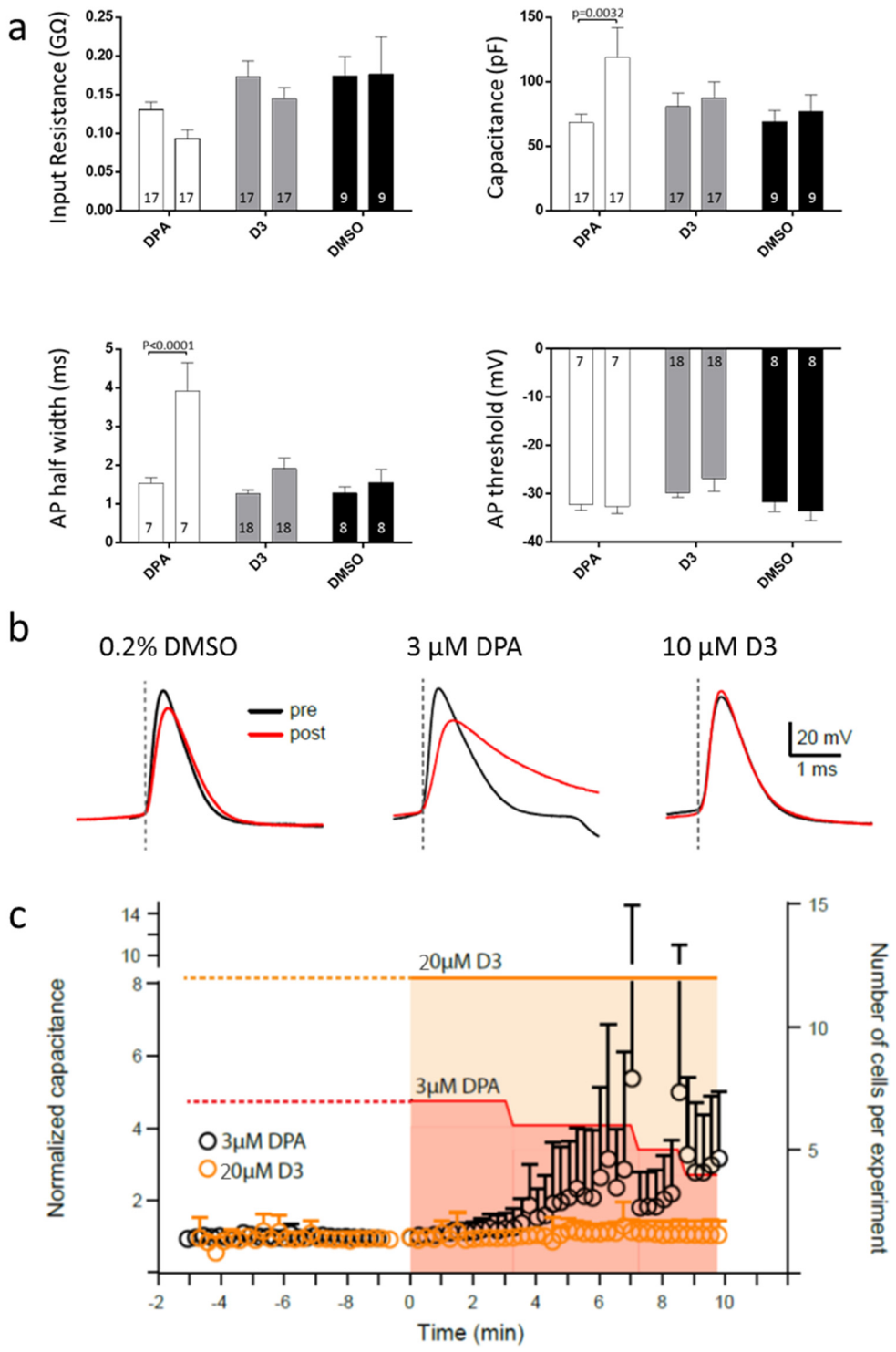

Figure S3. Comparison of the effects of DMSO, DPA and D3 on passive membrane and AP properties. Whole-cell recordings were carried out in cultured neurons without the expression of GPI-eGFP. (**a**) Comparisons of input resistance (Rn), membrane capacitance (Cm), AP width measured at 50% amplitude (FWHM), and AP threshold (APth) measured as the voltage at the first peak of the third derivative of the membrane

potential. Measurements for Rn and Cm were taken before (*Left bars*) and 5 min after (*Right bars*) the perfusion of DPA (2.5 μM, n=7; 3 μM, n=6; and 5 μM, n=4 cells; total pooled n = 17 cells), D3 (10 μM, n=6; and 20 μM, n=11 cells; total pooled n = 17 cells), and DMSO (0.2%, n = 9 cells). The only significant effect was the increase in Cm by DPA (from 68.31 ± 6.46 to 118.63 ± 23.33 pF; p=0.0032). The values for FWHM and APth were assessed before (*Left bars*) and 10 min after (*Right bars*) the perfusion of DPA (2.5 μM, n=7 cells), D3 (10 μM, n=6; and 20 μM, n=12 cells; total pooled n = 18 cells), and DMSO (0.2%, n = 8 cells). The only significant effect was the increase in FWHM by DPA (from 1.537 ± 0.140 to 3.911 ± 0.737 ms; p<0.0001). Significance was assessed by post two-way ANOVA Sidak's multiple comparisons tests with p-values adjusted for multiple comparisons. (**b**) Representative APs during three experimental conditions before (*pre*, *black*) and 10 min after (*post*, *red*) perfusion of the compounds indicated above the traces. Dashed vertical lines mark AP threshold. (**c**) Evolution of Cm changes and cell survival during the time following perfusion of 3 μM DPA or 20 μM D3. Left axis represents normalized mean Cm (± SEM) calculated as the ratio to the averaged value of the pre-perfusion period. Right axis shows the number of cells. The number of cells (dotted to solid lines) surviving the perfusion of DPA gradually diminished over the period of 10 min, whereas no cells were lost to D3 perfusion.

B Publication #2: Bringing to light the physiological and pathological firing patterns of human induced pluripotent stem cell-derived neurons using optical recordings

frontiers | Frontiers in Cellular Neuroscience

TYPE Original Research
PUBLISHED 17 January 2023
DOI 10.3389/fncel.2022.1039957

OPEN ACCESS

EDITED BY
Kevin Beier,
University of California, Irvine,
United States

REVIEWED BY
Jessica Elaine Young,
University of Washington, United States
Matthias Prigge,
Leibniz Institute for Neurobiology (LG),
Germany
Ken Berglund,
School of Medicine, Emory University,
United States

*CORRESPONDENCE
Istvan Mody
✉ mody@ucla.edu

†PRESENT ADDRESSES
Balint Szalontai,
Laboratory for Retinal Gene Therapy,
Department of Ophthalmology,
University Hospital Zurich, University of
Zurich, Zurich, Switzerland
Kurt Golcuk,
Department of Neuroscience,
School of Medicine, Johns Hopkins
Medicine, Baltimore, MD, United States

‡These authors have contributed
equally to this work

SPECIALTY SECTION
This article was submitted to
Cellular Neuropathology,
a section of the journal
Frontiers in Cellular Neuroscience

RECEIVED 08 September 2022
ACCEPTED 22 December 2022
PUBLISHED 17 January 2023

CITATION
Alich TC, Röderer P, Szalontai B,
Golcuk K, Tariq S, Peitz M, Brüstle O
and Mody I (2023) Bringing to light
the physiological and pathological
firing patterns of human induced
pluripotent stem cell-derived neurons
using optical recordings.
Front. Cell. Neurosci. 16:1039957.
doi: 10.3389/fncel.2022.1039957

Bringing to light the physiological and pathological firing patterns of human induced pluripotent stem cell-derived neurons using optical recordings

Therese C. Alich[1‡], Pascal Röderer[2,3‡], Balint Szalontai[1†], Kurt Golcuk[1†], Shahan Tariq[2], Michael Peitz[2,4], Oliver Brüstle[2] and Istvan Mody[1,5*]

[1]Institute of Experimental Epileptology and Cognition Research, Medical Faculty, University Hospital Bonn, Bonn, Germany, [2]Institute of Reconstructive Neurobiology, Medical Faculty, University Hospital Bonn, Bonn, Germany, [3]Cellomics Unit, LIFE & BRAIN GmbH, Bonn, Germany, [4]Cell Programming Core Facility, Medical Faculty, University of Bonn, Bonn, Germany, [5]Department of Neurology, David Geffen School of Medicine at UCLA, Los Angeles, CA, United States

Human induced pluripotent stem cells (hiPSCs) are a promising approach to study neurological and neuropsychiatric diseases. Most methods to record the activity of these cells have major drawbacks as they are invasive or they do not allow single cell resolution. Genetically encoded voltage indicators (GEVIs) open the path to high throughput visualization of undisturbed neuronal activity. However, conventional GEVIs perturb membrane integrity through inserting multiple copies of transmembrane domains into the plasma membrane. To circumvent large add-ons to the plasma membrane, we used a minimally invasive novel hybrid dark quencher GEVI to record the physiological and pathological firing patterns of hiPSCs-derived sensory neurons from patients with inherited erythromelalgia, a chronic pain condition associated with recurrent attacks of redness and swelling in the distal extremities. We observed considerable differences in action potential firing patterns between patient and control neurons that were previously overlooked with other recording methods. Our system also performed well in hiPSC-derived forebrain neurons where it detected spontaneous synchronous bursting behavior, thus opening the path to future applications in other cell types and disease models including Parkinson's disease, Alzheimer's disease, epilepsy, and schizophrenia, conditions associated with disturbances of neuronal activity and synchrony.

KEYWORDS

iPSC-derived sensory neurons, dark quencher genetically encoded voltage indicator, action potential firing patterns, inherited erythromelalgia, GABA, glutamate, co-cultures, synchronous burst firing

1. Introduction

Induced pluripotent stem cell (iPSC)-derived neurons represent a promising tool for modeling human neuropsychiatric and neurological diseases *in vitro* (Okano and Yamanaka, 2014). The possibility to generate unlimited numbers of disease and patient-specific neurons has been exploited to study a variety of pathological phenotypes ranging from epigenetic alterations and changes in gene expression to morphological, subcellular and biochemical pathologies. While a number of studies uncovered disease-specific changes in neuronal function, high-resolution assessments of neuronal activity and connectivity have remained challenging.

Action potential (AP) firing patterns, consisting of single spikes or complex bursting activity, are essential for communication between neurons and within neuronal networks. Temporal features of spike trains are critical for the communication between pre- and postsynaptic neurons. If neurons fire in bursts, information transfer within neuronal networks is augmented due to the enhanced probability of inducing postsynaptic neurons to fire APs (Lisman, 1997; Izhikevich et al., 2003) and increases the likelihood of synaptic potentiation (Pike et al., 1999). Yet, accurate und undisturbed detection of AP firing of single identified neurons, including fast successive APs within bursts, constitutes a major challenge. Finding an ideal method suited for monitoring the activity of hiPSC-derived neurons is difficult, as it should have single cell resolution and should be suitable for high throughput analyses, in order to account for heterogeneous populations of neurons. Furthermore, neuronal activity comprises many facets from hyperpolarization, subthreshold events to high-frequency AP trains, which should all be mapped by the method of choice. Ideally, the method should be non-invasive to not distort the activity of the monitored neurons. Electrophysiological methods are still the most widely used approaches to assess hiPSC-derived neuronal activity: multi electrode arrays (Thomas et al., 1972) can display the activity of whole neuronal ensembles, but cannot adequately resolve APs of single identified neurons, failing to discriminate different cellular subtypes. Patch-clamp techniques display the whole spectrum of neuronal activity at a single cell level (Neher and Sakmann, 1976) but are inherently time consuming, and invasive, as the interior of the cell is dialyzed by the intracellular solution in the patch pipette, which may have unpredictable effects on physiological intracellular events.

Genetically encoded optical activity sensors enable the targeting of specific neuronal subtypes and make possible the concomitant visualization of cellular ensembles. Genetically encoded calcium Indicators (GECIs) are the most widely used genetically encoded optical activity sensors and have been used in hiPSC-derived neuronal models (Real et al., 2018; Samarasinghe et al., 2021). However, GECIs have major drawbacks as they are only an indirect measure of neuronal activity, do not allow monitoring the whole spectrum of neuronal activity such as hyperpolarization and subthreshold events, and are too slow to resolve high frequency APs. Importantly, GECIs also act as calcium buffers and thereby interfere with intracellular calcium signaling (McMahon and Jackson, 2018), which can alter physiological firing patterns of neurons.

In contrast to GECIs, genetically encoded voltage indicators (GEVIs) directly and rapidly measure the electrical potential across the plasma membrane and thus constitute a desirable method to monitor neuronal activity. A major challenge associated with GEVIs is the minimal space, restricted to the plasma membrane, available for sensor molecule placement allowing for three orders of magnitude less GEVI molecules per cell than GECI molecules located in the cytoplasm (Peron et al., 2015). This paucity of GEVI molecules leads to the need for high illumination intensities in turn causing rapid photobleaching and phototoxic effects (Carlton et al., 2010). The sensor molecules in most GEVIs (Bando et al., 2019a,b; Kannan et al., 2019; Milosevic et al., 2020) are protein transmembrane domains, which span the plasma membrane and change the electrical properties of the cell increasing capacitance and decreasing membrane resistance (Akemann et al., 2009; Cao et al., 2013).

Here we use a recently published dark quencher hybrid GEVI (dqGEVI) method for the undisturbed visualization of hiPSC-derived neuronal activity. Compared to other GEVIs, the hybrid dqGEVI is non-invasive and preserves membrane integrity (Alich et al., 2021). The approach circumvents the insertion of transmembrane domains into the cell membrane by using a fluorescent protein tagged onto the outer leaflet of the plasma membrane through a glycosylphosphatidylinositol (GPI)-anchor. This method, together with a voltage-sensing dark fluorescence quencher, disperse orange 3 (D3), has been extensively tested and shown to lack adverse effects on neuronal properties (Alich et al., 2021). We used the dqGEVI for the first time in a human *in vitro* disease-modeling study involving iPSC-derived sensory neurons.

Chronic pain is the leading cause of disability worldwide (Rice et al., 2016) with a prevalence of up to 40% (Tsang et al., 2008; Johannes et al., 2010) and a comorbidity with a number of highly widespread disorders, such as cancer, diabetes and HIV-induced peripheral neuropathy. As a large percentage of patients report their pain treatment as unsatisfactory, new therapeutics and novel cellular models are urgently needed. Using dqGEVI we monitored the spontaneous activity of hiPSC-derived sensory neurons (hiPSCdSN) at physiological temperatures. We applied this approach to hiPSCdSN derived from patients with inherited erythromelalgia (EM), a genetic chronic pain disorder with recurrent attacks of pain, swelling and redness of distal extremities. We show that dqGEVI enables the detection of significant differences in bursting behavior when compared to hiPSCdSNs from a non-EM cell line, a

phenotype that has not been detected in a previous patch-clamp based study using the same cell line (Cao et al., 2016). Moreover, as in patients, where pain attacks can be triggered by mild increases in ambient temperature, dqGEVI enabled visualization of hyperexcitability in EM patient neurons upon temperature increase, a response absent in cells derived from the non-EM cell line.

To illustrate the general applicability of our approach we also recorded human iPSC-derived forward programmed GABA- and glutamatergic forebrain neurons termed iGABANs and iGlutNs, respectively (Peitz et al., 2020). In co-cultures of iGABANs and iGlutNs we observed spontaneous synchronous bursting behavior. This promising finding suggests that the dqGEVI will be broadly applicable to various other disease models such as Alzheimer's and Parkinson's disease, epilepsy and schizophrenia, conditions associated with disturbances of neuronal activity and synchrony (Uhlhaas and Singer, 2006).

2. Materials and methods

2.1. AAV production

The tetracycline operon system ("Tetbow" principle) (Sakaguchi et al., 2018) was used to enhance expression of GPI-eGFP, the genetically encoded component of the dqGEVI in iPSC-derived neurons. The template plasmid (pCAG Arc-eGFP-GPI) encoding GPI-eGFP was constructed by VectorBuilder, all other plasmids were purchased from Addgene. The coding region was subcloned to the pAAV-TRE-tdTomato-WPRE plasmid (Addgene ID: 104112) using the EcoRI and HindIII cut sites to give rise to the pAAV-TRE-GPI-eGFP-WPRE construct. This, and the pAAV-Syn1-tTA (Addgene ID: 104109) plasmids were used to produce recombinant adeno-associated viruses (rAAVs; mosaic "pseudotype" of AAV1 and AAV2) as described in our previous work (Alich et al., 2021) and originally by Hauck and Chen (2003). Functional titers (3.67 × 10e9 TU/ml for the TRE-GPI-eGFP-WPRE vector, and 5.81 × 10e9 TU/ml for the Syn1-tTA vector) were measured using *in vitro* limiting dilution assay.

2.2. hiPSC cultures

This study employed the wild type hiPSC-line UKBi013-A[1] and the patient hiPSC-line RCi001-A[2]. The use of hiPSC-lines was approved by the Ethics Committee of the Medical Faculty of the University of Bonn (approval number 275/08), and informed consent was obtained from the donors. hiPSCs were cultured in StemMACS iPS-Brew (Miltenyi Biotec) and split with EDTA during maintenance. Quality control of hiPSCs for pluripotency (flow cytometric analysis of Tra1-60 expression) and genomic integrity (SNP analysis) was performed on a routine basis before *in vitro* differentiation as previously described (Elanzew et al., 2020).

2.3. Differentiation of hiPSCs into sensory neurons

Differentiation of hiPSCs into sensory neurons was performed following the protocol from Chambers et al. (2012) with slight modifications: In detail single cell suspensions of hiPSCs were seeded at suitable densities in StemMAC iPS-Brew in the presence of 10 μM ROCK inhibitor Y-27632 on Geltrex coated T175-flasks at day 1. Initial seeding densities needed to be determined for each cell line and can range between 3×10^5 and 10×10^5 cells/cm^2. A total of 24 h after plating medium was changed to differentiation medium. Two basal media were used during differentiation: Medium 1 consists of Knock out DMEM with 20% Knock Out Serum Replacement, 2 mM (1x) GlutaMAX, 100 μM (1x) NEAA and 0.02 mM 2-mercaptoethanol. Medium 2 consists of Neurobasal Media supplemented with 1% N2 supplement, 2% B27 supplement, 2 mM (1x) GlutaMAX, and 0.02 mM 2-Mercaptoethanol. Between day 0 and day 3 cells were kept in Medium 1, from day 4 to 5 cells were kept in 75% Medium 1 and 25% Medium 2, for day 6 cells were kept in 50% Medium 1 and 50% Medium 2, from day 7 to 9 cells were kept in 25% Medium 1 and 75% Medium 2 and from day 10 to 14 differentiating cells were kept in 100% Medium 2. Neuronal differentiation was induced by dual-SMAD inhibition. 100 nM LDN 193189 and 10 μM SB 431542 were added from day 0 to day 6. To specify the differentiating cells into sensory neurons 3 μM CHIR 99021, 10 μM SU 5402 and 10 μM DAPT were added to the culture from day 3 to day 14. At day 14 of differentiation, cells were dissociated to single cells by treatment with accutase for 45–60 min, centrifuged at 400 × g for 10 min, resuspended in cold CryoStor CS10 freezing medium and frozen at −80°C in freezing boxes. Frozen cells were transferred to a liquid nitrogen tank for long-term storage after 24 h.

Frozen hiPSC-derived sensory neurons were thawed, counted and plated at a density of 40,000 cells per 12 mm coverslip (Neuvitro Corporation, GG-12-PLO-Laminin, Camas, WA, USA) in maturation media supplemented with 10 μM ROCK inhibitor Y-27632. Coverslips were pre-coated with 360 μg/ml Geltrex for 1 h at room temperature. Maturation medium consists of Neurobasal A Medium supplemented with 1% N2 supplement, 2% B27 supplement, 2 mM (1x) GlutaMAX, 0.02 mM 2-mercaptoethanol, 12 μg/ml gentamicin, 200 μM ascorbic acid, 0.1 μg/ml human recombinant laminin (BioLamina, LN521), 10 ng/ml GDNF, 10 ng/ml BDNF,

1 https://hpscreg.eu/cell-line/UKBi013-A

2 https://cells.ebisc.org/RCi001-A

10 ng/ml NGF, and 10 ng/ml NT3. Medium was changed after 24 h to remove ROCK inhibitor. After 3 days cells were treated with 1 μg/ml Mitomycin C (Sigma Aldrich, M4287) for 2 h at 37°C to inactivate proliferative cells. Recombinant adeno-associated viruses (rAAVs) were added on day 6 after thawing (2 μl AAV-Syn tTA; 2 μl AAV- TRE-GPI-eGFP-WPRE) and were incubated with the cells for 1 week without media change. Afterwards, the medium was changed twice per week. Cells were matured for at least 6 weeks prior to functional analysis.

2.4. Differentiation of hiPSCs into iGlutNs and iGABANs

Induced forebrain glutamatergic neurons (iGlutNs) and GABAergic neurons (iGABANs) were generated by controlled overexpression of NGN2 and ASCL + DLX2 in hiPSCs (lines iLB-C14-s11-NGN2 and iLB-C-133-s4-APD) as described (Rhee et al., 2019; Peitz et al., 2020). Mixed cultures comprising 80% iGlutNs and 20% iGABANs (both 8 days after transgene induction) were plated at a density of 1,000 cells/mm^2 in 24-well plates containing Matrigel-coated glass cover slips. The following day 50% of the medium was changed to fresh pre-warmed NBB27 medium (Neurobasal medium, 1x B27 supplement, 1x GlutaMax, 10 ng/ml BDNF, 2–4 μg/ml laminin and 1 μg/ml doxycycline). After 1 h rAAVs were added and incubated overnight after which the medium was changed to 0.5 ml/well of fresh pre-warmed astrocyte-conditioned NBB27. For the following 3 days medium was changed daily, and on day 4 post transduction mouse astrocytes generated from P1 pups were added in NBB27/FBS (Neurobasal medium, 1x B27 supplement, 1x GlutaMax, 10 ng/ml BDNF and 0.5% heat-inactivated FBS) medium to stabilize neuronal maturation. Medium changes with NBB27/FBS were done twice a week until the start of measurements.

2.5. Confocal imaging

To demonstrate plasma membrane targeting of the GPI-eGFP fusion protein, images of transgene-expressing neurons were taken using confocal laser scanning microscopy (Fluoview 1000, Olympus) at 40 × magnification. Cells were fixed with 4% paraformaldehyde for 10 min and coated with DAPI-Vectashield mounting medium (Vector Laboratories) prior to imaging.

2.6. Immunofluorescence characterization of hiPSC-derived sensory neurons

Cells fixed in 4% PBS-buffered paraformaldehyde for 10 min were permeabilized with 0.3% Triton X-100 in PBS for 15 min at room temperature, to stain for intracellular proteins. After washing, cells were incubated for 1 h at room temperature in blocking buffer (PBS, 5% normal donkey serum (NDS), 0.1% Triton X-100). Primary antibodies were incubated overnight at 4°C in PBS supplemented with 1% NDS and 0.1% Triton-X100 (mouse-anti-Islet1, Abcam, Cambridge, UK ab86501, 1:100; mouse-anti-Peripherin, Santa Cruz Biotechnology, Dallas, USA, sc-377093, 1:200; rabbit-anti-Brn3a, Merck, Darmstadt, Germany, AB5945, 1:200; rabbit-anti-Nav1.8, Alomone Labs, Jerusalem, Israel, ASC-016, 1:200). Cells were washed twice with PBS and incubated with secondary antibodies for 1 h at room temperature. Secondary antibodies were diluted 1:500 in PBS supplemented with 1% NDS and 0.1% Triton-X100 (donkey-anti-rabbit IgG-Alexa Fluor® 488, Thermo Fisher, Waltham, MA, USA, A-21206; donkey-anti-mouse IgG-Alexa Fluor® 594, Thermo Fisher; donkey-anti-goat IgG-Alexa Fluor® 647, Thermo Fisher, A-21203). Extracellular markers were stained accordingly, but without the permeabilization step and without Triton-X100 in any of the incubation and blocking solutions (mouse-anti-Nav1.7, Abcam, ab85015, 1:100; goat-anti-hRet, R&D Systems, Minneapolis, MN, USA, AF1485, 1:200). After washing, coverslips were mounted on high precision cover glasses using Fluoromount-G with DAPI (Invitrogen, 00-4959-52). Images were taken with ZEISS Axio Imager Z1 equipped with an Apotome 1.0.

2.7. Genomic DNA isolation and Sanger sequencing

Genomic DNA was isolated of wild type and patient hiPSC using Qiagen DNeasy Blood and Tissue Kit. The DNA section harboring the SCN9A V400M mutation in the patient cell line was amplified *via* PCR, using the NEB Q5® High-Fidelity 2X Master Mix with the 5′-ATT TCC ATT TTT CCC TAG ACG CTG-3′ forward, and the 5′-TAC CTC AGC TTC TTC TTG CTC TTT-3′ reverse, primers (Cao et al., 2016). Amplicons were purified and analyzed by Sanger sequencing.

2.8. Optical recordings

Reagents for electrophysiological and optical experiments were purchased from Sigma (St. Louis, MO, USA) unless indicated otherwise. Optical experiments were conducted using an Olympus BX61WI microscope (Olympus Corporation, Tokyo, Japan) equipped with epifluorescence and DIC. A scientific complementary metal-oxide-semiconductor (sCMOS) camera (Prime 95B, Teledyne Photometrics, Tucson, AZ, USA) was used to visualize neurons and to verify fluorescence. GPI-eGFP expressing cultured hiPSC-derived sensory neurons 8–10 weeks, and cortical neurons 10–13 weeks after viral transduction were transferred to a modified

submerged chamber (Hill and Greenfield, 2011) and perfused with HEPES-buffered ACSF (3 ml/min at 37 ± 0.5°C, in mM): 135 mM NaCl, 4.7 mM KCl,1 mM CaCl2, 1 mM MgCl2, 10 mM Hepes, and 10 mM glucose (pH was adjusted to 7.4 with NaOH). Recordings were started after a ∼5 min preincubation period with ACSF containing of the diazobenzene dye D3 (2 μM) in 0.02% DMSO. The sCMOS camera was controlled by μManager software (Edelstein et al., 2014). Expression of GPI-eGFP was verified using epifluorescence. Excitation illumination (470 nm) at 3–5 $mWcm^{-2}$ was provided with a custom made light source (parts from Thorlabs Inc, Newton, NJ, USA with a Luxeon Rebel 470 nm LED LXML-PB01-0040) that was driven by a custom made TTL switched stable current source. The excitation light as well as the collected fluorescence were filtered using a FITC filter set (Ex: HQ480/40x; Di: Q505LP; Em: HQ535/50 m, Chroma Technology Corp., Bellow Falls, VT, USA). For optical voltage imaging, frame rates of 976 FPS were achieved using smaller field of view [regions of interest (ROIs)] with 52 pixels in the vertical plane and variable pixel in the horizontal plane. Camera was used in 12 bit sensitivity mode resulting in a gain of 0.67 e-/ADU. Exposure time was 1 ms. No binning was applied. Imaging traces were usually recorded for 10 s.

For heat sensitivity experiments hiPSC - derived sensory neurons were heated to 40°C with a custom-made perfusion system. Temperature was calibrated before each recording and controlled for deviations from set temperature of 40°C before and after each recording. Imaging traces were recorded for 30 s. In some experiments, the Nav1.7 Inhibitor (PF-05089771, Tocris Cat. No. 5931, Batch No: 1A/225855) was applied to the cells after heating to 40°C (**Supplementary Figure 3B**).

For Nav1.7 specificity experiments the Nav1.7 Inhibitor (PF-05089771, end concentration 60 and 110 nM) was added to the ACSF and active cells were perfused (3 ml/min at 37 ± 0.5°C) with the custom-made perfusion system.

For all experiments a 100 mM stock solution was prepared in DMSO and stored at −20°C.

2.9. Image processing pipeline

The video frames were processed using a custom-written app in MATLAB (MathWorks, USA). The stack of frames was loaded as grayscale images. An image file from the whole stack was selected as a reference frame for further image processing and finding the ROIs of the cells. The reference frame was filtered using a 2D Gaussian kernel with a standard deviation of one for removing noise. The grayscale image was binarized using the adaptive threshold method. The cells in the field of view were segmented after applying morphological image processing operations and then the reference ROIs were automatically generated. The mean intensity in the ROI of each frame in the whole stack was calculated and used as the fluorescence signal of the corresponding cell. The extracted intensity for each frame was plotted to obtain the fluorescence signal in the time domain. A linear fit was applied to the fluorescence trace to detrend a small drift caused by the camera. Then, the intensity values were converted into ΔF/F (%) scale. Spikes were detected using a threshold value of 3–5 standard deviation above the mean (**Supplementary Figure 2**).

2.10. Patch-clamp experiments

For electrophysiological recordings whole-cell patch clamp recordings were amplified using a Multiclamp 700B amplifier (Molecular Devices, Sunnyvale, USA), low-pass filtered at 10 kHz and digitized at 50 kHz with a NI USB-6341 (National Instruments, Austin, TX, United States) controlled by Strathclyde Electrophysiology Software WinWCP (John Dempster, University of Strathclyde, Glasgow, UK). Data were stored on a hard disk for offline analyses. Pipettes were pulled from borosilicate glass (King Precision Glass, Inc., Claremont, CA, USA) using a DMZ Zeitz puller (Zeitz-Instruments, Martinsried, Germany). Patch pipettes had resistances of 3–5 MΩ and contained (in mM): 135 K-Gluconate, 5 KCl, 10 HEPES, 0.1 ethylene glycol-bis (2-aminoethylether)-N,N,N′,N′-tetraacetic acid (EGTA), 1 $MgCl_2$, 3 MgATP, 0.2 Na_2ATP at pH 7.2.

3. Results

3.1. Expression of dqGEVI and optical detection of spontaneous spiking activity in hiPSC-derived sensory neurons

Human induced pluripotent stem cells from a healthy donor with a wild type *SCN9A* gene (UKBi013-A) and an EM-patient, suffering from a gain-of-function mutation in the *SCN9A* gene (RCi001A) previously characterized as "EM3" in Cao et al. (2016) were differentiated into immature sensory neurons within 14 days using a small-molecule based protocol and cryopreserved (**Supplementary Figure 1**). Cells are referred to as EM patient hiPSCdSNs and control hiPSCdSNs (for EM patient and control cells, respectively). The dqGEVI genes were delivered *via* AAV-based transduction (see section "2 Materials and methods"), 6 days after thawing and plating of the hiPSCdSN (**Figure 1A**). Analysis of marker expression and optical recordings of hiPSCdSNs were performed after 6–8 weeks culture in growth factor containing medium. At that time hiPSCdSN showed clustering, forming ganglion-like structures and a dense neuronal network. Immunofluorescence analysis revealed expression of classic sensory neuron markers including BRN3A, ISLET1, PRPH, and hRET, as well as the peripheral neuron specific voltage gated sodium channels

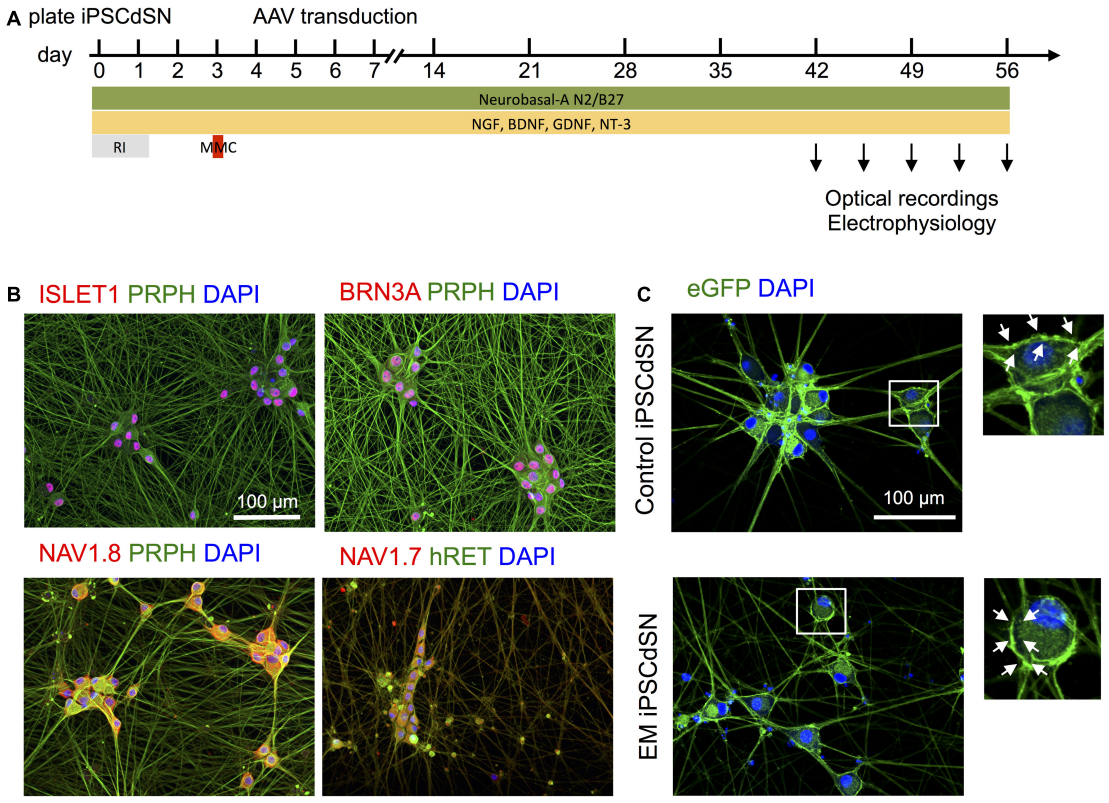

FIGURE 1
(A) *In vitro* cultivation and adeno-associated viruse (AAV) transduction paradigm for human induced pluripotent stem cell (hiPSC)-derived sensory neurons. RI, ROCK-Inhibitor, MMC: Mitomycin C. **(B)** Human induced pluripotent stem cell-derived sensory neuron (hiPSCdSN) express typical sensory neural marker, such as ISLET1, BRN3A, and PRPH, as well as peripheral sodium channels Nav1.7 and Nav1.8. **(C)** Dark quencher hybrid genetically encoded voltage indicator (dqGEVI) specifically labels the sensory neuronal cell membrane. EM, erythromelalgia.

Nav1.7 and Nav1.8 in virtually all neurons after 8 weeks of *in vitro* culture (Figure 1B). Expression of dqGEVI was confirmed by detection of native eGFP expression (Figure 1C). EGFP expression was robust and restricted to the plasma membrane at the soma with only a few of the cells expressing intracellular fluorescence, most likely at the ER membrane. There were no intracellular punctae as described elsewhere with other voltage indicators (Kiskinis et al., 2018).

Expression of dqGEVI does not affect passive or active membrane properties of primary mouse neurons (Alich et al., 2021). To verify these observations in hiPSCdSNs we performed manual patch-clamp experiments in cells transduced with dqGEVI and PBS as control. We did not observe differences in input resistance (R_{in}), membrane capacitance (C_m), time constant, and resting membrane potential (V_{rest}) after expression of dqGEVI in EM patient hiPSCdSN (pt) and control hiPSCdSNs (Ctrl) (R_{in}: pt: dqGEVI: 105.5 ± 11.34 MΩ (n = 11), PBS: 80.8 ± 9.99 MΩ (n = 11), Ctrl: dqGEVI: 61.1 ± 4.2 MΩ (n = 10), PBS: 48.3 ± 5.1 MΩ (n = 13), p = 0.27; C_m: pt: dqGEVI: 128 ± 10 pF (n = 11), PBS: 167 ± 26 pF (n = 11), Ctrl: dqGEVI: 169 ± 11 pF (n = 10), PBS: 231 ± 31 pF (n = 13), p = 0.15; time constant: pt: dqGEVI: 0.012 ± 0.0004 ms (n = 11), PBS: 0.011 ± 0.0006 ms (n = 11), Ctrl: dqGEVI: 0.010 ± 0.0007 ms (n = 10), PBS: 0.010 ± 0.0013 ms (n = 13), p = 0.06; V_{rest}: pt: dqGEVI: -53.1 ± 2.44 mV (n = 11), PBS: -58.8 ± 1.3 mV (n = 11), Ctrl: dqGEVI: -52.5 ± 1.41 mV (n = 10), PBS: -55.65 ± 1.2 mV (n = 13), p = 0.06; Kruskal-Wallis test, significance level α = 0.05) indicating that the integrity of the plasma membrane is fully preserved. Additionally, as we did not observe a difference in these parameters between control hiPSCdSN and EM patient hiPSCdSN, we conclude that the differences in firing patterns between control hiPSCdSN and EM patient hiPSCdSN were not due to differences in passive membrane characteristics.

3.2. A hyperactive phenotype in EM patient hiPSCdSNs

We assessed the number of spontaneously active cells in the EM patient hiPSCdSNs and control hiPSCdSNs using an automated cell finding and evaluation pipeline (described in

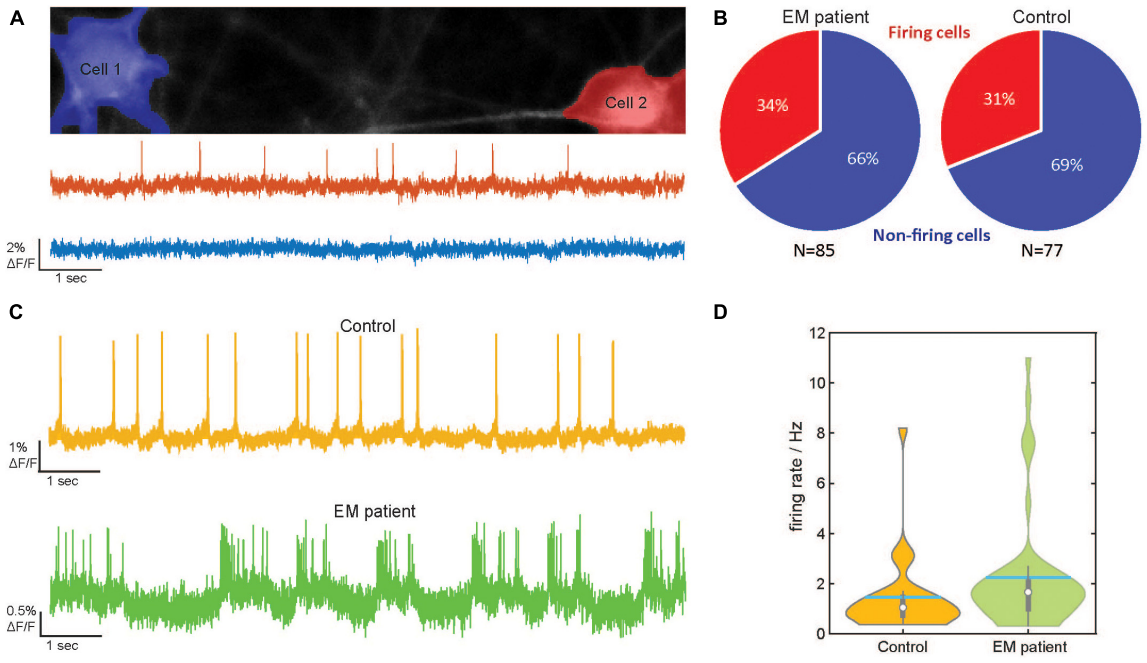

FIGURE 2
Optical detection of spontaneous spiking in human induced pluripotent stem cell -derived sensory neurons (hiPSC–SNs) from an erythromelalgia (EM) patient and control. **(A)** Top: Images of two (Cell 1 in blue and Cell 2 in red) control hiPSC–SNs expressing dark quencher hybrid genetically encoded voltage indicator (dqGEVI). Somata were detected with an automated soma detection and evaluation procedure. Bottom: Raw imaging traces of cell 1 (blue) and cell 2 (red). **(B)** Pie-graphs showing the percentage of spontaneously firing cells from EM patient (Total N = 85, active N = 29) and control (Total N = 77, active N = 24). **(C)** Representative raw imaging traces of spontaneous firing behavior of hiPSC-SNs from the EM patient (bottom) and control (top). **(D)** Violin plots of the firing rate distribution in the EM patient human induced pluripotent stem cell-derived sensory neurons (hiPSCdSNs) (N = 45) and the control hiPSCdSNs (N = 27). The thin vertical black line indicates the 95% confidence interval. The thick vertical black line indicates the interquartile range. The median is indicated by the white dot. Spiking frequency is significantly higher in hiPSCdSNs from EM patients (Wilcoxon Rank test, WRT, p = 0.03).

"2 Materials and methods"). The pipeline provides algorithms to automatically identify and segment neurons (**Figure 2A**, top), to extract the fluorescent signals and to detect spikes (**Figure 2A**, bottom). Other approaches for voltage imaging analysis make use of image processing algorithms (Kiskinis et al., 2018; Cai et al., 2021) to extract the fluorescent signal. Notably, in our analyses data were not filtered, smoothed or averaged for analysis as the single raw optical traces possessed sufficient signal to noise ratio for accurate spike detection (**Figures 2A, C**).

Analysis of the imaging traces revealed that in both groups about a third of the cells showed spontaneous activity (EM patient: 34% active cells of total n = 85; control 31% active cells of total n = 77; **Figure 2B**). These results are partially in line with the findings from Cao et al. (2016), who detected 35% spontaneously active EM neurons. However, in contrast to our data, only 0–14% of their control neurons showed signs of spontaneous activity. This discrepancy could be due to intrinsic heterogeneity among the hiPSCdSN preparations or variations among healthy donors. Disturbances of the cell interior dialysis of the intracellular solution by the patch-clamp technique used in their study may also account for these differences. The fraction of active EM patient hiPSCdSN, however, revealed a significantly higher firing rate in the EM patient hiPSCdSNs (mean spiking frequency 2.18 ± 0.35 s^{-1}, median 1.56) compared to the control hiPSCdSNs (mean spiking frequency 1.46 ± 0.3 s^{-1}, median 1.04; p = 0.03 Wilcoxon rank-sum test) (**Figures 2C, D**). Thus, EM patient sensory neurons show a hyperactive phenotype, a finding which is in line with previous observations and can be attributed to the gain-of-function mutation *SCN9A* gene encoding the voltage-gated sodium channel subunit alpha Nav1.7 (Cao et al., 2016). The specificity of this phenotype was further confirmed by the application of the specific Nav1.7 channel blocker PF-05089771, which at 60 and 110 nM concentrations blocked AP firing of the patient hiPSCdSNs (data not shown).

3.3. Burst AP firing in EM patient hiPSCdSNs

The temporal pattern of AP firing is essential for sensory information (pain) transmission, as spikes that occur in a bursty

TABLE 1 Number of bursting versus sporadically firing cells in erythromelalgia (EM) patient versus control human induced pluripotent stem cell-derived sensory neurons (hiPSCdSNs).

	Bursters	Sporadically firing cells	Marginal row totals
Control	4	26	30
EM patient	23	44	67
Total	27	70	97 (grand total)

Fischer's exact test $p = 0.049$.

pattern (burst spikes) can be transmitted across synapses more reliably than spikes occurring in an irregular (sporadic spikes) pattern (Lisman, 1997).

We therefore analyzed the bursting pattern of AP firing of the EM patient and control hiPSCdSNs on cells showing spontaneous activity. We found that control hiPSCdSNs discharge in sporadic fashion, while EM patient hiPSCdSNs discharge in a bursting pattern (**Figure 3A**, left shows example traces). The log-binned histograms of the time difference between the spikes, the inter-event intervals (IEIs; **Figure 3A**, right) show that the sporadically firing control cells can be fitted with a single exponential, whereas the bursting EM cells are well-fitted with two exponentials, representing the intra-burst intervals between APs (left peak) and the inter-burst intervals between two bursts (right peak). Exponential fits were performed on all cells with >20 APs. In EM patient hiPSCdSNs 15 out of 30 cells exhibited two distributions (average tau values: intra-burst intervals: 165 ± 38 ms; inter-burst intervals 1,750 ± 377 ms), the remaining 15 cells exhibited a single distribution (average tau values for single fit: 852 ± 220 ms). In control hiPSCdSNs 6 out of 24 cells exhibited two distributions (average tau values: intra-burst intervals: 313 ± 111 ms; inter-burst intervals 1,775 ± 603 ms), the remaining 18 cells exhibited a single distribution (average tau values for single fit: 974 ± 207 ms). There was no difference between intra-burst intervals and inter-burst intervals from EM patient hiPSCdSNs and control hiPSCdSNs in the cells exhibiting two distributions (intra-burst intervals $p = 0.028$; inter-burst intervals $p = 0.87$, Wilcoxon rank-sum test) and in the cells exhibiting a single distribution ($p = 0.69$, Wilcoxon rank-sum test) indicating that the quality of the bursts is not different between groups. To quantify these observations we categorized the cells into "bursters" and sporadically firing cells (**Table 1**). A "burster" was defined as having an epoch where at least one burst occurred in which a "burst" is defined as a cluster of spikes from a single neuron that fires with a higher rate than at a previous time (Lobb, 2014).

The results reveal that the fraction of bursters is significantly higher in EM patient hiPSCdSNs compared to control hiPSCdSNs (EM patient: total $n = 67$ Ctrl: total $n = 30$, Fisher's exact test $p = 0.049$) (**Table 1**). To further support our statement on the difference between bursting vs. non-bursting EM patient hiPSCdSNs vs. control hiPSCdSNs we performed a bootstrap Chi-square analysis on 30 randomly picked cells from the patients and the 30 Ctrl with 10,000 iterations without replications. The mean p-value from all iterations is 0.0179.

We also characterized the firing patterns of the cells using a continuous measure of burstiness. The burstiness parameter $\boldsymbol{B}$ was calculated as in previous papers (Goh and Barabási, 2008; Schleiss and Smith, 2016; Chen et al., 2018):

$$\mathbf{B} = (\sigma - \mu)/(\sigma + \mu)$$

where σ and μ denote the standard deviation and the mean of inter-event intervals (IEIs), respectively. The magnitude of B (−1, 1) correlates with the cell's burstiness with B = 1 indicating a bursty signal, B = 0 a neutral signal (Poisson process), where the IEIs follow an exponential distribution, and B = −1 indicating a completely regular (periodic) signal. We observed a significantly higher burstiness in the EM patient hiPSCdSNs compared to control hiPSCdSNs (Wilcoxon rank-sum test, $p = 0.02$) (**Figure 3B**).

Another measure of the burstiness of a cell is the accumulation of consecutive short IEIs, which represent the spikes within a burst. To categorize the IEIs of each cell into consecutive short (long) followed by short (long) (S->S, L->L), we plotted the IEIs of a cell against itself shifted by one and clustered the data using the k-means method with k = 3 for both groups (**Figures 3C, D**). The quality of the clustering was controlled by calculating the silhouette index for the clustering with k = 3. All values were >0.5. Average silhouette indexes were 0.70. ± 0.15 for EM neurons and 0.73 ± 0.14 for controls, indicative of a qualitatively median to good clustering. We counted the S->S intervals in the cells where a clustering was enabled by the presence of three obvious clusters. Cells with silhouette indices ≥0.5 were included in the analysis. In the EM patient group an average of 38.5 ± 4.7 S->S were counted compared to 16.1 ± 4.3 S->S intervals in the control. Statistical comparison of the data shows a significant difference (Wilcoxon rank-sum test, $p = 0.002$).

3.4. Elevated heat sensitivity in EM patient hiPSCdSNs

Recurrent attacks of pain and swelling in the distal extremities characteristic for inherited erythromelalgia are, amongst others, triggered by mild increases in ambient temperature. To elucidate if the present model can mimic the elevated heat sensitivity observed in EM patients, we increased the ambient temperature from 37°C (recording temperature) to 40°C (example traces shown in **Figure 4A**) in EM patient and control cells. The baseline frequencies in the EM patient hiPSCdSNs were significantly higher as compared to control hiPSCdSNs ($p = 0.005$, Wilcoxon rank-sum test), which reflects the increased excitability described in **Figure 2**. We observed

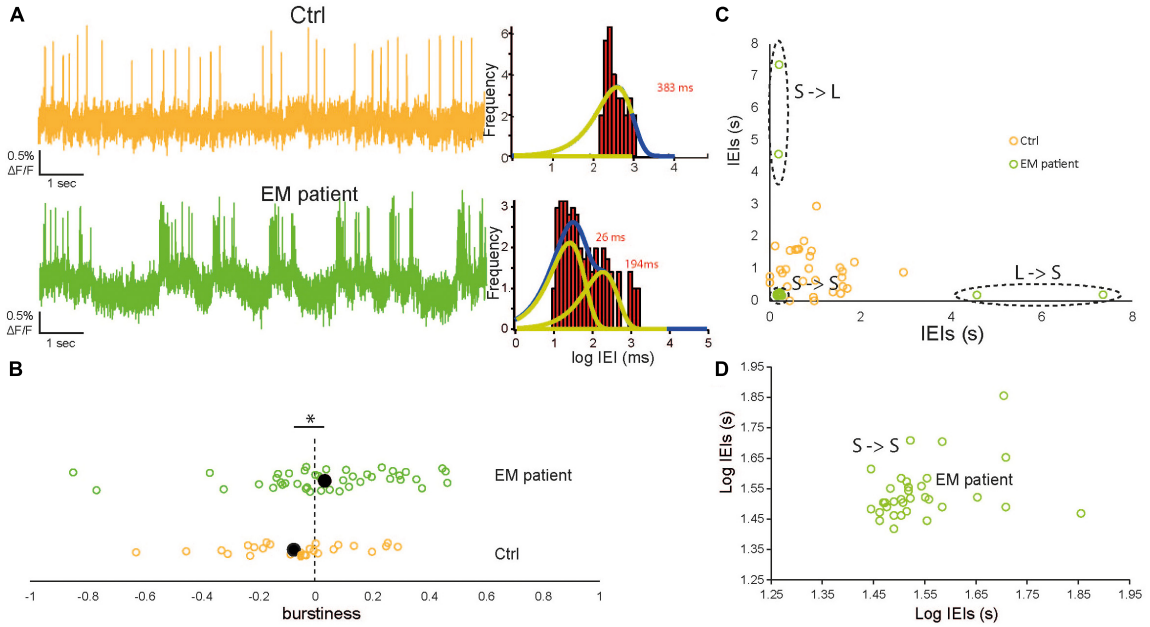

FIGURE 3
Increased spontaneous bursting discharge in erythromelalgia (EM) patientdSNs. **(A)** Left: Representative raw imaging traces of control human induced pluripotent stem cell-derived sensory neurons (hiPSCdSNs) (top, orange) showing a sporadic firing pattern and EM patient hiPSCdSNs (bottom, green) showing a clear bursting pattern. Right: Log-binned Interevent interval (IEI) histograms of the example EM patient hiPSCdSNs trace exhibited two distributions that were well fit with multiple exponential distributions whereas control hiPSCdSNs were well fit with a single exponential. Yellow lines indicate exponential fits. Blue lines indicate the sum of the fits. **(B)** Comparison of the burstiness of EM patient hiPSCdSNs and control hiPSCdSNs. Filled black dots indicate the average values. Burstiness is significantly higher in EM patient hiPSCdSNs (*EM patientdSNs N* = 45, control hiPSCdSNs *N* = 27; WRT **p* = 0.04). **(C)** Plot of the shifted IEIs for single cell examples of EM patient hiPSCdSNs and control hiPSCdSNs. Dotted black lines indicate clusters of short followed by short (S->S) Short followed by long (S->L) and L->S in the EM patient group. **(D)** Enlargement of the S->S cluster in **(C)** on a log scale.

a significant increase in firing frequency in the EM patient hiPSCdSNs () but not in the control hiPSCdSNs [EM patient hiPSCdSNs n = 10, 2.25 ± 0.21 to 3.12Hz ± 0.22 Hz at 40°C, p = 0.03; control hiPSCdSNs n = 6, 0.96 ± 0.22 to 0.99 ± 0.21 Hz at 40°C, p = 0.87, Wilcoxon signed-rank test (paired difference test), all errors are indicated as ± SEM **Figure 4B**. These observations are in line with the findings of Cao et al. (2016), further reinforcing the role of Nav1.7 channels in the elevated heat sensitivity observed in EM patients.

3.5. Exploration of dqGEVI for optical recording of hiPSC-derived forebrain neurons

To demonstrate a broader applicability of the dqGEVI platform for hiPSC-based neurological and neuropsychiatric disease modeling we expressed dqGEVI in mixed cultures of human hiPSC-derived forebrain neurons. The synchrony of neuronal firing is of major importance for information processing in the brain, and abnormal neuronal synchronization has been found in diverse neurological and neuropsychiatric diseases such as schizophrenia, epilepsy, autism spectrum disorder, Alzheimer's and Parkinson's reviewed in Uhlhaas and Singer (2006).

To generate defined populations of forebrain neurons we employed forward programming of iPSCs via overexpression of the transcription factors NGN2 and ASCL1 + DLX2 to generate induced glutamatergic (iGlutNs) and GABAergic neurons (iGABANs), respectively (Zhang et al., 2013; Yang et al., 2017). To ensure highly controlled and stable transgene expression, we used targeted insertion of doxycyclin-inducible transgene cassettes into the AAVS1 "safe harbor" locus as described (Rhee et al., 2019; Peitz et al., 2020).

For optical recording we used mixed cultures composed of 80% NGN2-induced and 20% ASCL1/DLX2-induced neurons. Upon transduction with the dqGEVI-expressing AAVs we imaged the spontaneous activity of these cultures (**Figure 5A**) at 37°C (batch of n = 48 neurons, mean firing frequency 2.57 s^{-1}) and calculated the correlation coefficient of the optical sampling points (**Figure 5B**) as a measure of synchronized activity between pairs of neurons using a sample of 18 pairs. The mean correlation coefficient was 0.436 ± 0.036, indicating a high degree of synchrony between neuronal pairs.

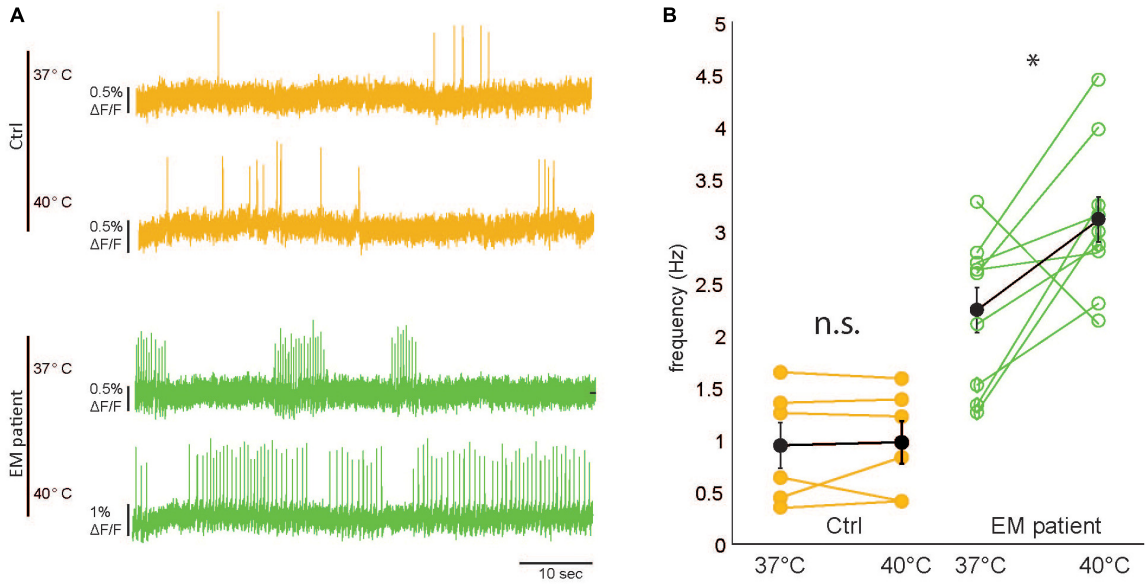

FIGURE 4
Erythromelalgia (EM) patient human induced pluripotent stem cell–derived sensory neurons (hiPSC–SNs) are hypersensitive to mild increases in ambient temperature. **(A)** Representative raw imaging traces of control hiPSC-SNs (top, orange) and EM patient–SNs (bottom, green) at 37 and 40°C. **(B)** Comparison of spike frequency filled black dots indicate average values. Error bars indicate SEM. [*EM patientdSNs N* = 10, control human induced pluripotent stem cell-derived sensory neurons (hiPSCdSNs) *N* = 6, Wilcoxon rank-sumtest, control: **p* = 0.87, EM patient: **p* = 0.027].

To demonstrate that the dqGEVI system can be scaled up toward a high throughput screening platform we enlarged the field of view (FOV) to 66 × 664 pixels to observe the synchronization between more cells. We were able to visualize the synchronous activity of six neurons in parallel (**Figure 5C**). The number of neurons in the FOV is thereby solely restricted by the capacity of the recording computer. The FOV can, without reservations in terms of sampling rate, be extended to 1,200 pixels (pixel size 11× 11 μm) in the horizontal plane, and paired with an increase in cell density the number of cells in the FOV can be further increased.

These data indicate that the present dqGEVI approach can be used to record both PNS and CNS neurons and that this method can be extended from single neurons to neuronal cohorts.

4. Discussion

In this study we employed a dqGEVI optical recording method to assess the spontaneous firing activity of hiPSC-derived sensory and forebrain neurons. This method represents the least invasive and still most accurate approach for AP detection and resolution during neuronal activity. In contrast to other GEVIs, in the dqGEVI the genetically encoded part of the sensor, the fluorescent protein (eGFP), is attached to the outside of the plasma membrane using a glycosylphosphatidylinositol anchor (GPI anchor) instead of transmembrane domains used in most of the other GEVIs such as rhodopsin-based and voltage sensitive domain (VSD)-based approaches reviewed in Yang and St-Pierre (2016), Knöpfel and Song (2019), Mollinedo-Gajate et al. (2021). The insertion of GPI-eGFP into the plasma membrane and the incubation with the voltage-sensing dark quenching molecule D3 has been shown to leave the membrane properties of the cells unaffected both in primary mouse neurons (Alich et al., 2021) and in hiPSC-derived neurons (present study).

In whole-cell patch-clamp recordings a significant opening in the plasma membrane and dialysis of the cells interior with the internal pipette solution might disturb the intracellular mechanisms of the neuron (Pusch and Neher, 1988). Intracellular ion concentrations are unavoidably disturbed by the dialysis of the cell's interior into the pipette and the pipette's contents into the cell. In addition, non-physiological intracellular Ca^{2+} buffering and the interference with endogenous Ca^{2+} buffers in these recordings poses a significant problem (Nägerl and Mody, 1998; Nägerl et al., 2000), but regrettably receives little attention. The intracellular solutions used in the whole-cell patch-clamp recordings contain various amounts of exogenous Ca^{2+} buffers and the most recently used molecules for optical recordings, the GECI, are themselves Ca^{2+} buffers (McMahon and Jackson, 2018). As cytosolic Ca^{2+} regulates many intracellular processes, it

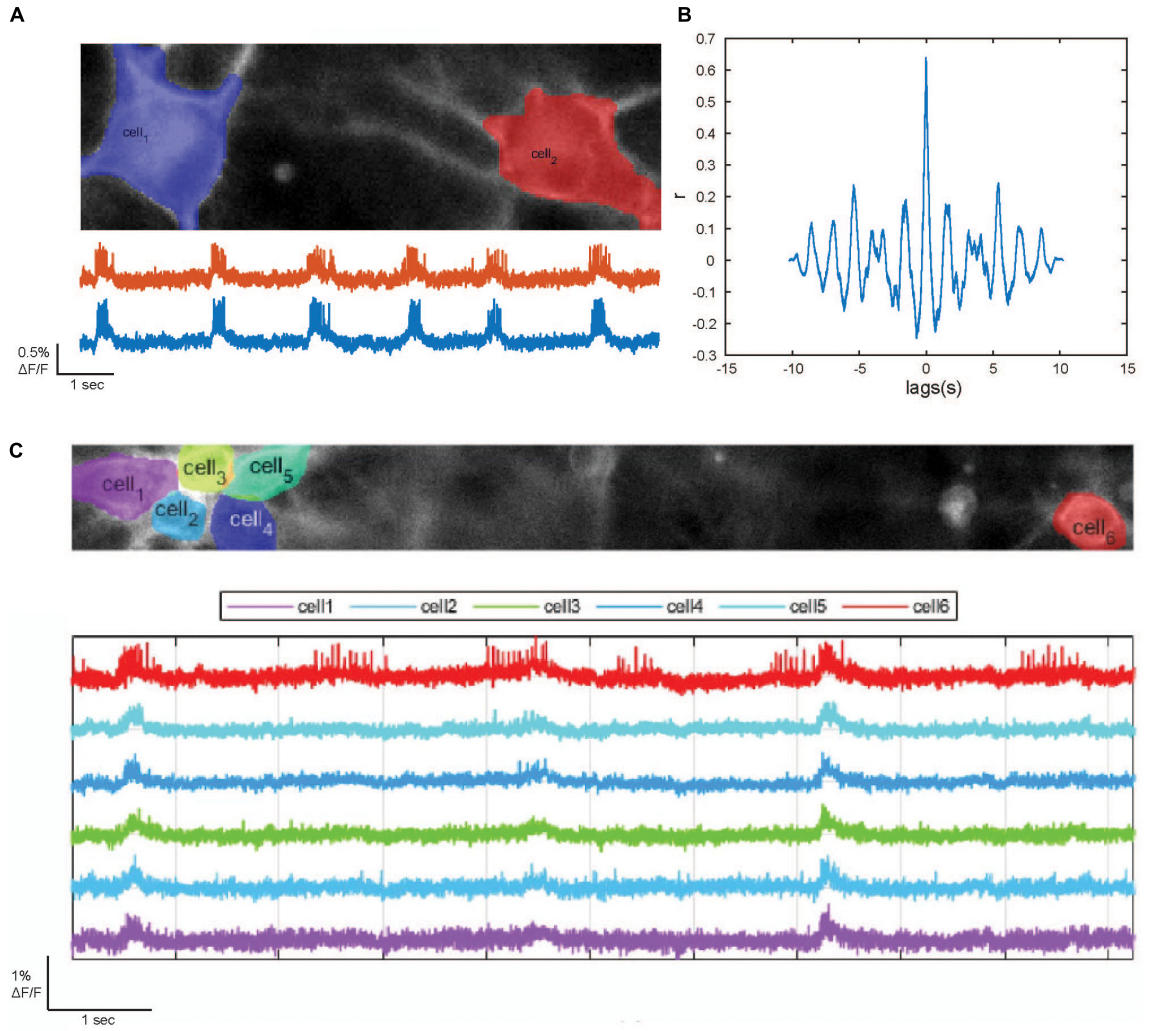

FIGURE 5
Optical detection of epileptogenic bursting behavior in human induced pluripotent stem cell (hiPSC)-derived forebrain neurons [induced forebrain glutamatergic neurons (iGluN) (80%) and GABAergic neurons (iGABAN) (20%)]. **(A)** Top: Automated detection of the somata of two example hiPSC-derived iGluN iGABAN neurons. **(B)** Cross-correlation between the fluorescence traces of two example neurons. **(C)** Upscaling of the dark quencher hybrid genetically encoded voltage indicator (dqGEVI) imaging system. Top: Automated detection of the somata of six hiPSC-derived forebrain neurons. Bottom: respective fluorescence traces.

greatly affects the behavior of neurons. Synaptically connected neurons, which form neuronal networks, use intracellular Ca^{2+} to regulate their membrane excitability and to control the network bursting pattern (Kudela et al., 2009) mainly by influencing Ca^{2+}-dependent K^{+} channels. Therefore, Ca^{2+} buffering in various recording methods is a major impediment for observing the physiological behavior of neurons, particularly their endogenous burst firing patterns.

The method employed here stands in sharp contrast to the whole-cell patch-clamp approach used by Cao et al. (2016), who previously investigated hiPSC derived sensory neurons from EM patients. Using the non-invasive dqGEVI approach we were able to observe the undisturbed spontaneous AP firing behavior of hiPSC-derived sensory and cortical neurons and could detect differences in AP firing phenotypes between patient and control neurons. The increased AP firing frequency, which we observed in the patient group is in line with previous patch-clamp based studies exploring patient cells from EM patients and mouse Nav1.7 mutant dorsal root ganglion (DRG) neurons (Dib-Hajj et al., 2005; Cao et al., 2016). These studies explained the increase in AP firing rate through a hyperpolarizing shift in activation and a depolarizing shift in steady-state inactivation of Na^{+} channels thus lowering the threshold for single APs. In addition to these observations, the dqGEVI method revealed

that the firing behavior in the EM patient-derived cells differs not only with regard to AP frequency, but also in their burst firing patterns.

A burst is a group of events that are separated by gaps that are all shorter than a critical time t_c and a gap between the bursts that is longer than t_c. Various methods have been used to differentiate between within bursts and between bursts time gaps, and to minimize misclassifications (Colquhoun and Sakman, 1985; Lieberman and Mody, 1998).

Using several methods of burst classification, we found a significantly larger fraction of "bursters" in the patient group. This finding might shed light on the pathophysiological mechanism of EM. If neurons fire in bursts, the information transmission within neuronal networks is increased due to the increased probability of inducing postsynaptic neurons to fire APs (Lisman, 1997; Izhikevich et al., 2003). This is of particular relevance for pain transmission, as burst firing of the dorsal root ganglion (DRG) cells increases the likelihood for pain information transmission to the postsynaptic pain projection neuron.

Heat evokes intense burning pain in EM patients (Drenth and Waxman, 2007). This is mimicked in our model where we observed a marked increase in mean firing frequencies upon slight increases in ambient temperature in Nav1.7 mutant cells, whereas the mean firing rate in control hiPSCdSNs only showed a minimal increase as in EM hiPSCdSNs (Cao et al., 2016) and in rat DRG neurons (Yang et al., 2016). It is long known that the firing pattern and the electrical activity of neurons is affected by changes in ambient temperature (Hodgkin and Katz, 1949; Dalton and Hendrix, 1962; Frankenhaeuser and Moore, 1963; Burrows, 1989). These temperature changes influence membrane excitability by altering ion channels and active transporters. The effect of temperature on neuronal excitability, however, is bidirectional. Temperature increases can trigger activation of transient receptor potential (TRP) channels. Upon stimulation these channels produce "generator potentials," which are small changes in voltage across the membrane. TRP channels are expressed in different subsets and at different expression levels thereby transducing thermal stimuli of different strength to produce these "generator potentials" (Vriens et al., 2014). Nav1.7 channels then act as amplifiers of these receptor potentials causing the cell to fire once the potential has reached a certain threshold (Waxman, 2006) thus contributing to an increase in excitability upon heating.

On the other hand, temperature increases can reduce input resistance by affecting potassium channels such as TREK2 and TRAAK, which are expressed in DRG neurons (Kang et al., 2005), thereby inhibiting APs firing and decreasing neuronal excitability. The minimal temperature effect on control neurons is thus likely to result from the balanced interaction between different channel types, TRP, K^+ and Na^+. We propose that the Nav1.7 gain of function mutation in the patient hiPSCdSNs shifts this balance toward a hyperexcitable phenotype as the receptor potentials are strongly amplified.

We observed 34% of spontaneously active cells in the EM patient group, which is in line with the findings from Cao et al. (2016), where their EM3 cells showed 35% active cells. A similar fraction of active cells, 31%, was detected in our control hiPSCdSNs. The comparable ratios of active versus non-active cells in the patient hiPSCdSNs and the control hiPSCdSNs may suggest that the fraction of active cells is independent of the sodium channel mutation and does not contribute to the EM phenotype.

We also demonstrate the usefulness of the optical voltage recordings in mixed cultures of glutamatergic and GABAergic forebrain neurons. Targeting gene expression to a defined subset of nerve cells using cell type specific promoters may refine the approach even further and enable deciphering the contribution of a particular neuronal subtype to a disease phenotype or to visualize differences in susceptibility toward pharmacological compounds. This strategy is, however, particularly challenging in hiPSC-derived neurons, because the currently available promoters are often leaky (resulting in non-specific transgene expression) and maintain a poor expression level, which is highly disadvantageous in voltage imaging. The bipartite expression system presented here provides a straight-forward solution for the latter problem. The weak, but neuron-specific Synapsin1 promoter maintains sufficient levels of the trans-activator protein to induce adequate levels of fluorescent protein expression *in trans* for imaging in the co-transduced cells. Following the same principle, other specific promoters such as the mGAD65 should be able to restrict high levels of voltage sensor expression to a population of cells, e.g., inhibitory neurons (Hoshino et al., 2021). Furthermore, diluting the trans-activator encoding rAAV also facilitates sparse, stochastic labeling of the transduced cells which can be beneficial for removing background fluorescence of overlapping cells when imaging subcellular compartments.

In addition to being suitable for the study of hyperexcitable phenotypes, as in the example of inherited EM, in future studies the dqGEVI approach may also distinguish between phenotypes associated with changes in hyperpolarizing currents elicited by mutations in potassium channels. As originally shown (Alich et al., 2021) dqGEVI is highly sensitive to both hyperpolarizing and depolarizing subthreshold potential changes. In view of the multitude of neuropsychiatric diseases associated with mutations in potassium channels reviewed in Imbrici et al. (2013) this opens the prospect to a high throughput optical screening method of compounds for the treatment of a multitude of neuropsychiatric disorders. As reprogramming and differentiation or direct conversion of somatic cells into induced neurons becomes more and more reliable and scalable, the analyzed cohorts will steadily increase, creating a demand for a fast system ready for high throughput analyzes. Upscaling the system to a 96-well format using preexisting

photodiode-based plate readers or automated camera based systems (e.g., HAMAMATSU FDSS/μCELL functional drug screening system) will increase the throughput and enable fast phenotyping of newly identified disease-associated mutations, as well as compound screening.

Data availability statement

The datasets analyzed for this study can be found in the Sciebo cloud storage of the University of Bonn (https://uni-bonn.sciebo.de/s/6XN3D3eDLWraHoe).

Ethics statement

The studies involving human participants were reviewed and approved by Ethics Committee of the Medical Faculty of the University of Bonn (approval number 275/08). The patients/participants provided their written informed consent to participate in this study.

Author contributions

TA, OB, and IM: conceptualization. TA, PR, BS, ST, and MP: data curation. TA, PR, KG, MP, and IM: formal analysis. TA, PR, MP, BS, and ST: investigation. OB and IM: funding acquisition. IM: project administration. TA, KG, and IM: software. TA, PR, and IM: visualization. TA, PR, BS, and MP: writing—original draft. TA, OB, IM, BS, and PR: writing—review and editing. All authors contributed to the article and approved the submitted version.

Funding

This work was supported by inovative medicine initiatives 2 joint undertaking under grant agreement No. 116072-NGN-PET (European Union's Horizon 2020 Research and Innovation Programme and EFPIA) to OB, European Regional Development Fund (NeuRoWeg; grants EFRE-0800407; EFRE-0800408) to OB, The Original idea of the dqGEVI research was supported by European Research Council Advanced Grant 339620 MULTIGEVOS to IM, and German Research Council DFG, SFB1089 to IM.

Acknowledgments

We thank Phuong Tran and Lydia Fischer for excellent technical assistance, S. Schoch and her laboratory for help with virus preparation, Anja Nitzsche for initial support with setting up the iPSCdSN cultures, H. Beck for his generous help providing the Prime95B camera and him and his laboratory members for discussions and comments. We also thank the European Bank for induced pluripotent Stem Cells (EBiSC) for providing the iPSC line RCi001-A, that was generated and deposited by Pfizer Limited (https://cells.ebisc.org/RCi001-A/).

Conflict of interest

OB was a co-founder and shareholder of LIFE & BRAIN GmbH.

The remaining authors declare that the research was conducted in the absence of any commercial or financial relationships that could be construed as a potential conflict of interest.

Publisher's note

Supplementary material

The Supplementary Material for this article can be found online at: https://www.frontiersin.org/articles/10.3389/fncel.2022.1039957/full#supplementary-material

References

Akemann, W., Lundby, A., Mutoh, H., and Knöpfel, T. (2009). Effect of voltage sensitive fluorescent proteins on neuronal excitability. *Biophys. J.* 96, 3959–3976. doi: 10.1016/j.bpj.2009.02.046

Alich, T. C., Pabst, M., Pothmann, L., Szalontai, B., Faas, G. C., and Mody, I. (2021). A dark quencher genetically encodable voltage indicator (dqGEVI) exhibits high fidelity and speed. *Proc. Natl. Acad. Sci.U.S.A.* 118, 1–12. doi: 10.1073/pnas.2020235118

Bando, Y., Grimm, C., Cornejo, V., and Yuste, R. (2019a). Genetic voltage indicators. *BMC Biol.* 17:1–12. doi: 10.1186/s12915-019-0682-0

Bando, Y., Sakamoto, M., Kim, S., Ayzenshtat, I., and Yuste, R. (2019b). Comparative evaluation of genetically encoded voltage indicators. *Cell Rep.* 26, 802–813. doi: 10.1016/j.celrep.2018.12.088.Comparative

Burrows, M. (1989). Effects of temperature on a central synapse between identified motor neurons in the locust. *J. Comp. Physiol. A.* 165, 687–695. doi: 10.1007/BF00611000

Cai, C., Friedrich, J., Singh, A., Eybposh, M. H., Pnevmatikakis, E. A., Podgorski, K., et al. (2021). VolPy: Automated and scalable analysis pipelines for voltage imaging datasets. *PLoS Comput. Biol.* 17:1–27. doi: 10.1371/journal.pcbi.1008806

Cao, G., Platisa, J., Pieribone, V. A., Raccuglia, D., and Kunst, M. (2013). Resource genetically targeted optical electrophysiology in intact neural circuits. *Cell* 154, 904–913. doi: 10.1016/j.cell.2013.07.027

Cao, L., McDonnell, A., Nitzsche, A., Alexandrou, A., Saintot, P. P., Loucif, A. J. C., et al. (2016). Pharmacological reversal of a pain phenotype in iPSC-derived sensory neurons and patients with inherited erythromelalgia. *Sci. Transl. Med.* 8, 225–245. doi: 10.1126/scitranslmed.aad7653

Carlton, P. M., Boulanger, J., Kervrann, C., Sibarita, J. B., Salamero, J., Gordon-Messer, S., et al. (2010). Fast live simultaneous multiwavelength four-dimensional optical microscopy. *Proc. Natl. Acad. Sci.U.S.A.* 107, 16016–16022. doi: 10.1073/pnas.1004037107

Chambers, S. M., Qi, Y., Mica, Y., Lee, G., Zhang, X. J., Niu, L., et al. (2012). Combined small-molecule inhibition accelerates developmental timing and converts human pluripotent stem cells into nociceptors. *Nat. Biotechnol.* 30, 715–720. doi: 10.1038/nbt.2249

Chen, L., Saito, T., Saido, T. C., and Mody, I. (2018). Novel quantitative analyses of spontaneous synaptic events in cortical pyramidal cells reveal subtle parvalbumin-expressing interneuron dysfunction in a knock-in mouse model of alzheimer's disease. *eNeuro* 5, 1–15. doi: 10.1523/ENEURO.0059-18.2018

Colquhoun, D., and Sakman, B. (1985). Fast events in single-channel currents activated by acetylcholine and its analogues at the frog muscle end-plate. *J. Phyiol.* 369, 501–557. doi: 10.1113/jphysiol.1985.sp015912

Dalton, J., and Hendrix, D. (1962). Effects of temperature on membrane potentials of lobster giant axon. *Am. J. Physiol.* 202, 491–494. doi: 10.1152/ajplegacy.1962.202.3.491

Dib-Hajj, S. D., Rush, A. M., Cummins, T. R., Hisama, F. M., Novella, S., Tyrrell, L., et al. (2005). Gain-of-function mutation in Nav1.7 in familial erythromelalgia induces bursting of sensory neurons. *Brain* 128, 1847–1854. doi: 10.1093/brain/awh514

Drenth, J., and Waxman, S. (2007). Mutations in sodium-channel gene SCN9A cause a spectrum of human genetic pain disorders. *J. Clin. Invest.* 117, 3603–3609. doi: 10.1172/JCI33297

Edelstein, A. D., Tsuchida, M. A., Amodaj, N., Pinkard, H., Vale, R. D., and Stuurman, N. (2014). Advanced methods of microscope control using μManager software. *J. Biol. Methods* 1:10. doi: 10.14440/jbm.2014.36

Elanzew, A., Nießing, B., Langendoerfer, D., Rippel, O., Piotrowski, T., Schenk, F., et al. (2020). The StemCellFactory: A modular system integration for automated generation and expansion of human induced pluripotent stem cells. *Front. Bioeng. Biotechnol.* 8:1–16. doi: 10.3389/fbioe.2020.580352

Frankenhaeuser, B. Y. B., and Moore, L. E. (1963). The effect of temperature on the sodium and potassium permeability changes in myelinated nerve fibres of *Xenopus* laevis. *J. Physiol.* 169, 431–437. doi: 10.1113/jphysiol.1963.sp007269

Goh, K., and Barabási, A. (2008). Burstiness and memory in complex systems. *Eur. Lett.* 81, 1–5. doi: 10.1209/0295-5075/81/48002

Hauck, B., and Chen, L. X. W. (2003). Generation and characterization of chimeric recombinant AAV vectors. *Mol. Ther.* 7, 419–425. doi: 10.1016/s1525-0016(03)00012-1

Hill, M., and Greenfield, S. (2011). The membrane chamber: A new type of in vitro recording chamber. *J. Neurosci. Methods* 195, 15–23. doi: 10.1016/j.jneumeth.2010.10.024

Hodgkin, B. A. L., and Katz, B. (1949). The effect of temperature on the electrical activity of the giant axon of the squid. *J. Physiol.* 109, 240–249. doi: 10.1113/jphysiol.1949.sp004388

Hoshino, C., Konno, A., Hosoi, N., Kaneko, R., Mukai, R., Nakai, J., et al. (2021). GABAergic neuron-specific whole-brain transduction by AAV-PHP.B incorporated with a new GAD65 promoter. *Mol. Brain* 14, 1–18. doi: 10.1186/s13041-021-00746-1

Imbrici, P., Camerino, D. C., and Tricarico, D. (2013). Major channels involved in neuropsychiatric disorders and therapeutic perspectives. *Front. Genet.* 4:1–19. doi: 10.3389/fgene.2013.00076

Izhikevich, E. M., Desai, N. S., Walcott, E. C., and Hoppensteadt, F. C. (2003). Bursts as a unit of neural information: Selective communication via resonance. *Trends. Neurosci.* 26, 161–167. doi: 10.1016/S0166-2236(03)00034-1

Johannes, C. B., Le, T. K., Zhou, X., Johnston, J. A., and Dworkin, R. H. (2010). The prevalence of chronic pain in United States adults: Results of an internet-based survey. *J. Pain* 11, 1230–1239. doi: 10.1016/j.jpain.2010.07.002

Kang, D., Choe, C., and Kim, D. (2005). Thermosensitivity of the two-pore domain K+ channels TREK-2 and TRAAK. *J. Physiol.* 564, 103–116. doi: 10.1113/jphysiol.2004.081059

Kannan, M., Vasan, G., and Pieribone, V. A. (2019). Optimizing strategies for developing genetically encoded voltage indicators. *Front. Cell. Neurosci.* 13:1–17. doi: 10.3389/fncel.2019.00053

Kiskinis, E., Kralj, J. M., Zou, P., Weinstein, E. N., Zhang, H., Tsioras, K., et al. (2018). All-optical electrophysiology for high-throughput functional characterization of a human iPSC-derived motor neuron model of ALS. *Stem Cell Rep.* 10, 1991–2004. doi: 10.1016/j.stemcr.2018.04.020

Knöpfel, T., and Song, C. (2019). Optical voltage imaging in neurons: Moving from technology development to practical tool. *Nat. Rev. Neurosci.* 20, 719–727. doi: 10.1038/s41583-019-0231-4

Kudela, P., Bergey, G. K., and Franaszczuk, P. J. (2009). Calcium involvement in regulation of neuronal bursting in disinhibited neuronal networks: Insights from calcium studies in a spherical cell model. *Biophys. J.* 97, 3065–3074. doi: 10.1016/j.bpj.2009.09.027

Lieberman, D. N., and Mody, I. (1998). Substance P enhances NMDA channel function in hippocampal dentate gyms granule cells. *J. Neurophysiol.* 80, 113–119. doi: 10.1152/jn.1998.80.1.113

Lisman, J. E. (1997). Bursts as a unit of neural information: Making unreliable synapses reliable. *Trends. Neurosci.* 20, 38–43. doi: 10.1016/S0166-2236(96)10070-9

Lobb, C. (2014). Abnormal bursting as a pathophysiological mechanism in Parkinson's disease. *Basal Ganglia* 3, 187–195. doi: 10.1016/j.baga.2013.11.002.Abnormal

McMahon, S., and Jackson, M. (2018). An inconvenient truth: Calcium sensors are calcium buffers. *Trends. Neurosci.* 41, 880–884. doi: 10.1016/j.tins.2018.09.005.An

Milosevic, M., Jang, J., McKimm, E., Zhu, M., and Antic, S. (2020). In vitro testing of voltage indicators?: Archon1, VSFP-butterfly in vitro testing of voltage indicators?: Archon1. *Eneuro* 7, ENEURO.60–ENEURO.20. doi: 10.1523/ENEURO.0060-20.2020

Mollinedo-Gajate, I., Song, C., and Knöpfel, T. (2021). "Genetically encoded voltage indicators," in *Optogenetics, advances in experimental medicine and biology 1293*, eds H. Yawo, et al. (Singapore: Springer Nature Singapore Pte), 209–224. doi: 10.1007/978-981-15-8763-4_12

Nägerl, U. V., and Mody, I. (1998). Calcium-dependent inactivation of high-threshold calcium currents in human dentate gyrus granule cells. *J. Physiol.* 509, 39–45. doi: 10.1111/j.1469-7793.1998.039bo.x

Nägerl, U. V., Mody, I., Jeub, M., Lie, A. A., Elger, C. E., and Beck, H. (2000). Surviving granule cells of the sclerotic human hippocampus have reduced Ca2+ influx because of a loss of calbindin-D(28k) in temporal lobe epilepsy. *J. Neurosci.* 20, 1831–1836. doi: 10.1523/jneurosci.20-05-01831.2000

Neher, E., and Sakmann, B. (1976). Single-channel currents recorded from membrane. *Nature* 260, 799–802. doi: 10.1038/260799a0

Okano, H., and Yamanaka, S. (2014). iPS cell technologies: Significance and applications to CNS regeneration and disease. *Mol. Brain* 7, 1–12. doi: 10.1186/1756-6606-7-22

Peitz, M., Krutenko, T., and Brüstle, O. (2020). Protocol for the standardized generation of forward programmed cryopreservable excitatory and inhibitory forebrain neurons. *STAR Protoc.* 1:100038. doi: 10.1016/j.xpro.2020.100038

Peron, S., Chen, T. W., and Svoboda, K. (2015). Comprehensive imaging of cortical networks. *Curr. Opin. Neurobiol.* 32, 115–123. doi: 10.1016/j.conb.2015.03.016

Pike, F. G., Meredith, R. M., Olding, A. W., and Paulsen, O. (1999). Rapid report: Postsynaptic bursting is essential for "Hebbian" induction of associative long-term potentiation at excitatory synapses in rat hippocampus. *J. Physiol.* 518, 571–576. doi: 10.1111/j.1469-7793.1999.0571p.x

Pusch, M., and Neher, E. (1988). Rates of diffusional exchange between small cells and a measuring patch pipette. *Eur. J. Phyiol.* 411, 204–211. doi: 10.1007/BF00582316

Real, R., Peter, M., Trabalza, A., Khan, S., Smith, M. A., Dopp, J., et al. (2018). In vivo modeling of human neuron dynamics and down syndrome. *Science* 362, 1–19. doi: 10.1126/science.aau1810

Rhee, H. J., Shaib, A. H., Rehbach, K., Brose, N., Rhee, H. J., Shaib, A. H., et al. (2019). An autaptic culture system for standardized analyses of iPSC-derived human neurons resource an autaptic culture system for standardized analyses of

iPSC-derived human neurons. *Cell Rep.* 27, 2212–2228. doi: 10.1016/j.celrep.2019.04.059

Rice, A. S. C., Smith, B. H., and Blyth, F. M. (2016). Pain and the global burden of disease. *Pain* 157, 791–796. doi: 10.1097/j.pain.0000000000000454

Sakaguchi, R., Leiwe, M. N., and Imai, T. (2018). Bright multicolor labeling of neuronal circuits with fluorescent proteins and chemical tags. *Elife* 7, 1–28. doi: 10.7554/eLife.40350

Samarasinghe, R. A., Miranda, O. A., Buth, J. E., Mitchell, S., Ferando, I., Watanabe, M., et al. (2021). Identification of neural oscillations and epileptiform changes in human brain organoids. *Nat. Neurosci.* 24, 1488–1500. doi: 10.1038/s41593-021-00906-5

Schleiss, M., and Smith, J. A. (2016). Two simple metrics for quantifying rainfall intermittency: The burstiness and memory of interamount times. *J. Hydrometeorol.* 17, 421–436. doi: 10.1175/JHM-D-15-0078.1

Thomas, C., Springer, P., Loeb, G., Berwald-Netter, Y., and Okun, L. (1972). A miniature microelectrode array to monitor the bioelectric activity of cultured cells. *Exp. Cell Res.* 74, 61–66. doi: 10.1016/0014-4827(72)90481-8

Tsang, A., Von Korff, M., Lee, S., Alonso, J., Karam, E., Angermeyer, M. C., et al. (2008). Common Chronic pain conditions in developed and developing countries: Gender and age differences and comorbidity with depression-anxiety disorders. *J. Pain* 9, 883–891. doi: 10.1016/j.jpain.2008.05.005

Uhlhaas, P. J., and Singer, W. (2006). Neural synchrony in brain disorders: Relevance for cognitive dysfunctions and pathophysiology. *Neuron* 52, 155–168. doi: 10.1016/j.neuron.2006.09.020

Vriens, J., Nilius, B., and Voets, T. (2014). Peripheral thermosensation in mammals. *Nat. Rev. Neurosci.* 15, 573–589. doi: 10.1038/nrn3784

Waxman, S. (2006). A channel sets the gain on pain. *Nature* 444, 831–832. doi: 10.1038/444831a

Yang, H., and St-Pierre, F. (2016). Genetically encoded voltage indicators: Opportunities and challenges. *J. Neurosci.* 36, 9977–9989. doi: 10.1523/JNEUROSCI.1095-16.2016

Yang, N., Chanda, S., Marro, S., Ng, Y., Janas, J., Haag, D., et al. (2017). Generation of pure GABAergic neurons by transcription factor programming. *Nat. Methods* 14, 621–628. doi: 10.1038/nmeth.4291

Yang, Y., Huang, J., Ma, M., Estacion, M., and Macala, L. (2016). Nav1.7-A1632G Mutation from a family with inherited erythromelalgia: Enhanced firing of dorsal root ganglianeurons evoked by thermal stimuli. *J. Neurosci.* 36, 7511–7522. doi: 10.1007/978-3-642-28753-4_202323

Zhang, Y., Pak, C., Han, Y., Ahlenius, H., Zhang, Z., Marro, S., et al. (2013). Rapid single-step induction of functional neurons from human pluripotent stem cells. *Neuron* 78, 785–798. doi: 10.1016/j.neuron.2013.05.029.Rapid

SUPPLEMENTARY INFORMATION

Bringing to light the physiological and pathological firing patterns of human iPSC-derived neurons using optical recordings

Alich TC ‡,[1], Röderer P ‡,[2,3], Szalontai B [,1], Golcuk K [1], Tariq S [2], Peitz M [2,4], Brüstle O [2] and Mody I [*,1,5]**

[1]Institute of Experimental Epileptology and Cognition Research, University of Bonn Medical Faculty & University Hospital Bonn, Venusberg-Campus 1, 53127 Bonn, Germany, therese.alich@ukbonn.de, balint.szalontai@uni-due.de, kgol@uni-bonn.de

[2]Institute of Reconstructive Neurobiology, University of Bonn Medical Faculty & University Hospital Bonn, Venusberg-Campus 1, 53127 Bonn, Germany, pascal.roederer@uni-bonn.de, tariqs3k@gmail.com, peitz@uni-bonn.de, brustle@uni-bonn.de

[3]LIFE & BRAIN GmbH, Cellomics Unit, Venusberg-Campus 1, 53127 Bonn, Germany

[4]Cell Programming Core Facility, University of Bonn Medical Faculty, Venusberg-Campus 1, 53127 Bonn, Germany

[5]Department of Neurology, Geffen School of Medicine at UCLA 635, Charles Young Drive South Los Angeles, CA 90095-733522/USA, mody@ucla.edu

‡ These authors contributed equally to this work

** Present address: Laboratory for Retinal Gene Therapy, Department of Ophthalmology, University Hospital Zürich, University of Zürich, Zürich, Switzerland

*** Correspondence:**
Istvan Mody
mody@ucla.edu

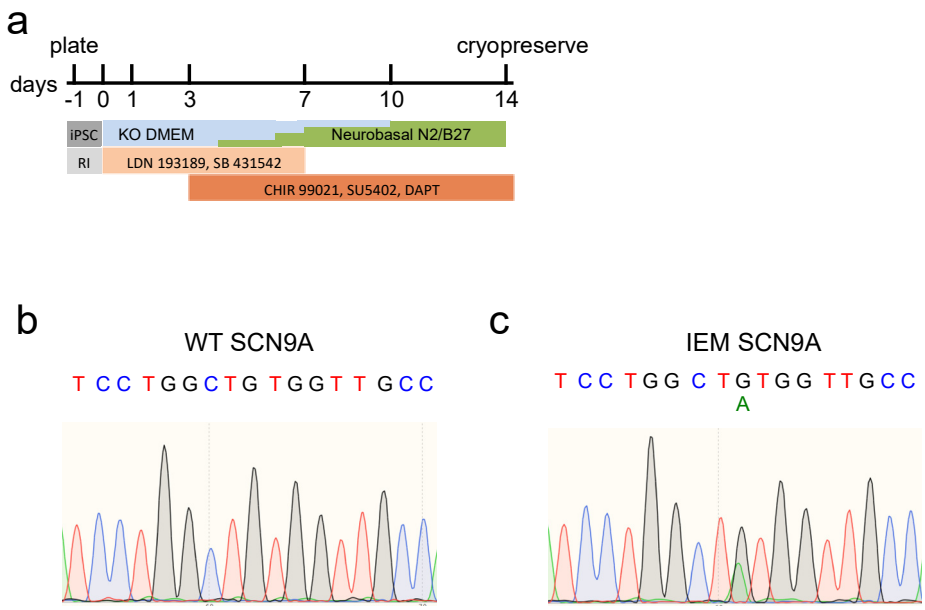

Supplementary Figure 1: *Generation of hiPSCdSN and validation of SCN9A mutation in patient hiPSC* **a)** Differentiation paradigm for the generation of human hiPSC-derived sensory neurons. hiPSC: induced pluripotent stem cells, RI: ROCK-Inhibitor **b, c)** Genotyping of wild type (b) and IEM-patient (c) hiPSC for V400M mutation in *SCN9A* gene. WT: wild type, IEM: inherited erythromelalgia.

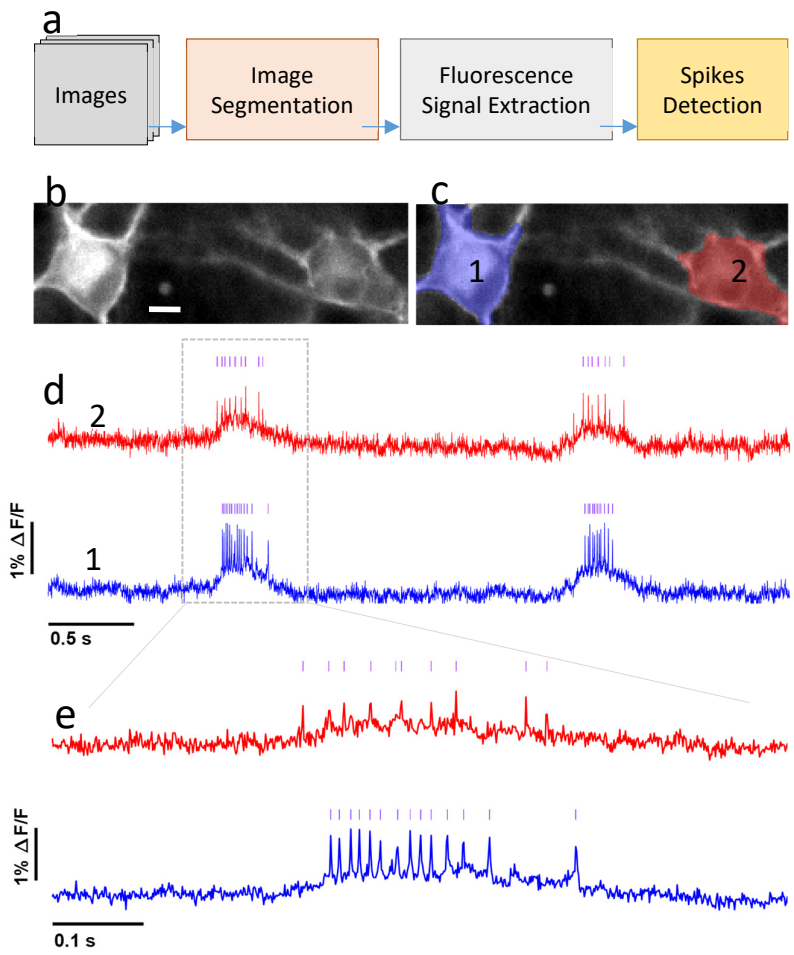

Supplementary Figure 2: *Cell detection pipeline*
The video frames were processed using a custom-written app in Matlab (MathWorks, USA). (a) The stack of frames was loaded as grayscale images. An image file from the whole stack was selected as a reference frame for further image processing and finding the ROIs of the cells. The reference frame was filtered using a 2D Gaussian kernel with a standard deviation of 1 for removing noise. The grayscale image was binarized using the adaptive threshold method. (b,c) The cells in the field of view were segmented after applying morphological image processing operations and then the reference ROIs were automatically generated. (d,e) The mean intensity in the ROI of each frame in the whole stack was calculated and used as the fluorescence signal of the corresponding cell. The extracted intensity for each frame was plotted to obtain the fluorescence signal in the time domain. A linear fit was applied to the fluorescence trace for baseline correction. Then, the intensity values were converted into ΔF/F (%) scale. Spikes were detected using a threshold value of 3-5 standard deviation above the mean.

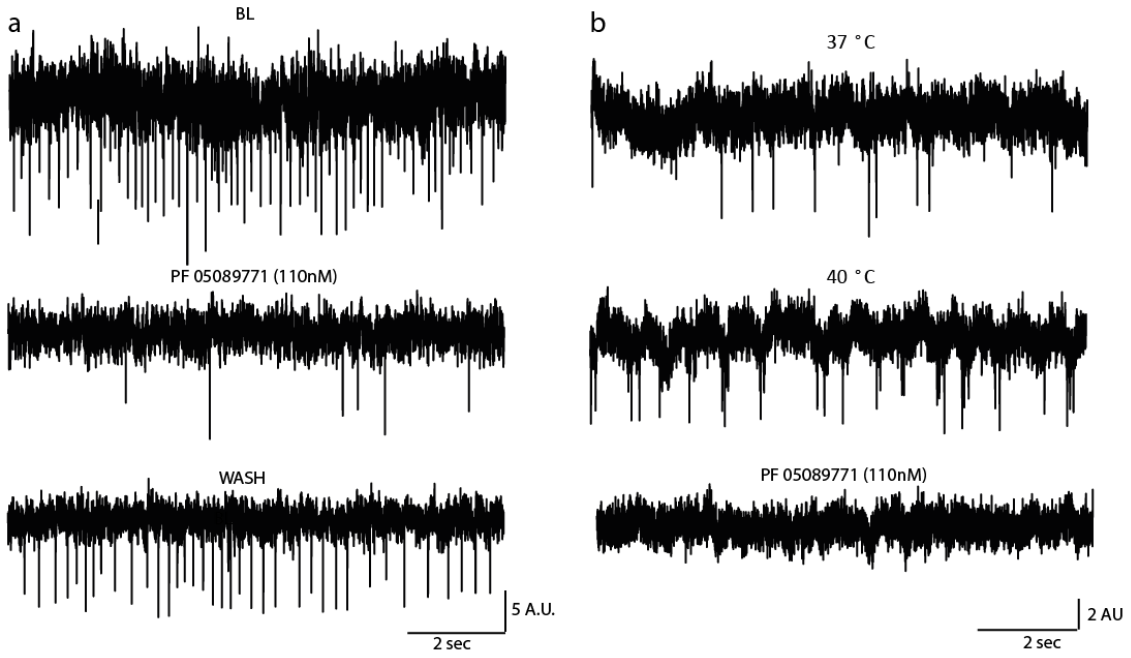

Supplementary Figure 3: Nav1.7 blocker reverses the hyperactive phenotype in EM patient hiPSCdSNs. (a) Representative traces of AP firing at baseline (*upper traces*), after 10 minutes of application of the Nav1.7 inhibitor PF-05089771 (*middle traces*) and 10 minutes after wash. (b) Representative traces show sporadic AP firing at 37°C (*upper traces*) increased firing at 40°C (*middle traces*) and elevated sensitivity to Nav1.7 inhibition at elevated temperatures (*lower trace*).

7 Acknowledgements

First and foremost, I would like to express my heartfelt gratitude to my supervisor, Professor Dr. Istvan Mody. His scientific passion has inspired me, and it is truly the driving force behind this work. I thank Professor Mody for his unwavering support and care, and I am especially thankful for the confidence he had in me. It has been an honor to work with someone who embodies such dedication and excellence.
I thank Professor Dr. Günter Mayer for his wonderful support in our past research project during my master thesis, which opened the path to my PhD studies in neurosciences. I want to thank him further for co-supervising this thesis.
My deepest thanks go to Professor Dr. Heinz Beck for his invaluable guidance and support at the start of my neuroscientific career. I thank Professor Beck for his advice, his generosity, and encouragement. I am glad to be able to continue my scientific career under his mentorship.
Milan Pabst's unwavering passion for science was instrumental in laying the foundation for this project. I am incredibly grateful for his commitment and his positive attitude. Although he is no longer with us, he continues to be an inspiration.
I would like to thank my friend and colleague Dr. Balint Szalontai for his brilliant biomolecular work. Without his expertise, this project would not have been possible. I thank Balint deeply for his advice, his support during difficult phases, and for the wonderful time we shared.
I would also like to extend my heartfelt thanks to Margit Reitze, Nicole Schönfelder, and Kristian Reichelt for all their support and for creating such a pleasant working atmosphere.
I would like to express my gratitude to Dr. Kurt Golcuk for his help on this project and for his outstanding support with all Matlab-related matters.
I am grateful to the lab of Professor Dr. Oliver Brüstle for the great collaboration which allowed me to work on such an interesting disease model.
I would also like to thank Phuong Tran and Lydia Fischer for their technical support throughout the project.
My special thanks go to Dr. Martin Schwarz for his insightful idea that moved the project forward.
I am grateful to the entire Beck lab, especially Dr. Thoralf Optiz and Dr. Tony Kelly, for valuable scientific discussions and advice.

Now it is time to thank my family who has supported me so strongly throughout.
My dear mother, who has always been in my heart.
My children, who give me the strength I need. My husband, who is my rock. My father, who has given me so much love and support throughout my life and is always there for us. My mother-in-law and my father-in-law for their great help in so many things. I couldn't have done it without all of you.